Charles University in Prague
Faculty of Science
Department of Physical and Macromolecular Chemistry

DIPLOMA THESIS

2-D simulations of electromigration processes

Viliam Kolivoška
Supervisor: Prof. RNDr. Bohuslav Gaš, CSc.
Prague 2008

Acknowledgements

I would especially like to thank Mgr. Jan Heyda for very helpful discussions and everyday encouragement in the work. I am deeply indebted to my supervisor, Prof. RNDr. Bohuslav Gaš, CSc., for the guidance of this thesis. I would also like to thank Doc. RNDr. Eva Tesařová, CSc., and RNDr. Vlastimil Hruška, who gave me a huge assistance in my work. I also thank RNDr. Ing. Jaroslav Hron, Ph.D. and Bc. Jaroslav Havrda who provided me a mathematical background of the finite element method. Last, but not least, I would like to thank my parents for the financial support during my studies.

Hereby I confirm that I have carried out the work independently, under the guidance of my supervisor, Prof. RNDr. Bohuslav Gaš, CSc. I also confirm that I have quoted all the sources properly.
I am aware of the fact, that the use of the results obtained in the presented thesis is possible only with a written agreement of Charles University.

Viliam Kolivoška

Contents

Abstract

In the presented thesis we introduce a computational model that can be used for 2-D and 3-D computer simulations of experiments in electrophoresis. The simulations are carried out by the aid of the finite element method (FEM). In particular, commercially available program Comsol Multiphysics 3.3 is employed. A general shape of continuity equation is chosen to express the mass, electric charge, momentum and energy conservation law. Diffusion, migration and convection terms are taken into account when formulating the mass conservation law. Both external (driving voltage) and internal (diffusion currents) terms are considered in the electric charge conservation law. Both constant voltage mode and constant current mode can be handled. A solvent is regarded as an incompressible Newtonian fluid. Both pressure-driven and electroosmotic flows can be taken into consideration. The heat convection as well as the heat diffusion is governed by the energy conservation law. Both strong and weak electrolytes (of any attainable valency) may be regarded as system constituents. Furthermore, the model can handle the ionic strength correction if desired. A task may be assigned either in Cartesian or cylindrical coordinates. The presented model was employed to solve four particular tasks. The first one inspects the electromigration in the setup in the Agilent 3DCE electrophoresis equipment. Changes in the electrolyte composition due to the electrolysis are inspected. The electroosmosis is also considered. The second task focuses on the lab-on-a-chip analysis in a gel. The injection cross is of the main interest. The analysis is carried out in the constant current mode. Four model anionic species are considered as the analytes and their resolution is inspected under various conditions.
The third task deals with the free flow electrophoresis equipment. Both the electric field and the pressure-driven bulk flow are applied simultaneously. Three model cationic species are considered as analytes and their resolution is analyzed. The last task investigates the thermal effects in a capillary. The temperature rises in the capillary as the electric current passes through the electrolyte (Joule heating). Both air and water cooling efficiency are inspected. The coolant velocity field and the resulting temperature map are analyzed under various conditions.

List of used symbols

$\Re^n$	n – dimensional space
n, N	natural number, number of the system constituents
$\aleph, \Re, C$	set of natural, real and complex numbers
t, x, S, V	time, distance, surface, volume
f, g, h	given functions
i, j, k, l	counting indices
$\Omega, \Omega(t)$	computational domain
$\partial\Omega, \partial\Omega(t)$	computational domain boundary
$\partial^2\Omega, \partial^2\Omega(t)$	unification of boundary intersections, a boundary of boundaries
$\Gamma, \Gamma_N, \Gamma_D, \Gamma_{N+D}$	boundary part, Neumann, Dirichlet and Newton boundary part
$V(t)$	test volume
$S(t), \partial V(t)$	test surface, test volume boundary
$X = (x, y, z)$, $X = (r, \varphi, z)$	arbitrary domain point in Cartesian and cylindrical coordinates
a, b, c, d	arbitrary boundary points
$\vec{n}, \vec{t}$	boundary normal vector, boundary tangent vector
$\nabla, \nabla., \nabla\otimes, \Delta$	*nabla* vector, *div*, *curl* and *Laplace* operator
.	inner product
$\otimes$	outer product
$\partial / \partial\vec{n}$	derivative with respect to the boundary normal vector
^{T}	matrix transposition
$A(X,t), \vec{B}(X,t)$	arbitrary scalar and vector system property
$M(t)$	total amount of A in $V(t)$, integral value of A over $V(t)$
$R(t)$	total rate of change of $M(t)$
$Q(X,t)$	source/sink term in $V(t)$
$P(t)$	production/consumption in $V(t)$, integral value of Q over $V(t)$
$\vec{J}(X,t), \vec{J}_i, \vec{J}$	general flux of a property *A*, substance flux, heat flux
$F(t)$	total flux of A through $\partial V(t)$, integral value of $\vec{J}$ over $\partial V(t)$
$\vec{v}_{V(t)}$	velocity of $V(t)$ in $\Re^n$
c_i	analytical concentration of *i*-th system constituent
c_{ij}	concentration of *j*-th ionic form of *i*-th system constituent
$\vec{J}_{i,dif}$, $\vec{J}_{dif}$	constituent diffusion flux, heat diffusion flux
$\vec{J}_{i,mig}$	constituent migration flux
$\vec{J}_{i,con}$, $\vec{J}_{con}$	constituent convection flux, heat convection flux
D_{ij}	diffusivity of *j*-th ionic form of *i*-th system constituent
u_{ij}	ionic mobility of *j*-th ionic form of *i*-th system constituent
z_{ij}	charge number of *j*-th ionic form of *i*-th system constituent
R	universal gas constant
T	absolute temperature
F	Faraday constant
$\vec{E}$	electric field strength vector

h_{ij}	molar fraction of *j*-th ionic form within *i*-th system constituent
$\vec{v}_i, v_{i,k}$	average constituent velocity, its component in *k*-th direction
$\vec{v}, v_k$	bulk flow velocity, its component in *k*-th direction
$\overline{D_i}$	effective constituent diffusivity
ρ	liquid density
ρ_e, ρ_{loc}	net electric charge density, local electric charge density
$\vec{j}, j$	current density vector, current density value
V	electric potential
κ	specific electric conductivity
$\vec{j}_{dif}$	diffusion current density
H_i	effective constituent charge
K_w	ionic product of water
G	*G*-function
$A_{i,j}, B_{i,j}$	arbitrary acid and base
$K_a(i,j), K_b(i,j)$	consecutive acidity constant, stepwise alkalinity constant
$K(i,j)$	consecutive general constant (either for an acid or for a base)
L_{ij}	global general constant of constituent
$\vec{b}, b_k$	body force vector, its component in *k*-th direction
$\vec{\vec{\sigma}}, \sigma_{kl}$	stress (surface) tensor, its *k,l*-entry
$p, \nabla p$	pressure, pressure gradient
$\vec{f}, f_k$	external (volume) force, its component in *k*-th direction
$\vec{\vec{\Im}}$	tensor governing the liquid properties
η	dynamic viscosity
E	general energy, internal energy
π_T	internal pressure at constant temperature
c_v	heat capacity at constant volume
$\vec{\vec{\lambda}}, \lambda$	thermal conductivity tensor, thermal conductivity scalar value
U	electric voltage, electric potential difference
I	electric current value, ionic strength
γ_{ij}	activity coefficient
a_{ij}	ionic activity
N_A	Avogadro's number
k_B	Boltzmann constant
ε	permittivity
$K_{a,app}(i,j), K_{b,app}(i,j)$	apparent acidity constant, apparent alkalinity constant
$K_{w,app}$	apparent ionic product of water
$u_{ij}(I)$	corrected mobility of *j*-th ionic form of *i*-th system constituent
$\kappa(I)$	corrected conductivity
$c_{ij}(I)$	corrected concentration

1. Introduction

Electrophoresis is a set of separation techniques that employ the electric field for the separation of species. Experiments in electrophoresis may either be conducted in a laboratory or simulated by the aid of mathematical methods. Of those, these three are usually employed:

(I) Finite difference method (FDM) is based on dividing the computational domain into non-overlapping segments. The governing equations are discretized and the system property values are evaluated at certain places of the geometry. FDM is used mainly when 1-D computational domains are wished to be inspected. Thus, this method may be applied in the simulations of experiments conducted in sufficiently narrow capillaries. The FDM can also, in principle, handle 2-D and 3-D problems, but it often encounters serious computational problems. Thus, more sophisticated methods are developed for 2-D and 3-D tasks.

(II) Finite volume method (FVM) is often employed when searching the solution in more-dimensional tasks. Similarly to the FDM, it also evaluates the properties at discrete places of the geometry. This method employs integrated forms (over finite volume) of governing equation. The divergence theorem is used to convert the volume integrals into the surface ones. They are evaluated as fluxes originating on the surfaces of neighboring finite volumes.

(III) Finite element method (FEM) is also based on integration of governing equations over finite volume. In the first step, the governing equation is multiplied by a smooth function (called the test function) and this product is integrated over volume. The Green's identity is employed to modify the resulting integral equation. Boundary conditions as well as initial conditions are applied and the integral equations are solved by means of numerical methods.

All the tasks in the presented thesis are solved by the aid of the finite element method. Commercially available software Comsol Multiphysics 3.3 was purchased for this purpose. This software enables one to solve sets of partial differential equations by means of the FEM. The software offers many kinds of physical tasks to be solved. Several application modes allow the tasks to be solved readily. The following application modes are available:

- Acoustics
- Convection and Diffusion
- Electromagnetics
- Fluid Dynamics
- Heat Transfer
- Structural Mechanics
- Electro-Thermal Interactions
- Fluid-Thermal Interactions

Governing equations may also be defined by the user if desired.

The *Fluid Dynamics application mode* employs the Navier-Stokes equations. This mode is used in the presented thesis to handle the liquid bulk flow (driven either by electroosmosis or by pressure).
The *Heat Transfer application mode* employs the energy conservation law. This mode is also applied in the presented thesis when temperature changes are wished to be inspected.
All other governing equations (electric field distribution, chemical equilibrium equations, electroneutrality equation, ionic strength correction equations and continuity equations for the system constituents) are defined by the author as no appropriate application modes were found in the software.

Four particular tasks are chosen to be solved by the presented computational model.

(I) The first task investigates the electromigration in the Agilent 3DCE electrophoresis equipment. The simulations are performed in order to study changes in the electrolyte composition due to the electrolysis. Forty simulations are carried out under various conditions. Moreover, the bulk flow driven by electroosmosis is inspected.

(II) This task deals with the lab-on-a-chip analysis in a gel. The electrokinetically driven sample injection is investigated. Four model anionic species are regarded as the analytes. Their resolution is investigated under various conditions (sixty-six simulations are carried out).

(III) Separation in the free-flow electrophoresis equipment is simulated in this task. Three model cationic species are regarded as the analytes. Pressure-driven bulk flow as well as electric field is applied and varied. The resolution of analytes is investigated.

(IV) This task focuses on the temperature effects in a capillary. The temperature rises as the electric current passes through the electrolyte. This phenomenon is known as Joule heating. Two particular geometry arrangements are inspected. Both air and water cooling is investigated.

2 Review of Present State of Knowledge

The review is divided into two parts. The first one deals with computer simulations of electrophoretic experiments in capillaries. The capillaries are usually considered as sufficiently narrow compared to their length and, thus, one-dimensional approaches may be used to describe the phenomena encountered in classical capillary electrophoresis (CE). The second part of the review handles two- and three-dimensional simulations. This approach is necessary when trying to describe complex geometries such as various injection sites, sample dispensers and mixing chambers.

2.1 Simulation Approaches in 1-D Geometries

Generally, serious problems are encountered when searching analytical solutions to solved tasks. Majority of problems cannot be solved in a closed analytical form. This brings the opportunity to employ numerical approaches. Several papers (Refs.[1], [2], [3], [4], [5], [6], [7], [8], [9] and [10]) have been published on numerical simulations. These works, however, lack the possibility of making general conclusions as models do not offer any analytical formulae for calculation of desired quantities. There is an original approach (to be found in Refs. [11] and [12]) that offers simulated electropherograms as a result of numerical simulations. However, as this model does not take a lot of important features into account, it was subsequently replaced by more sophisticated models.

A typical CE experiment is arranged by a capillary filled with uniform solution conventionally called the background electrolyte (BGE). Beside the BGE, the separation environment usually contains some analytes to be separated under the influence of electric field. The system is governed by the laws formulated for the mass transport (diffusion, convection and migration terms). As the analytes are usually thought to be charged species, strong Coulombic forces have to be taken into account. The behavior of charged species has to be governed by the macroscopic electroneutrality condition. Another condition to be satisfied is the electric field distribution, commonly expressed in terms of Kirchhoff's and Ohm's law. When chemical reactions take part in the system (e.g. dissociation of weak electrolytes), they have to be described by terms of the chemical equilibrium. Chemical reactions are commonly regarded as much „faster" than all other phenomena encountered in CE and, thus, the concept of equilibrium constants may be used. Majority of general laws governing the systems behavior are known from physical chemistry (see Ref. [13]) or can be found in specialized literature (Ref. [3]). Some of the laws describing the system behavior are nonlinear (e.g. concentration terms in denominator of the acid-base equilibrium formula). This feature causes difficulties when investigating the system behavior. Nevertheless, there are experimental setups that lead to a simplification of the equations. Under some circumstances, BGE may be regarded as a liquid of uniform composition along the capillary.

Unlike the BGE components, sample is injected only at a certain position in the capillary. It is commonly called the injection site. A small concentration of an analyte (when compared to BGE constituents' concentration) causes only a small disturbance in system properties (e.g. the conductivity or pH value). Under such conditions, continuity equations may be linearized and solved easily without computational problems or inaccuracies (in the framework of linearized model).

Gaš et al. (Ref. [14]) proposed a simulation model that optimizes the BGE composition in capillary zone electrophoresis (CZE). This work focuses on the interface between the sample region (contains BGE and sample) and the BGE region (contains only the BGE). The name „moving boundaries" is commonly used for this model as the sample region moves along the capillary under the influence of electric field. Four weak trivalent constituents (two acids and two bases) are allowed to form the BGE. One anionic constituent of sufficiently small concentration represents the sample. Thus, the model is proposed to simulate the separation of anionic analytes. As there is, in principle, no difference in treating anionic and cationic species, the model may be modified in order to describe the behavior of cationic analytes. The calculation begins with formulating the electroneutrality condition and the acid-base equilibrium equations. As there are five trivalent system components, fifteen equilibrium equations are to be solved. The model considers any H^+ and OH^- concentrations that obey the ionic product of water. There are four supplementary equations to be fulfilled: they are called the moving boundary conditions and represent the mass conservation law for each BGE constituent at the BGE-sample interface. Thus, twenty-one equations are to be solved simultaneously. This approach does not include the Kohlrausch regulation function. It is originally defined by Kohlrausch in Ref. [15] and governs the system behavior in isotachophoresis (ITP). Besides its widespread utility in ITP, Kohlrausch function was employed by Gebauer et al. (see Refs. [16], [17] and [18]) to calculate the sample zone composition in CZE. The applicability of this approach (proposed in Ref. [14]) is demonstrated by investigating phosphate buffer properties. Three anionic analytes (Cl^-, Br^- and salicylate) are employed to inspect how the analyte behavior can be affected by the BGE composition. Simulated results agree with experimentally obtained electropherograms.

Jaroš at al. (Ref. [19]) continued in the work initiated by Gaš at al. (Ref. [14]). A mathematical model based on the theory of moving boundaries was adapted and a user-friendly simulation program PeakMaster was introduced. PeakMaster program allows the BGE properties to be calculated and optimized. The designed BGE can be readily prepared and used in real analysis. The program, besides its other invaluable benefits, takes the ionic strength correction into account (dissociation constants as well as ionic mobilities depend on the ionic strength). The well-known theory of Debye, Hückel and Onsager (Refs. [20] and [21]) is supposed to predict the properties of simple binary electrolytes of ionic strength up to 10 mM (Ref. [13]). As a real BGE is usually more complicated ionic mixture, a sophisticated theory has to be employed. The theory of Onsager and Fuoss (Ref. [22]) is supposed to govern the properties of solution composed of any ionic mixture. According to Ref. [14], the dissociation constants and the moving boundary equations for all BGE constituents are formulated along with the electroneutrality condition and the ionic product of water. As the ionic strength is not known

initially, the calculus is performed by an iterative method. The first approximation puts all activity coefficients to be one. Governing equations are solved and, subsequently, new activity coefficients are determined *via* the formula of Debye and Hückel. The iterative procedure stops when the relative difference of subsequent values of activity coefficients is less than a sufficiently small number. Afterwards, actual mobilities are calculated employing Onsager-Fuoss model. Finally, the actual conductivity is calculated from corrected concentrations and ionic mobilities. Output data also contains the concentrations of all ionic forms of the system constituents in the sample region as well as in the BGE region. A use of PeakMaster is shown employing two examples. The first one considers separation of five anionic species - chloride, succinate, lactate, phenylacetate and caproate. Simulated and experimentally obtained electropherograms are nearly undistinguishable. The second example investigates the separation of complicated ionic assembly. PeakMaster program generally predicts the position of analyte peaks as well as system peaks (see next parts of the review for a deeper insight). The simulation results in the electropherogram that greatly resembles its experimentally obtained counterpart. As there is already a new version of PeakMaster program available, all its other features are discussed in subsequent parts of the review.

Poppe et al. (Refs. [23], [24], [25], [26] and [27]) introduced a linearized model of electrophoresis. The authors showed that linearized continuity equations lead to a matrix eigenvalue problem. Generally, the result of solving N x N square matrix comprises N matrix eigenvectors and N matrix eigenvalues. The ordered set of matrix eigenvalues is called the matrix spectrum. Since the water autoionization takes place, H^+ and OH^- ions originate. These ions are also regarded as the BGE components. Nevertheless, in the analysis performed under neutral pH (the region 5 – 9 is usually accepted and is called the safe pH region), these ions are of negligible concentrations. This simplifies the governing equations. Generally, N system constituents lead to N x N matrix problem (when omitting H^+ and OH^-) and, thus, N matrix eigenvalues are obtained. These conclusions have an invaluable impact on the indirect detection where BGE properties (the conductivity and the indirect UV response) are evaluated.

In chromatography, Crommen and co-authors (see Ref. [28]) figured out a remarkable phenomenon: when there is an analyte moving (by pure coincidence) as quickly as one of the system eigenzones, response of indirect detection reaches infinity values (in terms of absolute values). Poppe (Ref. [23]) continued in this way in electrophoresis and confirmed such a phenomenon here. He also showed (in Ref. [24]) that this phenomenon is connected with infinitely large matrix eigenvector components.

Despite all useful conclusions stated above, it should be borne in mind that the linearized model does not fully account for all phenomena encountered in CE. One such a phenomenon is well-known as the electromigration dispersion (EMD). Undesirable peak distortion and broadening is often explained in terms of EMD as a result of nonlinearity of electrophoresis. Gebauer et al. (Refs. [16] and [29]) and Horká and Šlais (Ref. [30]) defined a quantity called the relative velocity slope in order to evaluate the extent of EMD. This quantity is useful when predicting the analyte peak shape under particular conditions (e.g. when applicability of BGE is inspected for particular analysis).

Štědrý et al. (Ref. [31]) went ahead in direction of Poppe (in Refs. [23] and [24]). Employing linearized model of electromigration, they carried out a mathematical analysis of a basic representative arrangement of CE experiments. The authors focus on simulation of indirect-detection results. They take only strong electrolytes into account (the buffer constituents as well as the analytes) to prevent cumbersome equations that govern the behavior of weak electrolytes. They consider only one ion as the analyte. The BGE is composed of three ions, two of them being co-ions (related to the analyte one) and one is a counter-ion. All system constituents are thought to be univalent. As this work does not take the ionic strength correction into account, all properties of the ions are supposed to be constant. Thus, the conductivity can be calculated readily without iterative method (see Ref. [13]). All ions are expected to move exclusively under the influence of electric potential gradient (electromigration). Motion under the chemical potential gradient (diffusion) and caused by pressure drop or electroosmotic flow (convection) are ignored. Moreover, no thermal or sorption effects are assumed to play any role and radial distribution of all constituents is assumed to be time-independent. Under such circumstances, 1-D approach may be employed.
All components are supposed to show only small concentration changes in time. Thus, the transformation of variables can be done. Instead of solving problem with commonly defined concentrations, new perturbation variables are defined and implemented. The continuity equations are formulated at zero time for each system constituent. The system matrix is assembled and its eigenvalues are calculated. As there are four system constituents, four eigenvalues (called „eigenmobilities“ by the authors) are expected. The result of calculus is that two eigenmobilities are zero (they correspond to a water peak often encountered in real CE experiments), one eigenmobility is equal to that of the analyte (analyte peak, analyte zone) and one depends on the concentrations and mobilities of all buffer constituents. The last one is of the main interest as it is not affected by the properties of the analyte and is, thus, called the system eigenmobility. The authors define the term „eigenzone“ as a wave traveling along the capillary with a velocity proportional (through the electric field strength) to the eigenmobility. The waves tend to split and carry the disturbance (initially created by the sample injection) with given velocities. Input data (ionic mobilities as well as concentrations) is variable in order to investigate how the system peak mobilities are affected by the BGE composition. They find a situation where the system eigenmobility is equal to that of the analyte. This leads to the so-called resonance effect (notice the analogy with mechanical or electrical resonances). The analyte zone and the system zone comigrate and reach the detector site at the same time. Concentration profiles of BGE co-ions show the shape of the spatial derivative (a zigzag shape) of the original peak (it is supposed to be of the Gaussian shape). The indirect detection makes this effect visible. The amplitude of the resonance phenomenon grows in time proportionally and the signal can, at least in the framework of the linearized model, reach infinite values (in accordance with Ref. [23]). Furthermore, the authors derived a formula for calculating the relative velocity slope (Refs. [16], [29] and [30]). Thus, EMD can be predicted by the linearized model of electromigration.
Štědrý at al. (Ref. [32]) generalized the model introduced in Ref. [31]. The authors consider the linearized model of electrophoresis again. Unlike Ref. [31], weak electrolytes are allowed to

form the BGE and they may also be regarded as the analytes. Another restriction vanished – ions H^+ and OH^- are taken into consideration and, thus, the whole pH range may be inspected. Nevertheless, only univalent ions are regarded as system constituents (i.e. weak or strong univalent acids or bases).

Similarly as in Ref. [31], three constituents form the BGE and one ion represents the analyte. As the ions are not constrained to be strong anymore, the acid-base equilibrium equations have to be formulated for all constituents. The H^+ and OH^- ions contribute to the BGE conductivity. The model also allows H^+ and OH^- terms to be cancelled if reasonable (e.g. the H^+ term may vanish in alkalic pH range). Following Ref. [31], the continuity equation is formulated for each constituent. A new function (called the *G*-function) is defined and is implemented when solving the electroneutrality condition. As the analyte concentration is supposed to be negligibly small compared to that of BGE constituents, *G*-function does not take analytes into consideration. Concentrations of all charged forms of BGE constituents are expressed as a function of H^+ concentration. This forms the *G*-function with the H^+ concentration as the only unknown variable. Consequently, H^+ concentration is calculated and all other quantities are determined from it.

As it was done in Ref. [31], perturbation quantities are defined and the matrix eigenvalue problem is solved. The BGE conductivity is constrained to be spatially uniform as the sample injection causes only a small disturbance in it. Two quantities expressing the indirect detector response are calculated. The first one, the conductivity detection response, is defined in Ref. [33] and a simple formula for its calculation is suggested. The second one, the transfer ratio (Ref. [34]) is useful for indirect UV detection and the present work also allows it to be evaluated. The relative velocity slope can also be assessed (taking an electrolyte composed of weak ions into account). As there are four system constituents, initial disturbance splits into four waves. The significance of H^+ and OH^- terms in governing equations is investigated. Again, these terms may be cancelled from equations only when separation takes place in neutral pH region (concentrations of BGE components have to be larger than 1 mM). These conditions lead to a simplification in governing equations and guarantee two eigenmobilities to be close to zero. In other words, it means that there are two non-migrating system zones at the injection site („double water peak"). However, additional eigenzones of non-zero eigenmobilities are encountered beyond the safe pH region. In such cases, migrating waves arise as a consequence of significant concentrations of H^+ or OH^- ions. Mobilities of these zones have to be investigated as they can possibly lead to the resonance effects that are usually undesirable. Several other authors (Refs. [28], [35], [36], [37] and [38]) also investigated the behavior of eigenpeaks. Eigenpeaks emerging from significant concentrations of H^+ and OH^- were studied in Refs. [18] and [39]. Other authors (Refs. [40], [41], [42], [43], [44] and [45]) investigated system peaks in BGEs of complicated composition (various attainable ionic forms were taken into account).

Štědrý and co-authors (Ref. [46]) investigated a general case of *N* system constituents. This work is, in fact, a generalization of previous works (Refs. [31] and [32]). Any substance (regardless of its attainable valency) may be considered - weak (or strong) acids (or bases) or even ampholytes. This generalization makes the governing equations more complicated. The

model allows the behavior of any BGE to be simulated. Moreover, the model actually does not distinguish between the buffer components and the analytes and, thus, all system constituents are treated in the same way. As there are generally *N* constituents, the model becomes rather complicated (when compared to its earlier versions). On the other hand, a lack of transparency is prevailed by its great versatility. Again, the linearized shape of the continuity equation is assumed to govern all phenomena (Refs. [31] and [32]). It is formulated for each analyte bearing all its attainable forms in mind. The matrices are assembled, system eigenmobilities are calculated and time evolution of system is predicted (the model still omits diffusion). The BGE is thought to be composed of *N - 1* constituents and there is, thus, only one analyte in the sample region. Nevertheless, the model can, in principle, handle any number of analytes. Three simple buffers (acetic, phosphate and oxalic one, taking sodium as the counter-ion) show the usefulness of the model. Theoretical pH value and system eigenmobilities are calculated for each BGE (pH is a variable quantity as sodium concentration is allowed to change). Calculated pH plots resemble well-known „titration curves“. The eigenmobility dependencies show a remarkable behavior. The main feature to be highlighted is that curves of two different eigenmobilities never cross each other. There are conditions where at least one very fast eigenmobility is found. This brings the chance to observe the resonance phenomena with an analyte of the same effective mobility. Moreover, the present model offers more general conclusions to be done. In majority of BGEs, there is often one systemzone of very small eigenmobility (in terms of absolute values). It means that there is a zone standing at the injection site regardless of the presence of electric field applied. Thus, this zone may serve as the electroosmotic flow (EOF) velocity marker. This piece of knowledge has an invaluable impact on the real experiments as the EOF velocity can be comfortably assessed from the indirect detector record. However, when there is no eigenzone of zero eigenmobility, a neutral constituent has to be employed as the EOF marker.

Jaroš at al. (Ref. [47]) implemented the computer model introduced in Refs. [31], [32] and [46]. A new version of the simulation program PeakMaster is the result of this effort. Its old version is, unlike the improved descendant, based on the theory of moving boundaries (to be found in Refs. [14] and [19]). The computational model needs certain input data to be inserted. It comprises BGE composition, names of the analytes to be separated and desired simulation arrangement (capillary length, driving voltage, electroosmosis). PeakMaster program contains the database of compounds to be used readily as buffer constituents as well as the analytes. Majority of data is taken from the well-known Hirokawa's database (Refs. [48], [49], [50], [51] and [52]). Some data is provided by Včeláková et al. (Ref. [53]). The database is allowed to be modified if necessary.

Actual mobility and equilibrium constants of each system constituent are affected by the presence of all other system constituents through the ionic strength dependence. Computational models presented in Refs. [31], [32] and [46] omitted this feature and all calculations were performed using mobilities and equilirium constants extrapolated to zero ionic strength. The PeakMaster program takes the ionic strength correction into account. Onsager and Fuoss model (Ref. [22]) is implemented here. Nevertheless, the ionic strength correction can be left out if desired (this saves the computational time). The user interface enables one to choose the way of detection (direct, indirect or conductivity tracing). The main result of calculation is a

simulated electropherogram that can be compared with results of a real experiment. The peak shape (diffusion/EMD mimicking) is simulated by aid of Haarhoff – van der Linde‘s (HVL) function (Ref. [54]). Besides migration and diffusion, EOF (i.e. convection term) may also be taken into account if desired. An ideally flat EOF profile is assumed to avoid shearing effects.
The pH of the BGE is generally accepted to influence the behavior of electrophoretic system as some of constituents are weak acids (or bases) and their degree of dissociation (or protonation) is affected by the pH value. The H^+ activity is the first variable that is calculated at the beginning of the simulation. Once it is determined, all properties of the system constituents (effective mobilities, migration times) can be easily calculated. PeakMaster program also provides calculation of detection signal – the transfer ratio (UV indirect detection) and the molar conductivity detection response (indirect conductivity). The relative velocity slope is also assessed. The general properties of BGE (buffering capacity, ionic strength, conductivity) are also evaluated. The program is very useful when searching BGE to be used in a particular real separation as it can predict effective mobilities, and thus, the resolution among the analytes. It also calculates possible peak distortions and broadenings caused by EMD and resonance effects. A use of PeakMaster is demonstrated (Ref. [47]) by inspection of imidazole-oxalic buffer. Peakmaster predicts two eigenzones to arise and calculates their mobilities and, thus, also migration times in a real experiment. As a matter of fact, there are two system eigenpeaks in an experimentally obtained indirect UV and conductivity trace (EOF marker is used in a real experiment to determine the EOF velocity). Mobility values of both system peaks are determined. Although there is a small discrepancy between simulated and experimentally obtained system eigenmobilities (possibly caused by inaccurate data in the database), the program predicts system behavior without tedious trial-and-error experimental approaches.
Hruška at al. (Ref. [55]) introduced a mathematical model enabling time evolution of the electromigration system to be directly simulated and depicted. The model gave rise to a simulation program called Simul. It may be (along with PeakMaster program) downloaded as a freeware from the website (Ref. [56]). Its detailed mathematical background can be found in Refs. [4] and [5]. The model can handle any number of analytes or buffer constituents regardless of their attainable valency. Similarly to PeakMaster, also Simul is based on 1-D approaches.
All three kinds of particle movement i.e. migration, diffusion and (EOF driven) convection are taken into consideration when formulating the continuity equation for each system constituent. The electroosmotic flow is supposed to be uniform and no pressure effects are assumed to play any role. The electric field distribution is calculated taking the driving voltage as well as the diffusion currents into account. Conductivity accounts for H^+ and OH^- ions. Simul solves the continuity equation (partial differential equation - PDE) numerically by dividing the entire computational domain (capillary) into certain finite segments. Thus, finite difference method is employed (FDM, see Ref. [57] for a deeper insight). This method converts the set of original PDEs (time and spatial coordinate are independent variables) into a set of ordinary differential equations (ODEs, time is the only independent variable). ODEs are solved by means of the Runge-Kutta and predictor-corrector method (Ref. [58]). The electric field distribution is an ODE (in 1-D) and it is solved by the aid of Newton iterative method.

Time steps used in numerical simulation are either defined by the user or optimized by the program. A sufficient number of segments must be employed in order to avoid numerical problems.

The Simul program also offers saving the computational time by solving a part of the capillary rather than taking whole its range into account. A typical use of this approach is the capillary uniformly filled with the BGE everywhere and with the sample in a certain region, additionally. Computational domain expands as the sample region moves and broadens. Applicability of Simul is illustrated using three examples from the everyday practice. The first one considers separation of phenylacetic and caproic acid in TTAOH/oxalic acid/potassium buffer (TTAOH denotes tetradecyltrimethylamonium hydroxide). An experimentally obtained electropherogram shows a strange behavior (an unexpected zigzag-shaped peak). The Simul program is employed to inspect this problem. As there is an analogous peak in the simulated electropherogram, the peak is supposed to be a natural property of the BGE. The second example investigates the behavior of acetate ion zone in the sodium/phosphate buffer. Here, the electropherogram shows a zigzag-shaped peak. Identity of this peak can be easily clarified as Simul program can predict resonance phenomena. The last example shows the simulation of ITP separation with twenty-one ampholytes. An immobilized pH gradient is formed to mimic the conditions encountered in ITP. The analytes form their „ITP zones“ along the pH gradient. Simulated electropherogram resembles that one obtained from real ITP experiments.

Other authors (Refs. [9] and [59]) also introduced ITP simulations. Phenomena connected with splitting peaks (Ref. [60]), adsorpion effects (Refs. [61] and [62]), axial thermal effects (Ref. [63]) and peak distortion (Ref. [64]) were simulated as well.

Hruška et al. (Ref. [65]) inspected conditions where the electromigration matrix has complex eigenvalues. According to the theory of dynamic systems, such system should exhibit periodic solution (oscillation) in the resulting concentration profile.

Chemical oscillations are periodical changes in concentration of constituents driven by the chemical potential gradient. Electromigration systems can oscillate even when there is no gradient in chemical potential and the system is in the chemical equilibrium state. Here, the electric potential gradient is a force that creates the oscillations.

Favorable conditions for oscillations were searched and investigated in Ref. [65]. Simul program was used to predict the oscillatory behavior. The authors found a buffer (composed of imidazole and sebabic acid) that allows the oscillations to come into existence. Theoretically predicted periodical solution was later confirmed by the experiment. Experimentally obtained electropherograms confirmed oscillating pattern (in both CCD and DAD detection record). A buffer of slightly modified composition served as a sample (initial disturbance).

2.2 Simulation Approaches in 2-D and 3-D Geometries

Microfluidic devices in electrophoresis attract many researchers as they offer invaluable benefits over conventionally used appliances. Reduced time of analysis and lesser sample and buffer consumption are the main advantages. At the beginning, they were used for gel electrophoresis of small ions (Refs. [66], [67], [68], [69], [70], [71], [72] and [73]) as well as for the capillary gel electrophoresis of complicated assemblies (Refs. [74], [75], [76] and [77]). These pioneering works resulted into the lab-on-a-chip concept. Unlike classical capillary devices where pressure drop serves as a force that injects samples into the separation system, microdevices lack this option due to their complicated structure. Thus, electrokinetically driven injection is the only way that can be employed.

Ermakov et al. (Ref. [78]) introduced a 2-D mathematical model describing electrokinetically driven mass transport in two chip structures - injection cross and T-mixer. As the channel depth and wall properties are supposed to be uniform, 2-D model is supposed to describe all phenomena in good approximation. The model allows weak (or strong) acids (or bases) to participate in the mass transport. The diffusion Péclet number is employed to describe the competition between convection and diffusion transport. Electroneutrality condition is formulated and assumed to be obeyed everywhere. The model accounts for EOF and its velocity is supposed to be ideally flat and uniform as the channel diameter is much larger than the Debye radius. The thermal effects are not considered (see Ref. [79]).

Some of 2-D governing equations (e.g. the conductivity expression or the electroneutrality condition) are the same as in the 1-D models. However, there are equations (such as electric field distribution or mass conservation law) that differ from that ones stated in the 1-D models. The Navier-Stokes equations have no counterpart in 1-D models at all. All governing equations are solved employing the finite difference method. The simulation domain is covered by a rectangular grid. Simulated figures of the steady state flow in the injection cross are presented as the main result of the work. The injection cross is made of two perpendicularly crossing channels (the injection one and the separation one). One injection channel entry serves as a sample reservoir. Two injection parameters are regarded as being substantial. The first one is the amount of analyte in the sample plug. The second one is the standard deviation in the concentration over the sample plug. This parametes indicates the sample spatial dispersion. The ratio of the parameters, which should be as high as possible, is investigated. Input data (potentials imposed on particular channel entries) is variable and optimal conditions are found for the analysis. Cationic, anionic and neutral species are treated separately. Simulated results are compared with the experiments performed in Ref. [80].

The second part of Ref. [78] deals with the T-mixer that is made of three arms forming the shape of the letter „T“. The horizontal arms serve as buffer and sample reservoirs. The vertical one is employed to divert a mixed liquid away. The aim of this part of the work is to find conditions where diverted mixture is of the most uniform spatial profile. As an identical potential is imposed on the buffer and sample arm, the same bulk flow velocities are expected. Thus, the same volumes of buffer and sample are supposed to enter the outflow channel. The channel width is variable in order to optimize the mixing efficiency.

Ermakov et al. (Ref. [81]) continued in the way started in Ref. [78]. The behavior of pinched and gated injection is investigated in the injection cross. Pinched injection (partly described in Ref. [78]) is used when a compact well-defined sample plug is desired for the analysis. Variable sample volumes can be achieved by employing the gate injection. Both injection variants are accomplished in two steps. The first step (called the loading one) the sample moves from its reservoir and reaches the injection cross. In the second (dispensing) step, the loaded sample is forced to change its direction. The sample enters the separation channel where the analytes are separated. Similarly to Ref. [78], conditions are optimized in order to get the best sample properties (the highest possible analyte amount yet showing the lowest possible spatial dispersion). Simulated results are compared with experimental ones taken from Ref. [82].

Chatterjee (Ref. [83]) introduced a universal 3-D computational model. A general concept of transport phenomena in continuum is formulated. All conservation laws (i.e. stated for momentum, energy, mass and electric charge) can be handled. Generally, the continuity equation may be formulated for any quantity to be conserved. As the system is open (the fluxes may reach beyond the system), the inflow/outflow term has to be considered on the system boundaries. The equilibrium constants (expressed in terms of dissociation degrees) are employed to describe the chemical behavior of the system constituents. Each system constituent is taken as a simple species regardless of its attainable ionic forms.

The computational model is based on a rather complicated multi-block finite-volume scheme (finite volume method, FVM). The finite-volume method divides the computational domain into non-overlapping finite volume subdomains. A power-law scheme is employed to express the fluxes in each finite volume. Multi-block finite-volume technique is favorable for complex geometries as the domain decomposition reduces the order of matrices to be assembled and solved. Generally, the more simple matrices are created, the faster is to solve them.

Applicability of the present approach is illustrated by two examples. The first one considers a 3-D mixing chamber that markedly resembles a water tap as there are two inflow channels containing hot and cold water to be mixed together. 3-D flow and heat transfer phenomena are taken into account. The model investigates thermal profiles of water stream coming out from the outflow channel. The second example compares isoelectric focusing of a model analyte mixture with and without the bulk flow. Simulation of the EOF free system results to the profiles that resemble well-known figures obtained by other simulation approaches. Nevertheless, remarkable system behavior is observed when taking the convection into account. The pH gradient moves along the EOF and the pH change affects the ζ-potential. As the ζ-potential affects the EOF velocity retrospectively, convection profile cannot be regarded as flat anymore and it resembles a pressure-driven profile. These conditions lead to distorted peaks and, thus, to deterioration of robustness and separation efficiency.

3 Aims of Presented Thesis

The main result of the presented thesis is the proposal of a mathematical model and its implementation in the environment of Comsol Multiphysics 3.3 software. In particular, the presented model focuses on these problems:

- Mass conservation law (diffusion, migration and convection)
- Electric charge conservation law (driving voltage, diffusion currents)
- Momentum conservation law (Navier-Stokes equations, electroosmosis and pressure-driven bulk flow)
- Energy conservation law (thermal conduction and thermal diffusion)
- Ionic strength correction (corrected *pK* constants, corrected ionic mobility, corrected conductivity)
- Driving electricity modes (constant voltage mode, constant current mode)

The above model is employed to solve four particular tasks (in two or three dimensions):

- Inspection of changes in the electrolyte composition due to the electrolysis (electroosmosis is also taken into consideration)
- Simulation of the electrokinetic injection in the Lab-on-a-chip analysis
- Investigation of the separation in free-flow analyzer
- Thermal effects in a capillary (Joule heating and capillary cooling by the aid of water and air)

4 Results and Discussion

4.1 Mathematical Model of Electromigration

4.1.1 General Conservation Law

The system property behavior is often expressed in terms of the continuity equation. It is a differential equation that governs its conservation. Continuity equations can be written for any property that is wished to be conserved (e.g. mass, energy, electric charge or linear momentum) in a continuum.

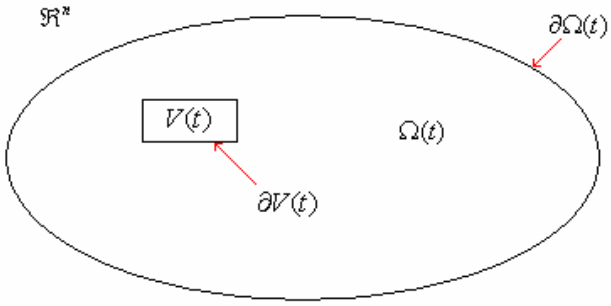

Fig. 1 Computational domain

Let us consider a subspace $\Omega(t) \subset \Re^n$ ($n \in \aleph$) that is conventionally called the computational domain and may generally change in time (Fig. 1). Time may attain any value from interval (0,*T*), *T*>0 being the end of the time domain. The domain boundary $\partial\Omega(t)$ connects $\Omega(t)$ with the rest of the space $\Re^n$.

Furthermore, let us consider a space subset $V(t) \subset \Omega(t)$ with its boundary $S(t) = \partial V(t)$. The subspace *V(t)* is usually called the test volume (its boundary *S(t)* is the test surface).

Let us define the total rate of change *R(t)* in *V(t)*

$$R(t) = \frac{d}{dt} M(t) \tag{1}$$

Here *M(t)* denotes the integral of a quantity *A* (that is going to be governed by upcoming continuity equation) over *V(t)*

$$M(t) = \int_{V(t)} A(x, y, z, t) dV(t) \tag{2}$$

The quantity *A* is generally space- and time-dependent but *M* is supposed to be space-independent as it is formed by integrating *A* over entire test volume.

There are two ways that can cause a change of *A* in *V(t)*. The first one considers changes induced by sources or sinks in the test volume

$$P(t) = \int_{V(t)} Q(x, y, z, t) dV(t) \tag{3}$$

Here *Q* denotes the source/sink term and *P(t)* is its integral over *V(t)*.

The second contribution originates from the flux (denoted $\vec{J}$) of *A* that passes through the test surface

$$F(t) = -\int_{S(t)} \vec{J}(x, y, z, t).\vec{n}(x, y, z, t) dS(t) \tag{4}$$

The dot "." was employed to denote the inner product. The sign "-" is in accordance with the agreement in which $\vec{n}$ is taken as the outer normal vector to *S(t)*.
The resulting equation

$$R(t) = P(t) + F(t) \tag{5}$$

may be expanded to

$$\frac{d}{dt}\int_{V(t)} A(x,y,z,t)dV(t) = \int_{V(t)} Q(x,y,z,t)dV(t) - \int_{S(t)} \vec{J}(x,y,z,t).\vec{n}(x,y,z,t)dS(t) \tag{6}$$

The divergence theorem may be applied to the right-hand side of the above equation

$$\frac{d}{dt}\int_{V(t)} A(x,y,z,t)dV(t) = \int_{V(t)} Q(x,y,z,t)dV(t) - \int_{V(t)} \nabla.\vec{J}(x,y,z,t)dV(t) \tag{7}$$

Here ∇ denotes the *Nabla* operator. The Reynolds transport theorem may be employed to modify the left-hand side of the above equation

$$\int_{V(t)} \frac{\partial A(x,y,z,t)}{\partial t} + \vec{v}_{V(t)}.\nabla A(x,y,z,t)dV(t) = \int_{V(t)} Q(x,y,z,t) - \nabla.\vec{J}(x,y,z,t)dV(t) \tag{8}$$

Here $\vec{v}_{V(t)}$ denotes the velocity of *V(t)* in $\Re^n$. The above integral identity can be rearranged to

$$\int_{V(t)} \left[\frac{\partial A}{\partial t} + \vec{v}_{V(t)}.\nabla A + \nabla.\vec{J} - Q \right] dV(t) = 0 \tag{9}$$

and is satisfied only when

$$\frac{\partial A}{\partial t} + \vec{v}_{V(t)}.\nabla A + \nabla.\vec{J} = Q \qquad \text{for} \qquad \forall t \in (0,T),\ \forall V(t) \subset \Omega(t) \tag{10}$$

This formula is well known as a general shape of the continuity equation. When Ω is supposed to be time-independent, the above equation reduces to

$$\frac{\partial A}{\partial t} + \nabla.\vec{J} = Q \tag{11}$$

This equation is the one that is used in the simulations, as no time-dependent computational domains are considered in the presented thesis. As we will see in next paragraphs, *A* may stand for several quantities, behavior of which will be investigated.

4.1.2 Mass Conservation Law

Let us consider a system with its boundary that consists of *N* species that we call the system constituents. Furthermore, a solvent (usually water) is present and is always regarded as a continuum (its molecular structure is fully neglected). The continuity equation may be employed to describe such a situation. Here, the analytical concentration of *i*-th system constituent c_i is taken as the variable governed by the general conservation law

$$\frac{\partial c_i}{\partial t} + \nabla.\vec{J}_i = 0 \tag{12}$$

The concentration represents the system quality (the amount of substance) related to the unit volume. The *Q* term is canceled as no sources or sinks of mass are allowed, such as chemical reactions among different system constituents. On the other hand, the acid-base equilibria of

individual constituents are considered. These cannot, however, alter the total, analytical concentration c_i of any species.

The substance flux is denoted $\vec{J}_i$. The three kinds of fluxes are considered in the model - diffusion, migration and convection:

$$\frac{\partial c_i}{\partial t} + \nabla.(\vec{J}_{i,dif} + \vec{J}_{i,mig} + \vec{J}_{i,con}) = 0 \tag{13}$$

The diffusion flux can be described in terms of the first Fick's law

$$\vec{J}_{i,dif} = -\sum_j D_{ij} \nabla c_{ij} \tag{14}$$

c_{ij} and D_{ij} are the concentration and diffusivity of *j*-th ionic form of *i*-th system constituent, respectively. The integer *j* may attain both positive and negative values, as the system constituents are allowed to be both positively and negatively charged (*j* = 0 holds for a neutral form). The diffusion motion of various ionic forms is treated separately as the ionic diffusivities may differ from each other. The diffusivity is related to the mobility through the Nernst-Einstein equation

$$D_{ij} = u_{ij} \frac{RT}{|z_{ij}|F} \tag{15}$$

Here u_{ij} and z_{ij} are the ionic mobility and charge number, respectively. *T* denotes the absolute temperature. The constants *F* and *R* are the Faraday constant and the universal gas constant, respectively.

The electromigration flux occurs in the presence of the electric field ($\vec{E}$ being the field strength) and can be expressed as follows

$$\vec{J}_{i,mig} = \sum_j \mathrm{sgn}(j) c_{ij} u_{ij} \vec{E} \tag{16}$$

The molar fraction defined as $h_{ij} = c_{ij}/c_i$ may be employed to modify the above equation

$$\vec{J}_{i,mig} = c_i \vec{E} \sum_j \mathrm{sgn}(j) h_{ij} u_{ij} = c_i \vec{v}_i \tag{17}$$

The sum in the middle part of the equation is the effective mobility and is useful when predicting the motion direction of system constituents. This quantity multiplied by the field strength is called the effective constituent velocity $\vec{v}_i$.

The convectional term is simply given by

$$\vec{J}_{i,con} = c_i \vec{v} \tag{18}$$

The system constituents are driven by the bulk flow of velocity $\vec{v}$ irrespective of their physical and chemical properties.

When merging all terms, the continuity equation obtains the form

$$\frac{\partial c_i}{\partial t} + \nabla.(-\sum_j D_{ij} \nabla c_{ij} + c_i \vec{v}_i + c_i \vec{v}) = 0 \tag{19}$$

This equation holds for all system constituents. The c_{ij} terms can be converted into the terms that contain c_i only. This can be easily done by using h_{ij} notation

$$\sum_j D_{ij}\nabla c_{ij} = \sum_j D_{ij}\nabla(c_i h_{ij}) = \sum_j D_{ij} c_i \nabla h_{ij} + \sum_j D_{ij} h_{ij}\nabla c_i = c_i \sum_j D_{ij}\nabla h_{ij} + \nabla c_i \sum_j D_{ij} h_{ij} \qquad (20)$$

As $\nabla D_{ij} = \vec{0}$, the above formula may be rearranged to

$$\sum_j D_{ij}\nabla c_{ij} = c_i \nabla \sum_j D_{ij} h_{ij} + \nabla c_i \sum_j D_{ij} h_{ij} = c_i \nabla \overline{D_i} + \overline{D_i}\nabla c_i \qquad (21)$$

Here $\overline{D_i}$ stands for the sum $\sum_j D_{ij} h_{ij}$ and is called the effective constituent diffusivity. As we will see in the next chapter, the h_{ij} fractions are affected by the local pH value. The final shape of the continuity equation is

$$\frac{\partial c_i}{\partial t} + \nabla.(-\overline{D_i}\nabla c_i - c_i \nabla \overline{D_i} + c_i \vec{v}_i + c_i \vec{v}) = 0 \qquad (22)$$

The continuity equation is an evolutionary equation as the left-most term is the time derivative of the governed quantity. One can object that there are also other terms that contain time-dependent terms (the velocity terms in *Nabla* operator). However, it should be borne in mind that these terms originate from forces (the electric or the pressure one) that are balanced by the viscous force effectively. As a result, steady state flows originate after "switching" the forces on immediately. Thus, the first term in the above equation is really the only one that vanishes when solving the stationary state problem. When diffusion is the only process that takes place in the system, the above equation takes the form

$$\frac{\partial c_i}{\partial t} = \nabla.(\overline{D_i}\nabla c_i) \qquad (23)$$

This governs the diffusion motion and is well-known as the second Fick's law.

The mass conservation law can also be analyzed from another point of view. The liquid density ρ may be also considered as the governed quantity

$$\frac{\partial \rho}{\partial t} + \nabla.(\rho \vec{v}) = 0 \qquad (24)$$

It is also a quantity (the mass) related to the unit volume. When constant in the space and time (incompressible fluid), we obtain

$$\nabla.\vec{v} = 0 \qquad (25)$$

This equation governs the movement of an incompressible liquid and is called the *incompressibility condition*. It is applied when dealing with the bulk flow (e.g. driven by the electroosmosis or by the pressure difference). The incompressibility condition is assumed to be satisfied when dealing with the electromigration in diluted liquid solutions.

4.1.3 Electric Charge Conservation Law

The continuity equation also governs the electric field distribution. The net electric charge density ρ_e is the quantity that is wished to be conserved

$$\frac{\partial \rho_e}{\partial t} + \nabla.\vec{j} = 0 \qquad (26)$$

Here $\vec{j}$ denotes the flux of the electric charge and is identical to the current density.

No sources or sinks of electric charge are considered. The question arises how the time derivative term can be regarded. There are at least two reasons why this term should be zero:
1) The electroneutrality condition states that the net electric charge density must be zero. So must its time derivative. There is an exception that breaks this rule - the electric double layer (EDL). However, the EDL layer is much thinner than the dimensions considered in electromigration in channels of micrometer dimension.
2) Even if there was a site of nonzero net electric charge density, its time derivative would equal zero when solving the stationary state problem.
The current density is, thus, simply given by

$$\nabla.\vec{j} = 0 \tag{27}$$

This is well known as the Kirchhoff‘s current law. There are, in principle, two terms that can contribute to the current density. The first one accounts for an external source of the electric field and can be described in terms of the Ohm’s law. A driving voltage forms the major part of electric field that forces charged particles to move along the field streamlines. Nevertheless, it should not be forgotten that charged particles also move along the concentration gradient due to diffusion. This movement also contributes to the total current density value. The Kirchhoff’s law takes the form

$$\nabla.(\kappa\vec{E} + \vec{j}_{dif}) = \nabla.(-\kappa\nabla V + \vec{j}_{dif}) = 0 \tag{28}$$

Here V is the electric potential caused by the external power supply, κ denotes the conductivity and $\vec{j}_{dif}$ stands for the diffusion current term. The conductivity is given by

$$\kappa = F\sum_{i,j}\left|z_{ij}\right|u_{ij}c_{ij} + Fu_H c_H + Fu_{OH}c_{OH} = F\sum_i c_i \sum_j \left|z_{ij}\right|u_{ij}h_{ij} + Fu_H c_H + Fu_{OH}c_{OH} \tag{29}$$

The right-hand terms account for the contribution of H^+ and OH^- ions.
The diffusion current term can be derived from the Faraday‘s law and the first Fick‘s law

$$\vec{j}_{dif} = F\sum_{i,j} z_{ij}\vec{J}_{ij,dif} + F\vec{J}_H - F\vec{J}_{OH} = -F\sum_{i,j} z_{ij}D_{ij}\nabla c_{ij} - FD_H\nabla c_H + FD_{OH}\nabla c_{OH} \tag{30}$$

This equation is used to assess the diffusion currents in the simulations.
Large concentration gradients may give rise to considerable diffusion currents. Large pH gradients are often accompanied by strong diffusion currents as H^+ and OH^- are the fast ions.
However, in most cases the driving electric field is much stronger than that generated by the diffusion currents.

4.1.4 Macroscopic Electroneutrality

As it has already been mentioned, the macroscopic electroneutrality forces the net electric charge density to be zero anywhere. This condition is satisfied only when all ionic forms of all species obey the condition

$$\sum_{i,j} c_{ij}z_{ij} + c_H - c_{OH} = 0 \tag{31}$$

The fraction h_{ij} may be used to modify the above equation

$$\sum_i c_i \sum_j h_{ij} z_{ij} + c_H - c_{OH} = \sum_i c_i H_i + c_H - c_{OH} = 0 \tag{32}$$

Here H_i is called the effective constituent charge. The H^+ and OH^- ion concentrations are bound by the ionic product of water K_w and thus, the above equation takes the shape

$$\sum_i c_i H_i + c_H - \frac{K_w}{c_H} = 0 \tag{33}$$

The left-hand side of this equation is called the *G*-function. It depends on the concentrations of all species as well as on c_H. The electroneutrality condition may, thus, simply be written as follows

$$G(c_1,...,c_N,c_H) = 0 \tag{34}$$

The last piece of work to be done is determination of all h_{ij} fractions. The next paragraph makes them computable by solving the chemical equilibrium equations.

4.1.5 Chemical Equilibrium Equations

The model does not account for any chemical reaction that leads to a change of overall (analytical) concentration c_i of respective species (*i*-th system constituent). It means that no chemical reaction between *k*-th and *l*-th system constituents is allowed. On the other hand, the acid-base reactions within one species are considered. They are assumed to be much "faster" than all other phenomena encountered. Thus, we assume the acid-base equilibrium to be reached at any time.

The acid $A_{i,j}$ is defined as a constituent that can dissociate the proton under appropriate conditions

$$A_{i,j} \leftrightarrow A_{i,j-1} + H^+ \quad K_a(i,j-1) = \frac{c_{i,j-1}}{c_{ij}} c_H \tag{35}$$

Here $j \le 0$ as the acids are negatively charged. On the contrary, the base $B_{i,j}$ is a constituent that can accept the proton

$$B_{i,j} \leftrightarrow B_{i,j+1} + OH^- \quad K_b(i,j+1) = \frac{c_{i,j+1}}{c_{ij}} c_{OH} \tag{36}$$

Here $j \ge 0$ as the bases are positively charged. The terms in left-hand sides of the above algebraic equations are called the consecutive equilibrium constants for acids and bases, respectively. The latter equation can be rearranged to

$$\frac{K_b(i,j+1)}{K_w} = \frac{c_{i,j+1}}{c_{ij}} c_H^{-1} \tag{37}$$

This equation is equivalent to that given for the acids. Thus, a new function *K* may be defined for acids

$$K(i,j-1) = K_a(i,j-1) \qquad (j \le 0) \tag{38}$$

and for bases

$$K(i,j+1) = \frac{K_w}{K_b(i,j+1)} \qquad (j \ge 0) \tag{39}$$

The concentration and molar fraction of any ionic form of any system constituent can be written as

$$c_{ij} = c_{i0} L_{ij} c_H^j \tag{40}$$

$$h_{ij} = h_{i0} L_{ij} c_H^j \tag{41}$$

Here c_{i0} and h_{i0} are the concentration and molar fraction of a non-charged form of *i*-th system constituent, respectively. L_{ij} is the global constituent constant (considered either for an acid or for a base) that depends only on the consecutive constants. It can be expressed for acids and bases, respectively, as

$$L_{ij} = \prod_{k=-1}^{j-1} K(i,k) \qquad\qquad L_{ij} = \prod_{k=+1}^{j+1} \frac{1}{K(i,k)} \tag{42}$$

The analytical concentration expression allows the fraction of the non-charged form to be evaluated

$$c_i = \sum_j c_{ij} = c_{i0} \sum_j L_{ij} c_H^j \quad \Rightarrow \quad c_{i0} = \frac{c_i}{\sum_j L_{ij} c_H^j} \quad \Rightarrow \quad h_{i0} = \frac{1}{\sum_j L_{ij} c_H^j} \tag{43}$$

Consequently, all h_{ij} may be calculated

$$h_{ij} = \frac{L_{ij} c_H^j}{\sum_k L_{ik} c_H^k} \tag{44}$$

Index *j* was replaced by *k* in the denominator in order to avoid misunderstandings. The integer *k* may attain the same values as *j*. The electroneutrality condition (in fact the *G*-function) can be written as follows

$$G(c_1,...,c_N,c_H) = \sum_i c_i \sum_j z_{ij} \frac{L_{ij} c_H^j}{\sum_k L_{ik} c_H^k} + c_H - \frac{K_w}{c_H} = 0 \tag{45}$$

This equation can be easily solved as c_H is the only unknown variable (all c_i values are given as input data).

4.1.6 Momentum Conservation Law

The behavior of bulk fluid motion is to be investigated. The linear momentum is the quantity which is to be conserved. It comprises two main properties of a moving fluid i.e. its mass and velocity. Rather than regarding the momentum itself the momentum related to the unit volume is considered. Its component in the respective direction is ρv_k, (*k* is any of *x*,*y*,*z* directions). We get

$$\frac{\partial(\rho v_k)}{\partial t} + \nabla.(\rho v_k \vec{v}) = b_k \tag{46}$$

We can hardly cancel the source term b_k this time as it forces the liquid to move which is exactly what is desired. A vector composed of three such source terms is called the body force $\vec{b}$. Several simple rearrangements (taking the mass conservation law into account) lead to the equation that can be written in the vector form as

$$\rho\left(\frac{\partial\vec{v}}{\partial t}+\vec{v}.\nabla\vec{v}\right)=\vec{b} \tag{47}$$

This is the general form of the Navier-Stokes equations. The body force can be either of volume or of surface character. Thus, the it can splits into two terms

$$\rho\left(\frac{\partial\vec{v}}{\partial t}+\vec{v}.\nabla\vec{v}\right)=\nabla.\vec{\vec{\sigma}}+\vec{f} \tag{48}$$

This equation is called the *Cauchy momentum equation* and governs the motion in any liquid that conserves mass. Symmetric tensor $\vec{\vec{\sigma}}$ is called the stress tensor and handles the surface forces whereas vector $\vec{f}$ accounts for any external volume force such as the gravity or the centrifugal force. The stress tensor can be further split into two terms, the first one being the pressure gradient and the second one being the gradient of so-called $\vec{\vec{\Im}}$ tensor that depends on the type of a liquid. The Navier-Stokes equations take the shape

$$\rho\left(\frac{\partial\vec{v}}{\partial t}+\vec{v}.\nabla\vec{v}\right)=-\nabla p+\nabla.\vec{\vec{\Im}}+\vec{f} \tag{49}$$

When a simple Newtonian fluid is considered, the equations read

$$\rho\left(\frac{\partial\vec{v}}{\partial t}+\vec{v}.\nabla\vec{v}\right)=-\nabla p+\nabla.\eta\left[(\nabla\otimes\vec{v})+(\nabla\otimes\vec{v})^{T}\right]+\vec{f} \tag{50}$$

Here $\otimes$ denotes the outer product (a matrix is created by the multiplication between a column vector and a row vector) and ^{T} stands for the matrix transposition. Quantity η is called the dynamic viscosity. As a liquid is thought to be incompressible, the Navier-Stokes equations are solved along with Eq. (25). These two equations are employed in the simulations. It should be mentioned that the external force $\vec{f}$ is a way to define the electroosmotic bulk flow.

4.1.7 Energy Conservation Law

There are some tasks in electrophoresis that require the temperature profile to be evaluated. The system quantity related to the unit volume (the energy density) is regarded as a variable that is governed by the continuity equation

$$\frac{\partial}{\partial t}\left(\frac{E}{V}\right)+\nabla.\vec{J}=Q \tag{51}$$

Here $\vec{J}$ denotes the heat flux and Q stands either for a heat source or a heat sink term (e.g. chemical reactions, friction). In particular, Joule heating is of the main interest here as the charged species migrate under the influence of the electric field.

The internal energy is a variable that will be considered. It may be assumed to depend on the volume as well as on the temperature

$$dE=\pi_{T}dV+mc_{v}dT \tag{52}$$

Here π_T and c_v denote the internal pressure (at constant temperature) and the specific heat capacity (at constant volume), respectively. The former one governs the interactions between the molecules (the potential energy contribution), the latter one describes the ability of a sample to assemble the internal energy when heated (the kinetic energy contribution). As the domain is supposed to be of constant volume, the former term cancels. The energy conservation law takes the form

$$\frac{mc_v}{V}\frac{\partial T}{\partial t}+\nabla.\vec{J}=Q \tag{53}$$

The heat flux consists of two contributions – the heat diffusion and the heat convection (the heat radiation is neglected as a continuum is considered). The former one is given by the Fourier's law of conduction

$$\vec{J}_{dif}=-\lambda\nabla T \tag{54}$$

Here λ stands for the thermal conductivity. Actually, a tensor $\vec{\vec{\lambda}}$ should be considered rather than the scalar number, as, generally the heat transport can depend on direction. Nevertheless, when dealing with a uniform liquid (as we consider here) all non-diagonal entries vanish in the tensor leaving the λ as a scalar number. It should be noticed that the Fourier's law resembles the first Fick's law that governs the diffusion of matter.
The heat convection term can be expressed as follows

$$\vec{J}_{con}=\frac{E}{V}\vec{v}=\frac{mc_vT}{V}\vec{v} \tag{55}$$

Vector $\vec{v}$ denotes the bulk flow velocity. The continuity equation takes the form

$$\rho c_v\frac{\partial T}{\partial t}+\nabla.(-\lambda\nabla T+\frac{mc_vT}{V}\vec{v})=Q \tag{56}$$

and may be rearranged to the shape

$$\rho c_v\frac{\partial T}{\partial t}+\nabla.(-\lambda\nabla T)+\rho c_v\vec{v}.\nabla T=Q \tag{57}$$

The incompressibility condition was used to obtain this equation. The Q term (of dimension power/volume) can be easily derived when the Joule heating is the only heat source and no heat sinks are considered

$$Q=\frac{UI}{V}=\frac{\left|\vec{E}\right|x\,jS}{V}=\frac{j^2}{\kappa} \tag{58}$$

Here U denotes the electric potential difference (voltage) and I is the resulting electric current. The current density value j accounts for both external and internal current sources. The equation

$$\rho c_v\frac{\partial T}{\partial t}+\nabla.(-\lambda\nabla T)+\rho c_v\vec{v}.\nabla T=\frac{j^2}{\kappa} \tag{59}$$

is employed in simulations where the temperature is changed by the electric current.

4.1.8 Ionic Strength Correction

The approach given above considers all ionic species as isolated (though charged) particles that do not interact with each other. The ionic strength correction takes the mutual ion-ion interactions into account. The ionic strength is defined as

$$I = \frac{1}{2}\sum_{i,j} c_{ij} z_{ij}^2 \tag{60}$$

It is the basic quantity that appears in the equation for the activity coefficient. In particular, the extended Debye - Hückel equation (Refs. [20] and [21]) is employed to calculate it

$$\log \gamma_{ij}(I) = -\frac{A z_{ij}^2 \sqrt{I}}{1 + B\sqrt{I}} + C z_{ij}^2 I + DI^2 + \ldots \tag{61}$$

The constants *A*, *B, C* and *D* are as follows

$$A = \frac{F^3}{4\pi N_A \ln 10}\sqrt{\frac{\rho_{loc}}{2\varepsilon^3 R^3 T^3}} \qquad B = \sqrt{\frac{2e^2 N_A}{\varepsilon kT}} \qquad C = 10^{-4} \qquad D = 0 \tag{62}$$

Here N_A, k and e are the Avogadro's number, the Boltzmann constant and the elementary charge, respectively. ε is the permittivity and ρ_{loc} stands for the local charge density (not to be confused with the net electric charge density ρ_e which is the macroscopic quantity and is equal to zero). The ion activities are given by

$$a_{ij}(I) = \gamma_{ij}(I) c_{ij}(I) \tag{63}$$

The activity of any neutral form a_{i0} equals its concentration c_{i0} as non-charged species are supposed to be unaffected by the presence of charged species. The acid-base equilibrium state can be expressed as

$$K_a(i, j-1) = \frac{a_{i,j-1}}{a_{ij}} a_H = \frac{\gamma_{i,j-1}}{\gamma_{ij}} \gamma_H \frac{c_{i,j-1}}{c_{ij}} c_H \tag{64}$$

$$K_b(i, j+1) = \frac{a_{i,j+1}}{a_{ij}} a_{OH} = \frac{\gamma_{i,j+1}}{\gamma_{ij}} \gamma_{OH} \frac{c_{i,j+1}}{c_{ij}} c_{OH} \tag{65}$$

The constants defined as

$$K_{a,app}(i, j-1)(I) = \frac{c_{i,j-1}}{c_{ij}} c_H \tag{66}$$

$$K_{b,app}(i, j+1)(I) = \frac{c_{i,j+1}}{c_{ij}} c_{OH} \tag{67}$$

are called the "apparent constants" (in spite of the fact that they are not constant as they depend on the ionic strength). The ionic product is in the form

$$K_w = a_H a_{OH} = \gamma_H \gamma_{OH} c_H c_{OH} \tag{68}$$

Similarly, the apparent ionic product of water is defined as

$$K_{w,app}(I) = c_H c_{OH} \tag{69}$$

The equations for apparent constants and the apparent ionic product of water are included in the electroneutrality condition and solved together as the *G*-function. This allows the corrected concentrations $c_{ij}(I)$ to be determined.

The ions influence each other also when they move in the electric field. Thus, the mobilities and the conductivity are affected by mutual interactions among charged species. The classical Onsager - Fuoss theory (Refs. [20], [21] and [22]) is employed to describe this effect. It is based on the assumption that all charged species are retarded by oppositely charged ions in their neighborhood.

Let us rewrite $ij \rightarrow f$ in order to have the next equations simpler. Let *M* be the total number of charged species, let *f' = 1, …, M*. The corrected mobility $u_f(I)$ can be calculated as

$$u_f(I) = u_f - \left(B_1 z_f u_f \sum_{n=0}^{5} C_n R_f^{(n)} + B_2 \left| z_f \right| \right) \sqrt{2} \frac{\sqrt{I}}{1 + B\sqrt{I}} \tag{70}$$

Here, the constants B_1 and B_2 are defined as

$$B_1 = \frac{e^3}{12\pi} \sqrt{\frac{N_A}{\varepsilon^3 k^3 T^3}} \qquad B_2 = \frac{e^2}{6\pi\eta} \sqrt{\frac{N_A}{\varepsilon k T}} \tag{71}$$

and C_n stands for the binomial coefficient

$$C_n = \binom{1/2}{n} \tag{72}$$

The $R_f^{(n)}$ coefficients are calculated as follows: let us assemble a square matrix (of *M* x *M* type) called *H* whose entry H_{jk} is given by

$$H_{jk} = \delta_{jk} \sum_{f'} \frac{z_{f'}^2 c_{f'}}{2I} \left(\frac{u_{f'} / \left| z_{f'} \right|}{u_{f'} / \left| z_{f'} \right| + u_j / \left| z_j \right|} \right) + \frac{z_k^2 c_k}{2I} \left(\frac{u_k / \left| z_k \right|}{u_j / \left| z_j \right| + u_k / \left| z_k \right|} \right) \tag{73}$$

Here δ_{jk} denotes Kronecker delta. Furthermore, let us create a column vector $\vec{R}^{(0)}$ (of *M* x *1* type)

$$\vec{R}^{(0)} = (R_1^{(0)}, ..., R_f^{(0)}, ..., R_M^{(0)})^T \tag{74}$$

Its *f*-th component is defined as follows

$$R_f^{(0)} = z_f - \left| \frac{z_f}{u_f} \right| \frac{\sum_{f'} z_{f'}^3 c_{f'}}{\sum_{f'} z_{f'}^2 c_{f'} \left| z_{f'} / u_{f'} \right|} \tag{75}$$

Consequently, the matrix multiplication is applied to $\vec{R}^{(0)}$ and vector $\vec{R}^{(1)}$ is constructed

$$\vec{R}^{(1)} = (R_1^{(1)}, ..., R_f^{(1)}, ..., R_M^{(1)})^T = (2H - E)\vec{R}^{(0)} \tag{76}$$

Here, *E* stands for a unit matrix of *M* x *M* type. The vector $\vec{R}^{(1)}$ is the first member of series whose general *p*-th element can be expressed as

$$\vec{R}^{(p)} = (2H - E)^p \vec{R}^{(0)} \tag{77}$$

The vectors $\vec{R}^{(0)},\ldots,\vec{R}^{(5)}$ are assembled in this order and their *f*-th components $R_f^{(0)},\ldots,R_f^{(5)}$ are used to calculate the corrected mobility $u_f(I)$. Thus, $u_{ij}(I)$ of any ionic form of any species can be determined using this approach. Finally, the corrected conductivity is given by

$$\kappa(I) = F\sum_{i,j}\left|z_{ij}\right|u_{ij}(I)c_{ij}(I) \tag{78}$$

The corrected conductivity can possibly affect the electric field distribution and all other phenomena encountered.

4.1.9 Transformation of the Variables into the Cylindrical Coordinates

There are several problems in electrophoresis that possess a symmetry. This feature can help one to save the computation time as the computational domain or even the space dimension can be reduced. Let us take a very simple capillary arrangement as an illustrative example. The capillary is supposed to be a cylinder with a radius *r* and a height *z*. It can be formed by rotation of the rectangle (*r*.*z*) around the *z* axis (Fig. 2).

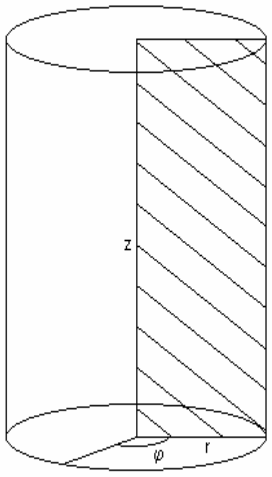

Fig. 2 Cylindrical coordinates

The cylindrical symmetry allows all system parameters to be independent of the angle φ.

Let us consider a scalar $A = A(x,y,z)$ and a vector variable $\vec{B} = (B_x, B_y, B_z) = (B_x(x,y,z), B_y(x,y,z), B_z(x,y,z))$ that stand for all system properties used in calculations. The transformation of coordinates searches for the variables $A = A(r,\varphi,z)$ and $\vec{B} = (B_r(r,\varphi,z), B_\varphi(r,\varphi,z), B_z(r,\varphi,z))$.

The following relations are employed

$$\frac{\partial A}{\partial x} = \cos\varphi\frac{\partial A}{\partial r} \qquad \frac{\partial A}{\partial y} = \sin\varphi\frac{\partial A}{\partial r} \tag{79}$$

$$\frac{\partial^2 A}{\partial x^2} = \frac{\sin^2\varphi}{r}\frac{\partial A}{\partial r} + \cos^2\varphi\frac{\partial^2 A}{\partial r^2} \qquad \frac{\partial^2 A}{\partial y^2} = \frac{\cos^2\varphi}{r}\frac{\partial A}{\partial r} + \sin^2\varphi\frac{\partial^2 A}{\partial r^2} \tag{80}$$

$$\Delta A = \nabla.(\nabla A) = \frac{1}{r}\frac{\partial A}{\partial r} + \frac{\partial^2 A}{\partial r^2} + \frac{\partial^2 A}{\partial z^2} \qquad \nabla.\vec{B} = \frac{B_r}{r} + \frac{\partial B_r}{\partial r} + \frac{\partial B_z}{\partial z} \tag{81}$$

The symmetry allows $\frac{\partial A}{\partial\varphi} = 0$ and $\frac{\partial\vec{B}}{\partial\varphi} = \vec{0}$ to be obeyed. The general continuity equation takes the shape

$$\frac{\partial A}{\partial t} + \frac{J_r}{r} + \frac{\partial J_r}{\partial r} + \frac{\partial J_z}{\partial z} = \frac{\partial A}{\partial t} + \nabla_{rz}.(J_r, J_z) + \frac{J_r}{r} = 0 \qquad \nabla_{rz} = \left(\frac{\partial}{\partial r}, \frac{\partial}{\partial z}\right) \tag{82}$$

Here J_r and J_z denote the fluxes of a quantity *A* that is governed by the general continuity equation. The term J_r / r has no counterpart in the continuity equation stated in the Cartesian coordinates.

The mass conservation law has the form

$$\frac{\partial c_i}{\partial t}+\nabla_{rz}.\left(-\overline{D}_i\nabla_{rz}c_i-c_i\nabla_{rz}\overline{D}_i+c_i\vec{v}_i+c_i\vec{v}\right)+\frac{1}{r}\left(-\overline{D}_i\frac{\partial c_i}{\partial r}-c_i\frac{\partial\overline{D}_i}{\partial r}+c_iv_{i,r}+c_iv_r\right)=0 \tag{83}$$

Here $v_{i,r}$ and v_r denote the system constituent and bulk-flow velocity component in *r*-direction, respectively.

The incompressibility condition reads

$$\nabla_{rz}.(v_r,v_z)+\frac{v_r}{r}=0 \tag{84}$$

The electric field distribution is given by

$$\nabla_{rz}.(-\kappa\nabla_{rz}V+\vec{j}_{dif})+\frac{1}{r}\left(-\kappa\frac{\partial V}{\partial r}+j_{dif,r}\right)=0 \tag{85}$$

Here, the term $j_{dif,r}$ denotes the diffusion current vector component in *r*-direction.

The Navier-Stokes equations are transformed into the shape

$$\rho\left(\frac{\partial v_r}{\partial r}+\vec{v}.\nabla_{rz}v_r\right)=-\frac{\partial p}{\partial r}+\eta\left(\frac{\partial^2v_r}{\partial r^2}+\frac{\partial^2v_r}{\partial z^2}\right)+\frac{\eta}{r}\left(\frac{\partial v_r}{\partial r}-\frac{v_r}{r}\right) \tag{86}$$

$$\rho\left(\frac{\partial v_z}{\partial r}+\vec{v}.\nabla_{rz}v_z\right)=-\frac{\partial p}{\partial z}+\eta\left(\frac{\partial^2v_z}{\partial r^2}+\frac{\partial^2v_z}{\partial z^2}\right)+\frac{\eta}{r}\frac{\partial v_z}{\partial r} \tag{87}$$

and the energy conservation law obtains the form

$$\rho c_v\frac{\partial T}{\partial t}+\nabla_{rz}.(-\lambda\nabla_{rz}T)+\left(-\frac{\lambda}{r}\frac{\partial T}{\partial r}\right)+\rho c_v(v_r,v_z).\nabla_{rz}T+\frac{1}{r}\rho c_vv_rT=\frac{j^2}{\kappa} \tag{88}$$

The *G*-function and the equations dealing with the ionic strength correction do not require any transformation.

4.2 Boundary Conditions

4.2.1. Boundary Value Problem

The subspace Ω (called the computational domain) is the region where a system quantity *A* is governed by a differential equation. The boundary conditions (BCs) are the equations that govern the boundary $\partial\Omega$. Searching for the solution in Ω and $\partial\Omega$ is called the boundary value problem. If there were no boundary conditions stated to the governing equation, it would be impossible to determine the value of the system quantity in Ω and $\partial\Omega$. Even when the governing equation is not a differential one (e.g. electroneutrality), its BCs have to be defined. Several types of boundary conditions may be stated.

In fact, the BCs are not the only conditions that constrain the solution. For instance, when the c_H value is to be calculated, we *a priori* search for $c_H\in R^+$. However, $c_H\in C$ may be obtained when wrong solving parameters are chosen. However, complex solution is not

physically possible. Such a solution must be rejected and the task recalculated with proper solving parameters.

4.2.2 Dirichlet Boundary Condition

The Dirichlet BC refers to the condition that fixes *A* value on a part of the system boundary (usually called the Dirichlet boundary part Γ_D)

$$A(a,t) = f(a,t) \quad \forall a \in \Gamma_D \quad \Gamma_D \subset \partial\Omega \tag{89}$$

Here *a* is a boundary point and *f* denotes a given function defined on Γ_D. The Dirichlet BC usually forces the boundary value to be maintained in time. The Dirichlet BC stands for a big reservoir that would be connected to the system *via* the corresponding boundary.
There are some situations where a time-dependent Dirichlet BC is necessary. A time-dependent function *f* is employed in such cases and the boundary value changes in time.

4.2.3 Neumann Boundary Condition

Let $\vec{J}$ be the flux of the governed system quantity *A*. The Neumann BC (defined on Γ_N - the Neumann boundary part) determines the rate of change rather than the *A* value itself. In $\Re^1$ it can be written as

$$\frac{\partial}{\partial x} A(b,t) = g(b,t) \quad \forall b \in \Gamma_N \quad \Gamma_N \subset \partial\Omega \tag{90}$$

Here *g* is a given function defined on Γ_N and *b* is arbitrary Neumann boundary part point.
In more-dimensional space the BC takes the shape

$$\frac{\partial}{\partial \vec{n}(b)} A(b,t) = \vec{n}(a).\nabla A(b,t) = g(b,t) \quad \forall b \in \Gamma_N \quad \Gamma_N \subset \partial\Omega \tag{91}$$

The left-hand term denotes the derivative of *A* with respect to the boundary outer normal vector $\vec{n}$. This formulation is rather cumbersome as the governed quantity is in the *Nabla* operator. In practice, it is more convenient to formulate the Neumann BC as

$$\vec{n}(b).\vec{J}(b,t) = g(b,t) \tag{92}$$

If $g = 0$ the BC takes the shape

$$\vec{n}(b).\vec{J}(b,t) = 0 \tag{93}$$

This is what is used when the boundary part is wished to be “impermeable” for *A*.
It should be mentioned that the Neumann BC has to be consistent with the equation that is stated to. In particular, the flux vector $\vec{J}$ is the only variable that may by governed the Neumann BC. The same vector variable emerges in the corresponding governing equation. A chapter “Weak Formulation” is devoted to dealing with the boundary conditions when solving the corresponding differential equation.

4.2.4 Mixed Boundary Condition

This BC is applicable for describing the boundary behavior when various types of boundary parts are necessary. The entire system boundary is split into the subsets Γ_D and Γ_N ($\partial\Omega = \Gamma_D \bigcup \Gamma_N$) (see Fig. 3). Thus, there is a part of the boundary part where the quantity value is maintained whereas the rest of the system boundary has a prescribed flux value. The mixed BC is expressed as

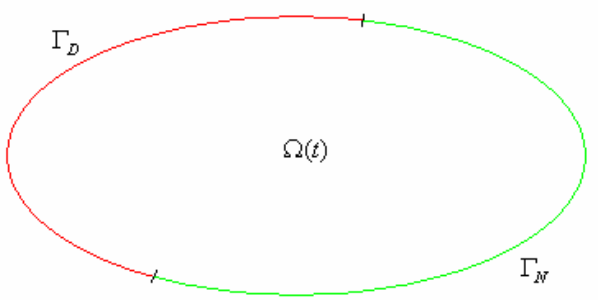

Fig. 3 Illustration of a mixed BC. The system boundary is divided into two parts

$$A(a,t) = f(a,t) \quad \forall a \in \Gamma_D \tag{94}$$

$$\vec{n}(b).\vec{J}(b,t) = g(b,t) \quad \forall b \in \Gamma_N \tag{95}$$

4.2.5 Newton Boundary Condition

This type of BC is a linear combination of the Dirichlet BC and the Neumann BC. Unlike the previous case, it may operate on the entire system boundary simultaneously. It is defined as

$$\alpha A(a,t) + \beta \vec{n}(a).\vec{J}(a,t) = h(a,t) \quad \forall a \in \Gamma_{N+D} \quad \Gamma_{N+D} \subset \partial\Omega \tag{96}$$

Here h is a function defined on $\partial\Omega$ and α,β are non-zero real functions.

4.2.6 Boundary Conditions Imposed on the Mass Conservation Law

Several types of boundary conditions are used when dealing with the mass conservation law. Let us consider a general boundary part $\Gamma \subset \partial\Omega$ ($\Gamma = \Gamma_D \vee \Gamma = \Gamma_N$). When desired to be impermeable, the zero Neumann BC is usually imposed. In other words, the flux vector is perpendicular to the boundary outer normal vector and no substance may penetrate it. The zero Neumann BC can be expressed as

$$\vec{n}(a).\left[-\overline{D}_i(a,t)\nabla c_i(a,t) - c_i(a,t)\nabla\overline{D}_i(a,t) + c_i(a,t)\vec{v}_i(a,t) + c_i(a,t)\vec{v}(a,t)\right] = 0 \quad \forall a \in \Gamma_N \tag{97}$$

There are several ways to express the BC when Γ is permeable. The Dirichlet BC is often employed

$$c_i(a,t) = f_i(a,t) \quad \forall a \in \Gamma_D \tag{98}$$

Here f_i is usually a time-independent function as a constant concentration is required to be maintained on the boundary.

A non-zero Neumann condition of various shapes can also be imposed on the permeable wall

$$\vec{n}(a).\vec{J}(a,t) = g(a,t) \quad \forall a \in \Gamma_N \tag{99}$$

A function $g \neq 0$ determines the flux that passes through the boundary. Several smart functions may be employed here, such as

$$g(a,t) = \vec{n}(a).\vec{J}(a,t) \tag{100}$$

This BC is tricky as the quantities cancel each other (the so-called nothing-doing condition)

$$0 = 0 \quad \forall a \in \Gamma_N \tag{101}$$

Another condition that may be used here is defined as

$$g(a,t) = \vec{n}(a).\left[c_i(a,t)\vec{v}_i(a,t) + c_i(a,t)\vec{v}(a,t)\right] \tag{102}$$

This BC forces all non-diffusion terms to cancel each other on the boundary

$$\vec{n}(a).\left[-\overline{D}_i(a,t)\nabla c_i(a,t) - c_i(a,t)\nabla\overline{D}_i(a,t)\right] = 0 \quad \forall a \in \Gamma_N \tag{103}$$

The *g* function can be also defined as

$$g(a,t) = \vec{n}(a).\left[\overline{D}_i(a,t)\nabla c_i(a,t) + c_i(a,t)\nabla\overline{D}_i(a,t) + c_i(a,t)\vec{v}_i(a,t) + c_i(a,t)\vec{v}(a,t)\right] \tag{104}$$

and the BC acquires the form

$$2\vec{n}(a).\left[-\overline{D}_i(a,t)\nabla c_i(a,t) - c_i(a,t)\nabla\overline{D}_i(a,t)\right] = 0 \quad \forall a \in \Gamma_N \tag{105}$$

The three approaches discussed above eliminate the convection and migration terms. The only term that remains is diffusion. This possibly eliminates numerical problems that can often develop on the boundaries in time.

Of course, there are more BCs that can be stated to the mass conservation law. Trial-and-error simulations are often performed in a hope to find the appropriate set of boundary conditions capable of solving the continuity equations without unfavorable numerical problems.

4.2.7 Boundary Conditions Imposed on the Electric Field Distribution Law

The electrophoretic runs can be conducted in two electric driving modes: (1) *constant voltage mode* and (2) *constant current mode*. The former mode is usual when separating the charged species or determining their mobilities. The latter one is often employed in the lab-on-a-chip electrophoretic runs.

Both the constant current and constant voltage mode can be handled by the present approaches. This part of the presented thesis shows that the BCs are not only the complementary formulae stated to the Kirchhoff‘s current law. In fact, the electric modes are governed by the BCs.

Let us take a simple rectangle as an illustrative example of the computational domain (Fig. 4). The system boundary consists of two horizontal impermeable walls (denoted collectively as Γ_W) and two vertical boundaries that are identical with the electrodes (Γ_R and Γ_L). The entire computational domain is filled with an electrolyte.

The *constant voltage mode* is easier to be implemented as the simple mixed BC can be employed. The electric potential values on the electrodes attain the values that are determined by the functions *f* and *g* (Fig. 4). Thus, the electrodes are the Dirichlet boundaries. The driving voltage is usually constant

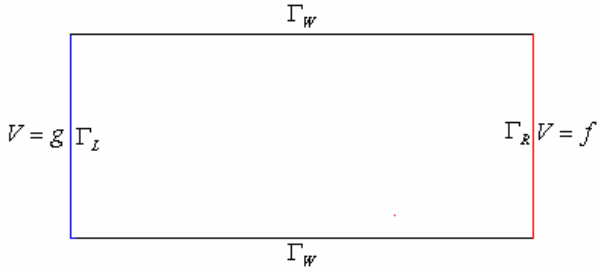

Fig .4 Constant voltage mode arrangement

in time but there are some tasks that require time-dependent potentials to be imposed. The zero Neumann BC is imposed on the non-conducting wall. The final set of BCs reads

$$V(a,t) = f(a) \quad \forall a \in \Gamma_R \quad \text{(right electrode)} \tag{106}$$

$$V(b,t) = g(b) \quad \forall b \in \Gamma_L \quad \text{(left electrode)} \tag{107}$$

$$\vec{n}(c).\vec{j}(c,t) = 0 \quad \forall c \in \Gamma_W \quad \text{(non-conductive wall)} \tag{108}$$

The *constant current mode* is more difficult to be arranged. The conductivity often tends to change in time as the ions move in the electric field. This means that the electrode potentials must change in time in order to maintain the constant current value. The time-dependent Dirichlet BC is inapplicable here as conductivity changes are a result of electromigration and are unpredictable. The conductivity-dependent Dirichlet BC would seem to solve the problem. Unfortunately, this BC causes serious computational problems that make it useless.

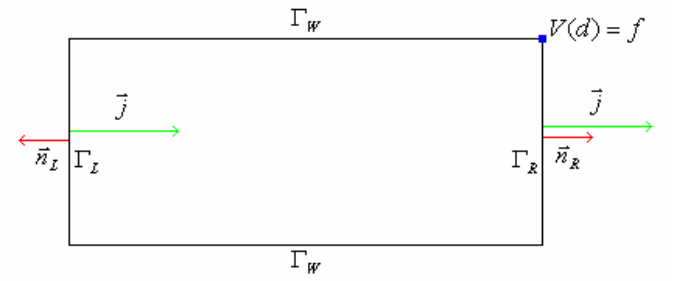

Fig .5 Constant current mode arrangement I

(I) Neumann BC set is more appropriate to be used here (Fig. 5). The following Neumann BC set is employed here

$$\vec{n}_R(a).\vec{j}(a,t) = j \quad \forall a \in \Gamma_R \quad \text{(right electrode)} \tag{109}$$

$$\vec{n}_L(b).\vec{j}(b,t) = -j \quad \forall b \in \Gamma_L \quad \text{(left electrode)} \tag{110}$$

$$\vec{n}_W(c).\vec{j}(c,t) = 0 \quad \forall c \in \Gamma_W \quad \text{(non-conductive wall)} \tag{111}$$

Here j determines the electric current density on the electrodes. However, a set of pure Neumann BCs lacks a point with a given potential value. This causes problems in the calculation of the electric field calculation and no unambiguous solution can be found. These troubles may be overcome by stating the so-called point condition that is a condition stated to the existing boundary condition. It is usually sufficient to define it at one point

$$V(d) = f(d,t) \quad d \in \partial^2\Omega \quad \partial^2\Omega = \Gamma_i \bigcap \Gamma_j \quad i, j = R, L, W \tag{112}$$

Arbitrary function f makes the electric field distribution able to be calculated but does not affect the required electric current density value.

(II) An alternative BC set was found. It also allows the constant current electric field distribution to be calculated. It employs the mixed BC. No point condition is required here as a g function provides a fixed potential value that prevents numerical problems from arising (Fig. 6). The BCs are

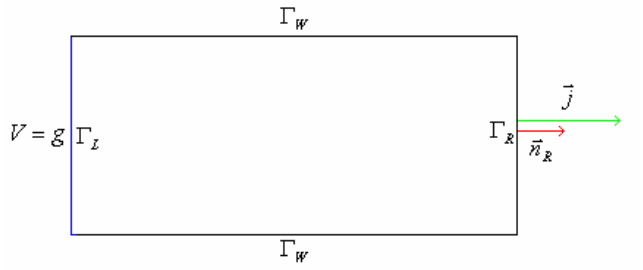

Fig .6 Constant current mode arrangement II

defined as follows

$$\vec{n}_R(a).\vec{j}(a,t) = j \quad \forall a \in \Gamma_R \text{ (Neumann BC, right electrode)} \tag{113}$$

$$V(b) = g(b) \qquad \forall b \in \Gamma_L \text{ (Dirichlet BC, left electrode)} \tag{114}$$

$$\vec{n}_W(c).\vec{j}(c,t) = 0 \quad \forall c \in \Gamma_W \text{ (Neumann BC, non-conductive wall)} \tag{115}$$

The current density value is determined by the Neumann BC imposed on the right electrode. Several tasks were solved and their results investigated in order to reveal possible differences between the two mentioned BC sets for constant current mode. As no differences were found, the two BC sets seem to be equivalent.

4.2.8 Boundary Conditions Imposed on the Electroneutrality Equation

As this electroneutrality equation is algebraic, its BC may be of the same shape

$$G(a,t) = 0 \quad \forall a \in \Gamma_D \tag{116}$$

regardless of whether the boundary is wished to be permeable or impermeable (it is the zero Dirichlet BC by definition).

The Neumann BC may also be employed

$$\vec{n}(a).\left[\xi \nabla c_H(a,t)\right] = 0 \quad \forall a \in \Gamma_N \quad \xi = 0 \tag{117}$$

Both BCs exhibit the same results.

4.2.9 Boundary Conditions Imposed on the Momentum Conservation Law

The classical Dirichlet boundary condition is used when the bulk flow value is known on the boundary

$$v_x(a,t) = f_x(a,t) \wedge v_y(a,t) = f_y(a,t) \wedge v_z(a,t) = f_z(a,t) \tag{118}$$

$$\vec{v}(a,t) = (v_x, v_y, v_z) = (f_x, f_y, f_z) = \vec{f}(a,t) \quad \forall a \in \Gamma_D \tag{119}$$

This BC is called the *inflow/outflow velocity condition* as it is predominantly used to for the open boundaries.

The *no slip condition* forces the velocity to attain the zero value on the boundary

$$v_x(a,t) = 0 \wedge v_y(a,t) = 0 \wedge v_z(a,t) = 0 \tag{120}$$

$$\vec{v}(a,t) = (v_x, v_y, v_z) = \vec{0} \quad \forall a \in \Gamma_D \tag{121}$$

This BC is imposed when dealing with pressure-driven flows.

The *pressure condition* defines a certain pressure p_0 on the boundary. It is given by

$$\vec{n}(a).\left[-p(a,t)E + \eta(\nabla \otimes \vec{v}(a,t)) + \eta(\nabla \otimes \vec{v}(a,t))^T\right] = -p_0(a,t)\vec{n}(a) \quad \forall a \in \Gamma_N \tag{122}$$

The *slip boundary condition* forces the liquid to flow perpendicularly to the boundary normal vector

$$\vec{n}(a).\vec{v}(a,t) = 0 \wedge \vec{t}(a).\left[-p(a,t)E + \eta(\nabla \otimes \vec{v}(a,t)) + \eta(\nabla \otimes \vec{v}(a,t))^T\right].\vec{n}(a) = 0 \quad \forall a \in \Gamma_N \tag{123}$$

Here $\vec{t}$ denotes the boundary tangent vector at a given point. This boundary condition is used for defining the electroosmotic flow and also when dealing with symmetrical problems in which no flux can pass the symmetry axis.

The *normal flow condition* constrains the velocity vector to be perpendicular to the boundary tangent vector

$$\vec{t}(a).\vec{v}(a,t) = 0 \wedge \vec{n}(a).\left[-p(a,t)E + \eta(\nabla \otimes \vec{v}(a,t)) + \eta(\nabla \otimes \vec{v}(a,t))^T\right].\vec{n}(a) = 0 \quad \forall a \in \Gamma_N \tag{124}$$

The *neutral boundary condition* does not control the motion direction with respect to the boundary

$$\left[-p(a,t)E + \eta(\nabla \otimes \vec{v}(a,t)) + \eta(\nabla \otimes \vec{v}(a,t))^T\right].\vec{n}(a) = 0 \quad \forall a \in \Gamma_N \tag{125}$$

An inclined flow through the boundary is usually governed by this BC.

4.2.10 Boundary Conditions Imposed on the Energy Conservation Law

The Neumann BC is used on a boundary part where a certain heat flow is required

$$-\vec{n}(a).\vec{J}(a,t) = J_0(a,t) \wedge \vec{J}(a,t) = -\lambda \nabla T(a,t) + \rho c_p T(a,t)\vec{v}(a,t) \quad \forall a \in \Gamma_N \tag{126}$$

Here, scalar J_0 defines the flux value that passes through the boundary either by diffusion or by convection. When no flux is allowed to pass the boundary part, the above equation reduces to the shape

$$-\vec{n}(a).\vec{J}(a,t) = 0 \quad \forall a \in \Gamma_N \tag{127}$$

This equation is called the *insulation wall condition*.

Dirichlet BC is imposed when the temperature is wished to be constant

$$T(a,t) = T_0(a,t) \quad \forall a \in \Gamma_D \tag{128}$$

This is what is called the *constant temperature condition*.

There are some tasks that wish the computational domain to be divided into several domain parts (subdomains): Ω_k, $k = 1, \ldots N$. Thus, new (internal) boundaries come into existence. When wished to be permeable, the BC takes the shape

$$\vec{n}(a).(\vec{J}_i(a) - \vec{J}_j(a)) = J' \quad \forall a \in \Gamma_{ij} \quad \Gamma_{ij} = \Omega_i \cap \Omega_j \quad \Omega = \bigcup_k \Omega_k \tag{129}$$

Here $\vec{J}_i$ and $\vec{J}_j$ denote the heat fluxes that act on the internal boundary Γ_{ij} from adjacent subdomains Ω_i and Ω_j, respectively. The BC is called the *heat flux continuity condition* when $J' = 0$. The *heat flux discontinuity condition* refers to $J' \neq 0$.

4.3 Weak Formulation

This chapter brings an insight into the way of solving the differential equations by means of the finite element method.

Let us consider a simple computational domain Ω (Fig. 7) with a Neumann (Γ_N) and a Dirichlet (Γ_D) boundary part. The boundary is collectively denoted $\partial\Omega$. The mass conservation law may serve as an example of a governing equation. Its *strong formulation* reads

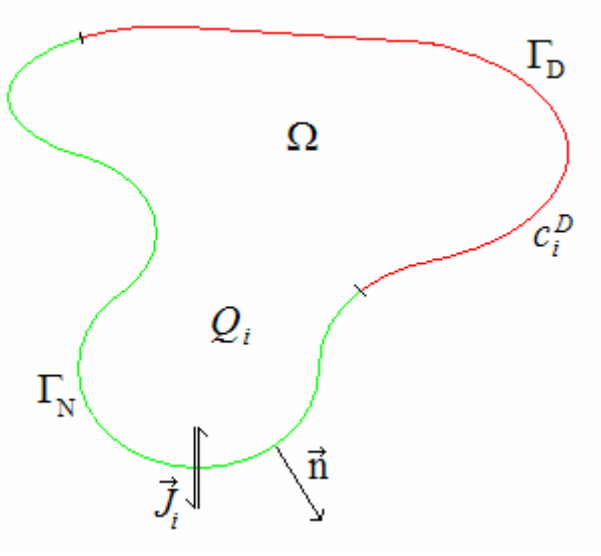

Fig. 7 Computational domain

$$\frac{\partial c_i(X,t)}{\partial t} + \nabla.\vec{J}_i(X,t) = Q_i(X,t) \quad \forall X \in \Omega \quad t \in (0,T) \tag{130}$$

The source Q_i term is not cancelled this time in order not to lose a general shape of the equation. The source term may represent the chemical reaction term. The task must be completed with the boundary conditions

$$c_i(a) = c_i^D(a) \quad \forall a \in \Gamma_D \tag{131}$$

$$\vec{J}_i(b).\vec{n}(b) = g(b) \quad \forall b \in \Gamma_N \tag{132}$$

as well as with the initial condition

$$c_i(X, t=0) = c_i^0(X) \quad \forall X \in \Omega \tag{133}$$

here c_i^0 denotes the concentration at zero time.

The concentration c_i is assumed to belong to

$$L^2([0,T], W^{1,2}(\Omega)) \tag{134}$$

Here $W^{1,2}(\Omega)$ denotes the space of "well-behaved" functions

$$W^{1,2}(\Omega) = \left\{\forall c_i : \exists \nabla c_i, \int_\Omega |c_i|^2 dV + \int_\Omega |\nabla c_i|^2 dV < +\infty\right\} \tag{135}$$

The left-hand integral constrains the concentration value. The right-hand one treats the concentration gradient in a similar way.

Let us take a smooth function $\varphi \in C_0^\infty(\Omega)$. Here, the subscript $_0$ denotes that φ is zero on Γ_D. The governed quantity must also belong to $C_0^\infty(\Omega)$. As c_i need not necessarily attain zero value on the Dirichlet boundary part, a new (shifted) variable is defined

$$\tilde{c}_i = c_i - c_i^D \quad \Rightarrow \quad \tilde{c}_i(a) = c_i^D(a) - c_i^D(a) = 0 \quad \forall a \in \Gamma_D \quad \Rightarrow \quad \tilde{c}_i \in C_0^\infty(\Omega) \tag{136}$$

Let us multiply the strong formulation by φ and integrate the product over Ω

$$\int_\Omega \frac{\partial c_i}{\partial t}\varphi dV + \int_\Omega \nabla.\vec{J}_i \varphi dV = \int_\Omega Q_i \varphi dV \tag{137}$$

This is what is called the *weak formulation* of the equation. The function φ is usually called the test function. The Green's identity may be employed to modify the second integral in the left-hand side of the equation

$$\int_\Omega \frac{\partial c_i}{\partial t}\varphi dV + \int_{\partial\Omega} \vec{J}_i.\vec{n}\,\varphi dS - \int_\Omega \vec{J}_i.\nabla\varphi dV = \int_\Omega Q_i\varphi dV \quad (138)$$

Thus, the weak formulation has one invaluable benefit over the strong one: it does not contain the governed quantity in *nabla* operator. This makes it easier to be solved.

The domain boundary is divided into two parts. Thus, the above equation takes the shape

$$\int_\Omega \frac{\partial c_i}{\partial t}\varphi dV + \int_{\Gamma_D} \vec{J}_i.\vec{n}\,\varphi dS + \int_{\Gamma_N} g\varphi dS - \int_\Omega \vec{J}_i.\nabla\varphi dV = \int_\Omega Q_i\varphi dV \quad (139)$$

Here, the Neumann boundary condition formulation was employed. The Dirichlet term vanishes as φ attains zero value on Γ_D

$$\int_\Omega \frac{\partial c_i}{\partial t}\varphi dV = -\int_{\Gamma_N} g\varphi dS + \int_\Omega \vec{J}_i.\nabla\varphi dV + \int_\Omega Q_i\varphi dV \quad (140)$$

The dependence on the time may either be handled by integrating the equation over time domain (very weak formulation) or by the finite difference method (FDM). The latter approach is applied here.

There are two ways to employ the finite difference method. The first one is called the *explicit method* and can be described by the formula

$$\int_\Omega \frac{c_i^{N+1} - c_i^N}{h}\varphi dV = -\int_{\Gamma_N} g^N\varphi dS + \int_\Omega \vec{J}_i^N.\nabla\varphi dV + \int_\Omega Q_i^N\varphi dV \quad (141)$$

Here h stands for the discrete time step that approximates the time derivative. The quantities c_i^N and c_i^{N+1} denote the concentrations at ^{N} - th and $^{N+1}$ - th time level, respectively. Notice that the above equation is time-independent. It can be rearranged to

$$\int_\Omega c_i^{N+1}\varphi dV = \int_\Omega c_i^N\varphi dV - h\int_{\Gamma_N} g^N\varphi dS + h\int_\Omega \vec{J}_i^N.\nabla\varphi dV + h\int_\Omega Q_i^N\varphi dV \quad (142)$$

Here, all right-hand side terms denote the variables at ^{N} – th time level. This approach allows c_i^{N+1} to be directly calculated. The first computational step employs the initial condition c_i^0 to obtain c_i^1.

The *implicit method* employs the formula

$$\int_\Omega \frac{c_i^{N+1} - c_i^N}{h}\varphi dV = -\int_{\Gamma_N} g^{N+1}\varphi dS + \int_\Omega \vec{J}_i^{N+1}.\nabla\varphi dV + \int_\Omega Q_i^{N+1}\varphi dV \quad (143)$$

Here, all right-hand side terms denote the variables at $^{N+1}$ – th step. Thus, the equation cannot be easily rearranged to obtain c_i^{N+1}. It must be solved by means of iterative numerical methods. As the latter method is known as being of greater numerical stability, it is employed.

4.4 Inspection of Electromigration Behavior in some Electrophoretic Configurations

4.4.1 Electrolysis of Background Electrolyte in Agilent 3DCE Electrophoresis

4.4.1.1 Geometry Arrangement

We inspect electromigration in the setup in the Agilent 3DCE electrophoresis equipment. A cylindrical vessel is filled with the electrolyte solution (Fig. 8). A separation capillary is embedded in a metal electrode and both are immersed in the solution. The height of the flask is 25 mm and its radius is 3 mm. The length of the electrode part immersed in the flask is 10 mm. The inner and the outer diameters of the capillary are 75 μm and 365 μm, respectively. The inner and the outer diameters of the electrode are 410 μm and 1000 μm, respectively. Thus, there is a gap between the capillary and the electrode filled with the electrolyte solution. The electrode base – capillary inlet distance is adjustable and denoted as *x*. The outer electrode edge is curved with the radius of 250 μm. The inner electrode edge and both capillary edges are curved with the radius of 25 μm.

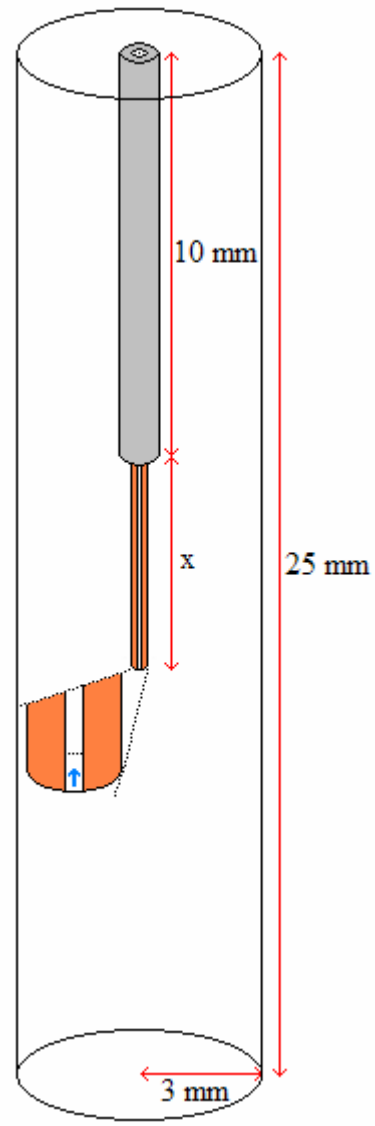

Fig. 8 The 3-D electrode image. x denotes the capillary inlet – electrode base distance. The capillary (orange) is embedded in the electrode (silver).

4.4.1.2 Symmetry

As the geometry is of the cylindrical shape, the cylindrical symmetry may be employed. A 2-D half cross-section is considered as a computation domain. This approach enables this configuration to be solved as a 2-D problem, as the angle coordinate need not be considered, which saves the computational time. Consequently, all governing equations are in the form employing the cylindrical coordinates.

4.4.1.3 Further Assumptions

No ionic strength correction is considered in order to save the computational time. Thus, the calculation employs the ionic mobilities and the *pK* values as constants extrapolated to zero ionic strength. The temperature is assumed to be constant (298.15 K) as no thermal effects are supposed to play any significant role.

4.4.1.4 Buffer Composition

At zero time, the computational domain is filled with the background electrolyte of uniform composition. In particular, sodium and acetic acid are chosen as the buffer components. No analyte is considered. Both sodium and acetic acid are regarded as weak electrolytes. Tab. 1 gives the complete information about buffer parameters (the ionic mobilities and the *pK* constants are taken from the PeakMaster database).

Tab. 1

Species	c/(mM)	u/e.u.	pK(+1)	pK(-1)
Sodium	10	51.9	13.7	-
Acetic acid	20	42.4	-	4.756

e.u. - electrophoretical unit

The upper capillary end Γ_{UCE} (see Fig. 9) is the only part of the system boundary that permeates the buffer components. Thus, the constant Dirichlet BC is imposed to the continuity equations here. The BC approximates a very long capillary filled with the electrolyte of uniform composition that is equal to that at zero time. The rest of the system boundary parts are impermeable for the buffer components and the zero Neumann BC is imposed here.

4.4.1.5 Metal Electrode

The metal electrode has positive potential and, thus, the constant Dirichlet BC is stated to the electric field distribution equation here. The upper capillary end forms the counter-electrode with zero potential (all simulations are performed under the constant voltage mode). The rest of the system boundaries are assumed to be ideally non-conductive and, thus, the zero Neumann BC is imposed here.

4.4.1.6 Modifications

As it has already been mentioned, the electrode base – capillary inlet distance is adjustable. This parameter is allowed to attain eight respective values: -1, 0, 1, 2, 3, 5, 8 and 11 mm. In the first configuration (x = -1 mm), the capillary is hidden

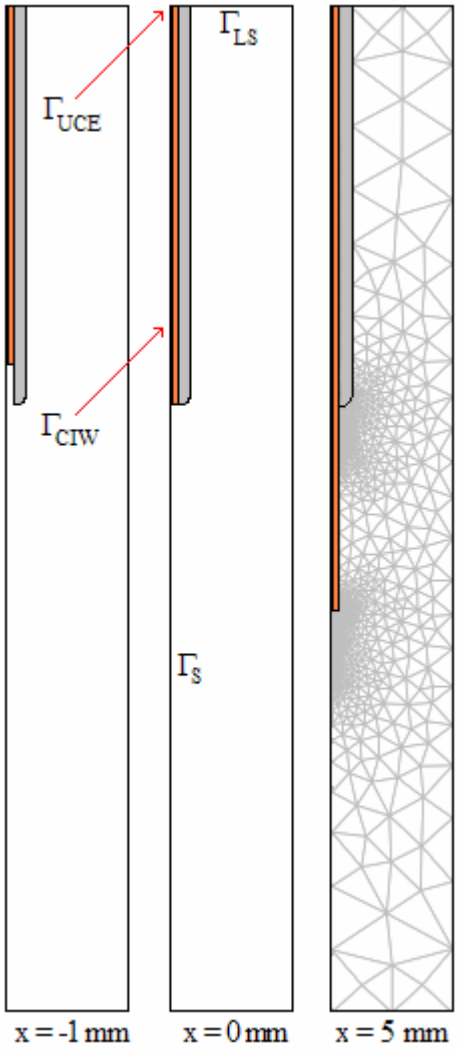

Fig. 9 Three particular geometry arrangements. The symbols denote the names of the boundaries:
Γ_S - symmetry axis
Γ_{CIW} - capillary inner wall
Γ_{UCE} - upper capillary end
Γ_{LS} - liquid surface
The most-right figure shows the computational mesh employed.

in the electrode. The second one (x = 0 mm) is the situation where the capillary end is at the same level as the electrode base. The rest of the geometries consider the capillary sticking out of the electrode base.
The capillary electric field strength is another variable parameter. It may attain five respective values: 5.55, 27.7, 55.5, 85.0 and 125 kV/m (determined at t = 0).
Thus, forty particular simulations are to be carried out and their results analyzed.

4.4.1.7 Inspection of Electrolysis Phenomena

The main result of this part of the thesis is the study of rate of changes that occur in the electrolyte composition under various conditions, especially with various length of the capillary sticking out of the electrode. As the metal electrode is positively charged, the acetic acid concentration is supposed to increase in its vicinity. As its concentration is maintained at the upper capillary end by the constant Dirichlet BC, its total amount should increase in time. On the other hand, the positively charged sodium is assumed to depart from the electrode vicinity and escape the domain through the constant Dirichlet boundary. These two phenomena are believed to decrease the pH value in the electrode vicinity and, consequently, in the capillary. The extent of these phenomena is to be investigated.

4.4.1.8 Results

All simulations really show a decrease in the buffer pH value in time (see Fig. 10).

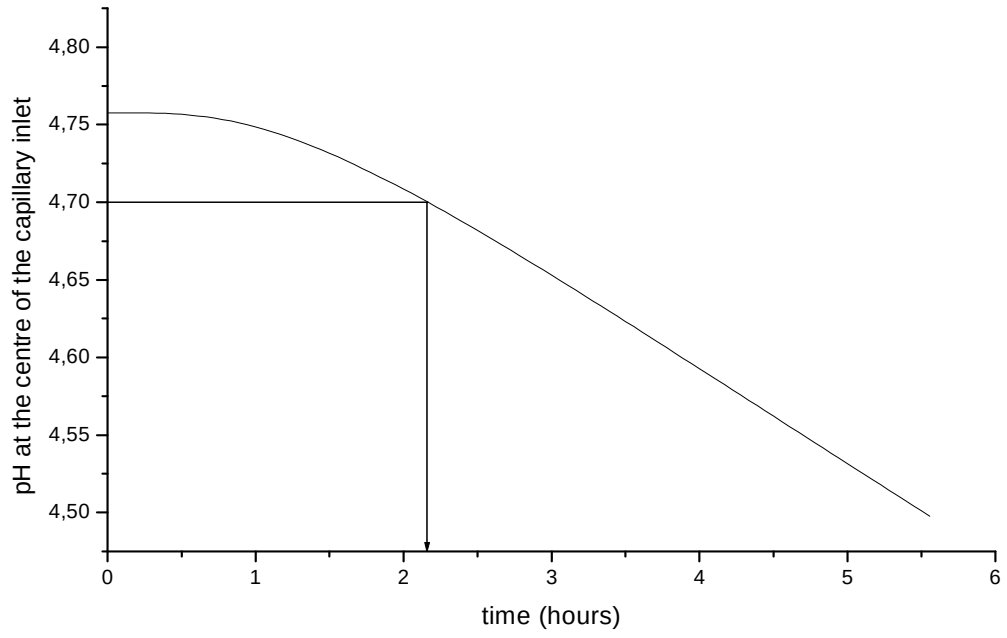

Fig. 10 The pH value in time. Conditions: electric field strength 55.5 kV/m, x = 5 mm. The arrow denotes the time when pH = 4.70 is reached.

The initial pH value of the BGE is 4.76. There are several possibilities to quantify the extent of its change. The pH = 4.70 is chosen to depict the situation where the buffer pH value starts to differ from that at $t = 0$. The pH value is determined at the centre of the capillary inlet (see the blue arrow in Fig. 8).
The time required to reach this change is evaluated. The time is strongly affected by the geometry arrangement as well as by the capillary electric field strength (Fig. 11).

Two particular configurations (with x = -1 mm and x = 1 mm) were chosen to be analysed in detail.

Hidden capillary arrangement x = -1 mm.
This situation may happen when a mistake is done in the capillary preparation. The electric field in the capillary region is highly homogenous (Fig. 12) whereas the rest of the domain is of heterogeneous field. As the capillary cross-section is much smaller than the electrode surface, the capillary field strength is several orders of magnitude stronger than that beyond it. There is a small region at the inner electrode surface with a high electric field. The streamlines tend to concentrate here and touch the inner electrode surface. The rest of the electrode surface is exposed to a very weak field that cannot cause any particle movement in this region.

This experimental setup is far away from being desirable as there is almost no distance between the electrode inner space and the capillary base. The electrochemical reactions alter the pH value strongly in the close neighborhood of the capillary region (Fig. 13). Thus, a buffer of altered composition enters the capillary immediately. In particular, only two seconds are required to change the pH value.

Capillary arrangement with x = 1 mm.
This experimental setup may be encountered when a too short capillary tip sticks out of the electrode. Similarly to the former case, the capillary field strength attains a high value (Fig. 14). However, a weak electric field is at the electrode surface and, thus, the electrophoretic movement is of lesser and the diffusion is of higher significance.

The capillary wall prevents the buffer altered by electrolysis to be passed straightforward into the capillary region (Fig. 15). Thus, a much longer time is required to induce the pH change here. Under these circumstances, the analysis may be carried out without undesirable effects.

Capillary arrangements with x = 2 - 11 mm.
These arrangements have longer electrode base – capillary inlet distance so the time to cause the pH change in the capillary inlet is also longer. The spatial hindrance is very effective. This is useful to be realized when long separation times are required.

Other dependence worth studying is the way the capillary field strength affects the time of the pH change. Five respective field strength values try to encompass the ones used in the real experiments. The stronger the imposed field is, the shorter times are required (Fig. 11).

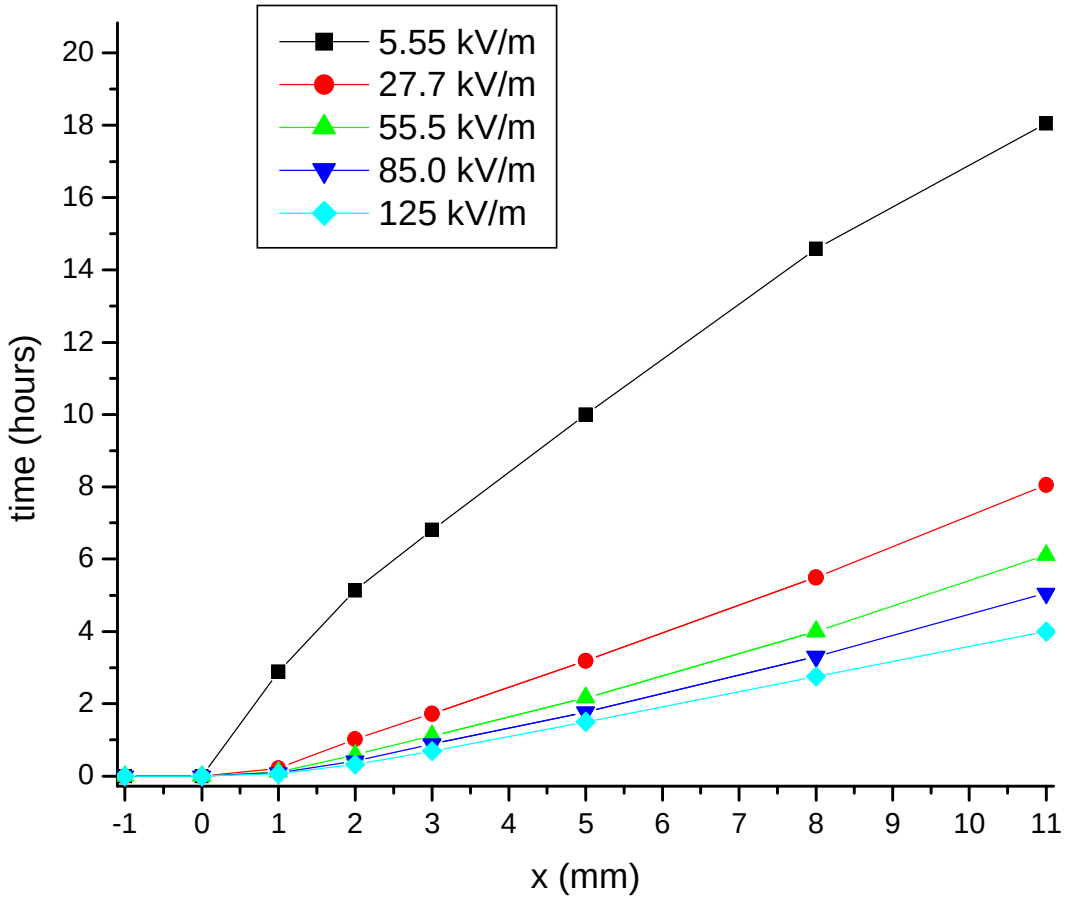

Fig. 11 Times required to cause the pH change (from 4.76 to 4.70) for eight geometries and five electric fields. Longer capillary tip sticking out of the electrode requires longer time to the pH change. Strong electric field tends to shorten the time.

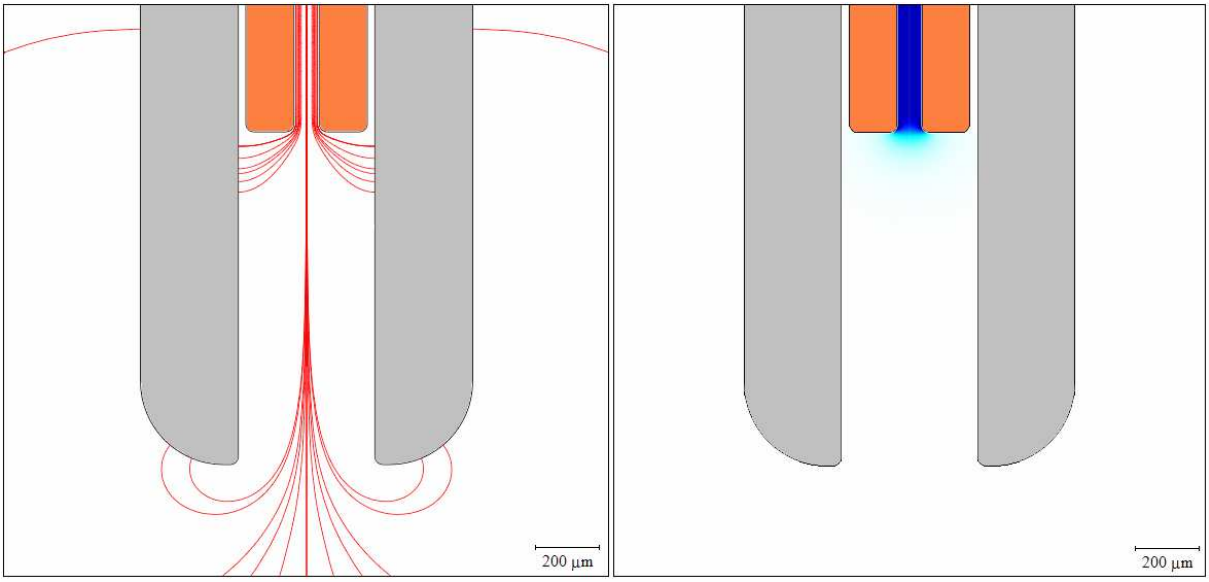

Fig. 12 The arrangement with x = -1 mm. The field streamlines (left picture) and the field strength value (right picture) is pictured. Capillary field strength: 55.5 kV/m (blue colour denotes the strong electric field to be found in the capillary).

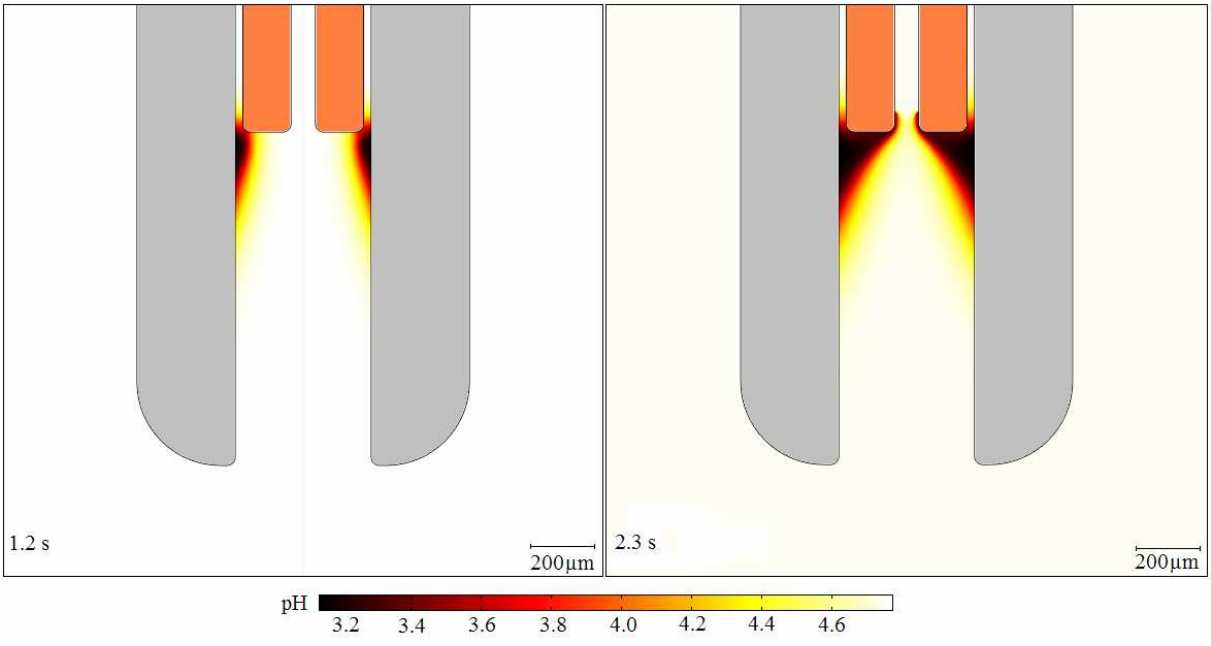

Fig. 13 The arrangement with x = -1 mm. The pH profiles at 1.2 s (left picture) and at 2.3 s (right picture) are depicted. Very short time is sufficient to alter the pH value. Capillary field strength: 55.5 kV/m.

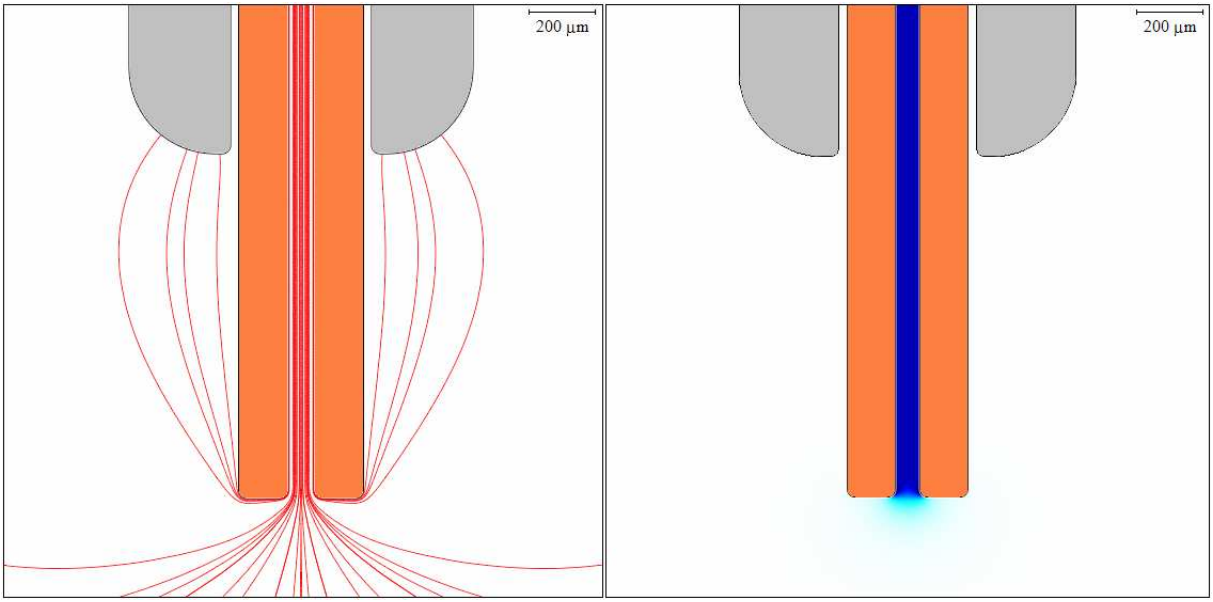

Fig. 14 The arrangement with x = 1 mm. The field streamlines (left picture) and the field strength value (right picture) are shown. Capillary field strength 55.5 kV/m.

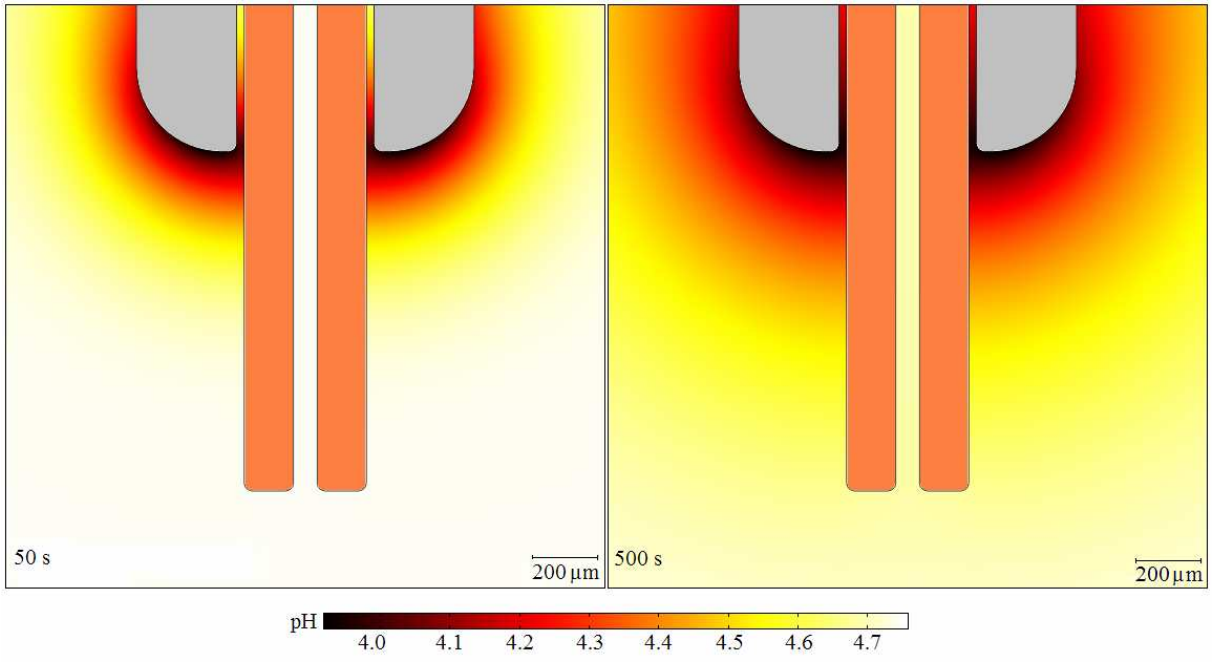

Fig. 15 The arrangement with x = 1 mm. The pH profiles at 50 s (left picture) and at 500 s (right picture) are depicted. Long time is necessary to cause the pH change. Capillary field strength 55.5 kV/m.

4.4.1.9 Electroosmosis

The previous analysis did not account for influence of the electroosmotic movement. It may be, however, also taken into account. When an uncoated silica capillary is employed, the electroosmotic velocity vector has upward z – direction in the capillary region: it flows up in the capillary, (a coated capillary with the reversed EOF vector can also be analyzed, of course). The bulk velocity vector can be determined on Γ_{CIW}

$$\vec{v}(a) = (0,0,-u_{EOF}(a)\frac{\partial V(a)}{\partial z}) \quad \forall a \in \Gamma_{CIW} \tag{144}$$

Here u_{EOF} is the electroosmotic flow mobility. This is a BC stated to the Navier-Stokes equations. There are a lot of situations where this BC formulation causes computational problems. This is not striking as it contains the electric potential. It is governed by another differential equation (the electric field distribution) that is solved along with the Navier-Stokes equations.

This problem can be overcome by stating the electroosmotic velocity instead of the mobility. This approach may be used without inaccuracies when no large conductivity changes evolve in time. As the simulations focus on slight pH changes, this assumption is supposed to be fulfilled.

The zero normal flow condition is imposed on the symmetry axis Γ_S (no liquid may pass through it)

$$v_r(b) = 0 \quad \forall b \in \Gamma_S \tag{145}$$

The normal flow BC is imposed on the liquid surface Γ_{LS} as well as on the upper capillary end Γ_{UCE}. There are two ways how the bulk flow can be handled on the rest of the boundary parts (the vessel base and its vertical wall, the electrode and the outer capillary surface). In particular, the *slip condition* and the *no slip condition* may be employed. The former one constrains the velocity vector to be perpendicular to the boundary normal vector and the latter one forces the velocity value to be zero. Both BC sets are investigated for several values of electroosmotic mobility (or, rather velocity) values.

Particularly, the EOF mobilities of 0, ±1, ±2, ±3, ±4, ±5, ±10, ±15, ±20, ±25, ±30, ±35, ±50, ±100 and ±200 e.u. are analyzed. The geometry arrangement with x = 5 mm and of the field strength of 55.5 kV/m is presented as an illustrative example.

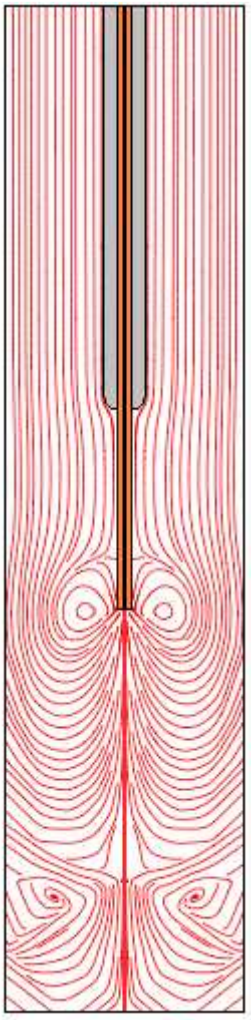

Fig. 16 The bulk flow streamlines tend to create vortices in the vessel. The homogenous field is in its upper part. The field streamlines may only cross through the boundaries Γ_{UCE} and Γ_{LS}. Simulating Conditions: u_{EOF} = 50 e.u, no slip BC is imposed on the rest of system walls.

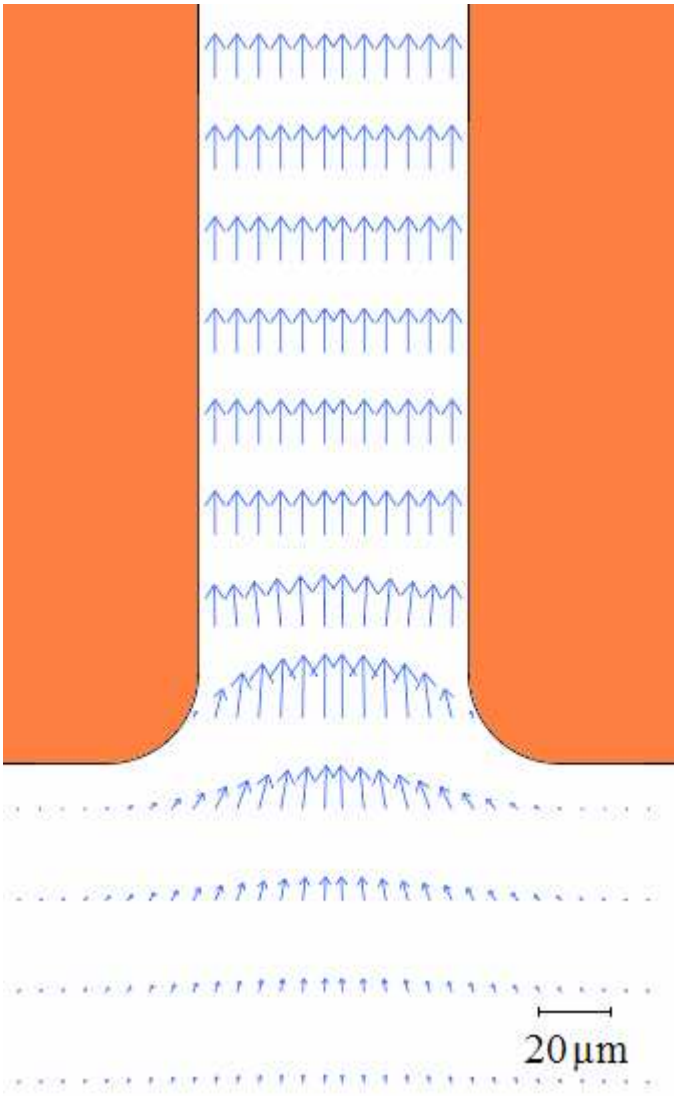

In both cases of BC sets, the bulk flow velocity field was investigated. At first sight, the velocity size and its direction are rather complicated in the vessel (Fig. 16). The velocity streamlines tend to create vortices at the capillary inlet as well as close to the electrode base. On the other hand, the velocity field has a homogenous profile in the upper part of the vessel as well as in the capillary region (Fig. 17).

Fig. 17 EOF-driven bulk flow velocity field. Arrows indicate the flow vector length and orientation. The velocity field of a uniform profile is in the capillary.

The liquid is supposed to be pumped from the vessel into the capillary when positive EOF mobility values are considered. This phenomenon may possibly decrease the time required to alter the pH value in the capillary. Conversely, when a capillary with reversed EOF is employed, the EOF velocity vector is of opposite direction. Under such circumstances, a “fresh” buffer enters the domain through the upper capillary end. This slows down or prevents the pH changes from arising.

Low EOF flowing up in the capillary causes small changes in the time required to attain the pH change due to electrolysis. On the other hand, even small values of the reversed EOF mobility strongly suppress the pH changes in the capillary, which is favorable. The pH value does not change at all when reversed EOF of mobility greater than 5 e.u. is considered (Fig. 18).

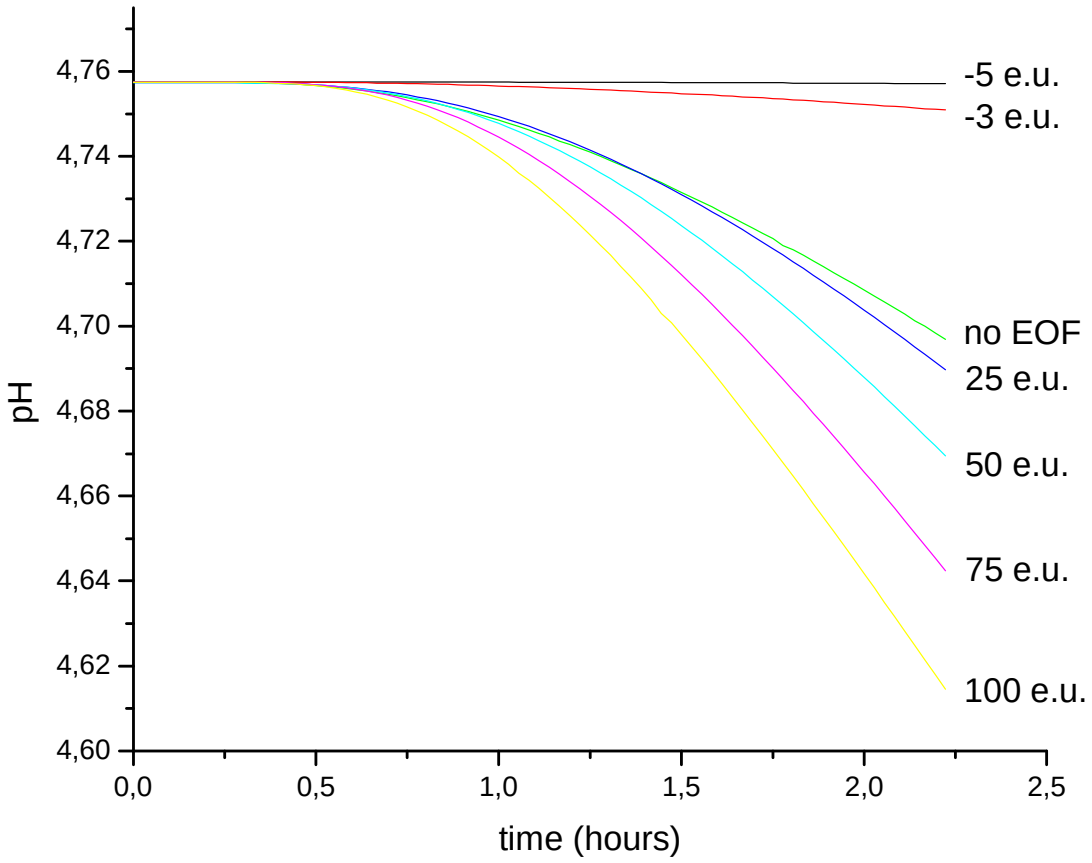

Fig. 18 The pH value in the capillary tip when the EOF is considered. Simulation conditions: field strength 55.5 kV/m, x = 5 mm

No significant difference between the *slip* and the *no slip* condition is observed (Fig. 19). This suggests that the velocity field in the capillary is independent of that in the vessel region.

The electrode immersion in the vessel is also varied. All formerly performed simulations employed the arrangement with the electrode immersion of 10 mm (let us call it the shallow arrangement). The deep arrangement (the immersion of 15 mm) is also considered (Fig. 20).

There is a good motivation for investigating the deep arrangement. As the liquid departs the vessel (when positive EOF values are considered), there must be a region where the electrolyte concentration is decreased. It is in the vicinity of the liquid surface as it is the only boundary part of the vessel where the normal flow BC is imposed. It is worth noticing that this decrease is of a purely artificial origin. It should be investigated whether it can cause some artificial pH changes. The shallow arrangement seems to be more sensitive to them as the capillary inlet is closer to the liquid surface. If there were any discrepancies between the arrangements results, the artificial effects would be significant.

The times needed to attain nearly the same values for both electrode immersion values and for all EOF mobility values (results not shown). It suggests that no artificial effects are supposed to play any substantial role here.

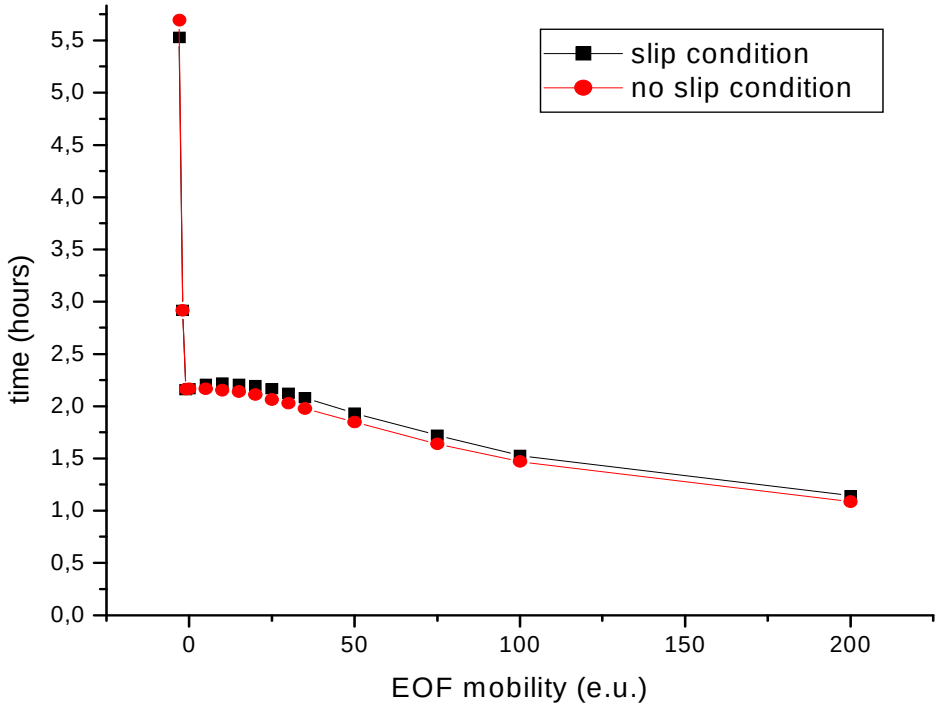

Fig. 19 The two BC sets reveal no significant difference in times required to cause the pH change.

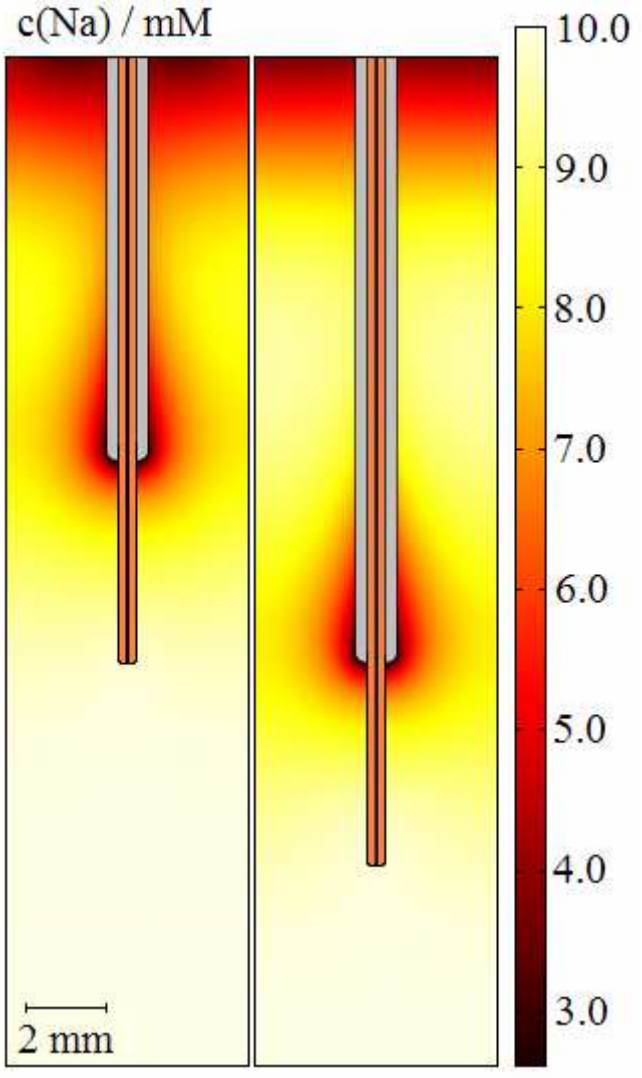

Fig. 20 The shallow and the deep electrode arrangement (x = 5 mm, u_{EOF} = 50 e.u.). The sodium concentration profile is pictured at t = 4000 s. The deep electrode arrangement reveals the separation of the artificial (at Γ_{LS}) and the natural (at the electrode) concentration gradients.

4.4.2 Electromigration Behavior in Chip Electrophoresis Structures

As it has already been mentioned, the lab-on-a-chip techniques are of rising interest nowadays as they offer a lot of benefits over conventional approaches. There are several chip structures that can be investigated by means of computer simulations. One of them is the channel intersection that serves as the injection site for the samples to be separated. This part of the thesis focuses on the injection and the analysis of four virtual analytes by gel electrophoresis in the lab-on-a-chip device.

4.4.2.1 Geometry Arrangement

The computational domain is formed by two channels perpendicularly crossing each other (Fig. 21). The channels are of same width (50 μm). The vertical one serves as the injection channel whereas the horizontal one is employed as the separation channel. The channel intersection is of the main interest as most of the substantial processes take place here. The intersection has round corners (radius 10 μm) as it is in the reality (this also prevents numerical problems from arising in computation). The four arms are denoted U, R, D, L according to their position. The upper one (U) serves as the sample reservoir whereas the lower one (D) is the sample waste. The left (L) and right (R) arm are the buffer inlet and outlet, respectively. The detector is placed in the outlet channel 2 mm downstream from the channel intersection. The open boundaries are called Γ_U, Γ_R, Γ_D, Γ_L and the rest of the boundary is denoted Γ_0.

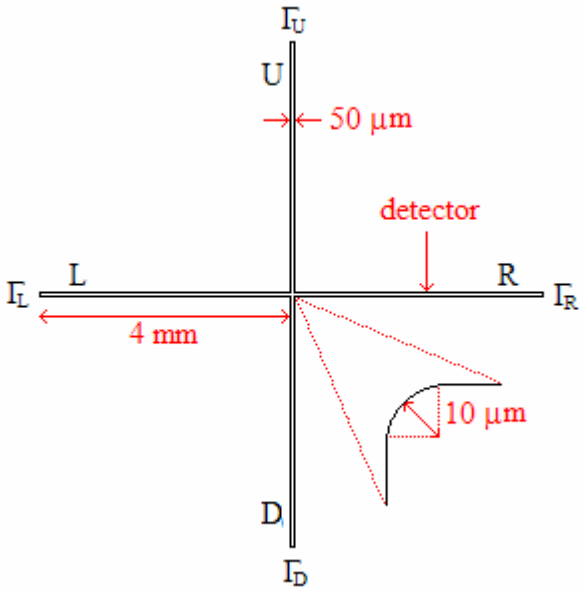

Fig. 21 The injection cross geometry

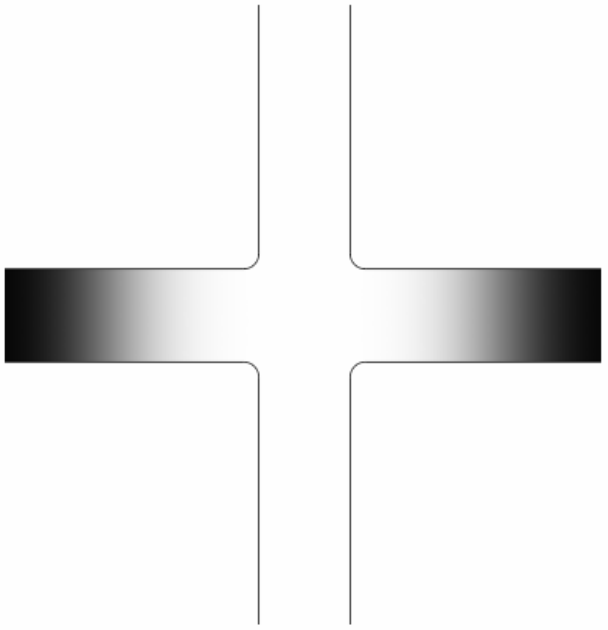

Fig. 22 The gel region (black colour)

4.4.2.2 Assumptions

The third dimension is not considered as the channel depth is supposed to be uniform and, thus, a 2-D model is employed. No ionic strength correction and thermal effects are considered.

4.4.2.3 Separation Environment and Analytes

The left and the right arms of the injection cross are filled with the BGE containing hydrophilic gel as a sieving medium (Fig. 22). The upper and the lower arms are filled with free BGE. The BGE is composed of two constituents: Na^+ and TAPS (tris(hydroxymethyl)methylaminopropanesulfonic acid). They are of a uniform concentration in all channels (Tab. 2). Four weak anionic constituents are regarded as the analytes. They have the same mobilities in the free BGE. However, their mobilities are different when they are in the gel-filled region. The analytes represent the species composed of long-chain molecules (e.g. DNA fragments) that can be separated in the gel according to the length. No change in mobility of sodium, TAPS, H^+ and OH^- is considered as these species are regarded as being small enough to pass the gel sieving environment without retardation.
The gel is not supposed to affect the acid-base equilibrium of any species. Moreover, it is assumed to prevent the bulk flows, either electroosmotic or laminar ones, from arising.

Tab. 2

Species	c (mM)	c_{INJ} (mM)	*u* (e.u.)	u_{GEL} (e.u.)	pK(+1)	pK(-1)
Sodium	20	20	51.9	51.9	13.7	-
TAPS	40	40	25.0	25.0	-	8.3
A_1	-	0.1	27.0	5.0	13.7	-
A_2	-	0.1	27.0	10.0	13.7	-
A_3	-	0.1	27.0	15.0	13.7	-
A_4	-	0.1	27.0	20.0	13.7	-

c_{INJ} – concentration of species in sample reservoir (upper arm) at t = 0
u_{GEL} – electrophoretic mobility of the constituent in the gel-filled region
e.u. – electrophoretical unit

4.4.2.4 Electric Field Distribution

All simulations are performed in the constant current mode. The separation process is accomplished in two steps. The first one is called the injection step and employs the electric field that forces the analytes to move downwards from the sample reservoir through the channel intersection into the sample waste. The second one is called the separation step. The analytes migrate from the channel intersection into the right arm of the separation channel.
The electric current distribution has to satisfy the Kirchhoff's current law. Its integral shape has the form

$$\sum_i I_i(t) = 0 \quad i = U, R, D, L \quad \forall t \in (0, T) \tag{146}$$

Here I_i denotes the electric current value in *i*-th arm. It is governed by the boundary condition that is imposed on respective open boundary. Its values may attain both positive and negative values according to the current direction with respect to the boundary outer normal vector.

As the channels are of uniform cross-section, the above equation also holds for the current density values j_i.

The symbols $j_U^{inj}, j_R^{inj}, j_D^{inj}, j_L^{inj}$ and $j_U^{sep}, j_R^{sep}, j_D^{sep}, j_L^{sep}$ denote the electric current density value in respective arms in the injection and separation step, respectively (Figs. 23,24).

The quantity j_U^{inj} is the one that forces the analytes to move downwards during the injection step (Fig. 23). It is never varied and attains the value (3000 A.m^{-2}) in all simulations. This ensures the constant amount of the analytes to enter the channel intersection. The current densities j_L^{inj} and j_R^{inj} always attain identical value in order to create the symmetrical simulation arrangement. This value is called the constraint current density $j_L^{inj} = j_R^{inj} = j_c$ and is variable. The constraint current forces a pure buffer to enter the channel intersection from the horizontal arms. The quantity j_D^{inj} is calculated so that the electric distribution satisfies the Kirchhoff's current law. A fraction defined as $\lambda_{inj} = j_c / j_U^{inj}$ is employed to show the relative significance of the constraint current density. It is allowed to attain six respective values: 0, 0.0417, 0.0833, 0.0167, 0.250 and 0.333. However, it should be mentioned that the real constraint current is twice as high as there are two streams that constrain the sample flow.

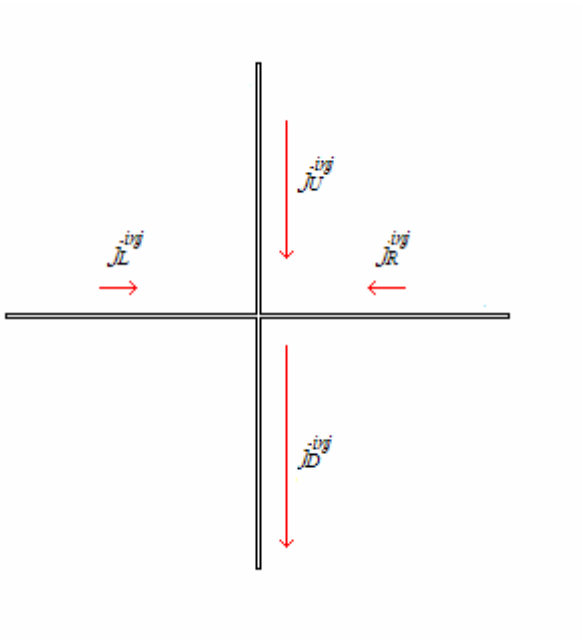

Fig. 23 Electric current density vector directions in the injection step (it takes first five seconds)

The current density j_R^{sep} causes the sample motion in the separation step (Fig. 24). It is constant (3000 A.m^{-2}) in order to maintain constant separation velocities and, thus, also migration times of the analytes. The values of j_U^{sep} and j_D^{sep} attain identical value denoted

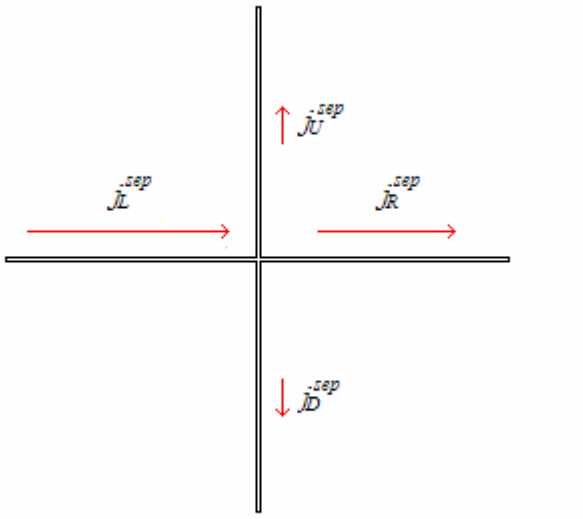

Fig. 24 Electric current density vector directions in the separation step (it takes next 25 s).

$j_U^{sep} = j_D^{sep} = j_p$ and called the pull back current density. It is variable and serves to prevent sample leakage from arising. The value of j_L^{sep} is adjusted to allow the current law to be obeyed. The fraction $\lambda_{sep} = j_p / j_R^{sep}$ is employed to depict the relative significance of the pull back stream. It may attain eleven respective values 0, 0.0417, 0.0833, 0.167, 0.250, 0.333, 0.417, 0.500, 0.583, 0.667 and 0.833. The real pull back strength is double as high as there are two streams that pull the injected sample back to the sample reservoir and the sample waste.

The constraint current is believed to affects the shape of analyte zone. The zone is diluted in the sample waste as a pure buffer enters the channel intersection from horizontal arms.
The pull back current prevents the sample leakage from arising in the separation step. The current density is applied in the upper and lower arms and pulls the sample from the injection cross back to the vertical arms. This is, along with the constraint stream, assumed to affect the separation of the analytes.
Both λ_{inj} and λ_{sep} are variable in the steps given above. Thus, sixty-six simulations are carried out and their results investigated.
For an easy overview we denote the simulations according to the scheme $\lambda_{inj} \rightarrow \lambda_{sep}$. For instance, the simulation employing $\lambda_{inj} = 0.583$ and $\lambda_{sep} = 0$ is denoted as $0.583 \rightarrow 0$.

4.4.2.5 Results

Zero constraint current density leaves the horizontal arms blind in the injection step - no electric field is in this region (Fig. 25, left panel). Current densities in upper and lower arm attain the same value.
Non-zero constraint current density values make the horizontal arms active and, thus, a stronger electric field is in the lower arm (Fig. 25, right panel). This dilutes the sample.
Although there is no field strength in the horizontal arms when no constraint current is applied, the diffusion tends to spread the analytes into this region (Fig. 26, left panel). The steady state is never reached as the diffusion operates permanently. This makes the separation worse as a longer sample plug is injected into the separation channel.
The constraint current confines the sample stream and reduces the diffusion effect (Fig. 26, right panel). This reduces the sample plug width injected into the separation channel. However, the sample concentration is lowered. This can possibly make the detection limit worse.

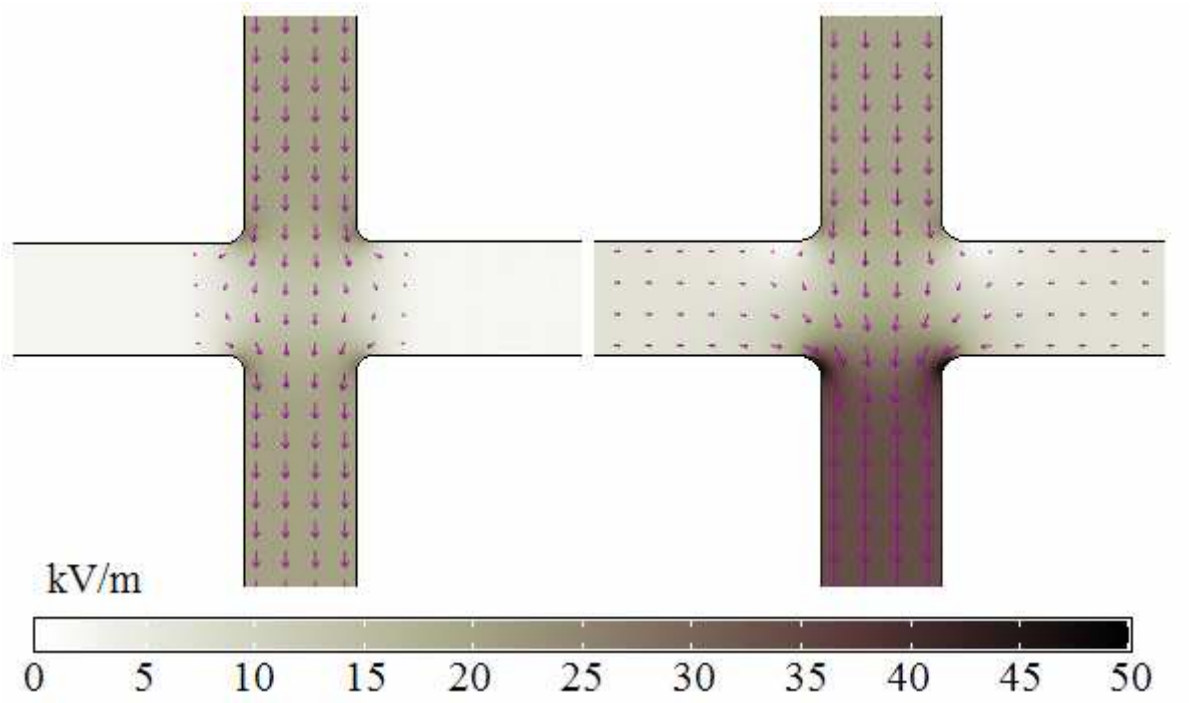

Fig. 25. Electric field distribution in injection step (t = 4 s) for 0 → 0 (left picture) and 0.333 → 0 (right picture). Arrows indicate the electric field strength vector. No field is in the horizontal arms when no constraint current is employed. Conversely, considerable field is in this region when constraint current is applied.

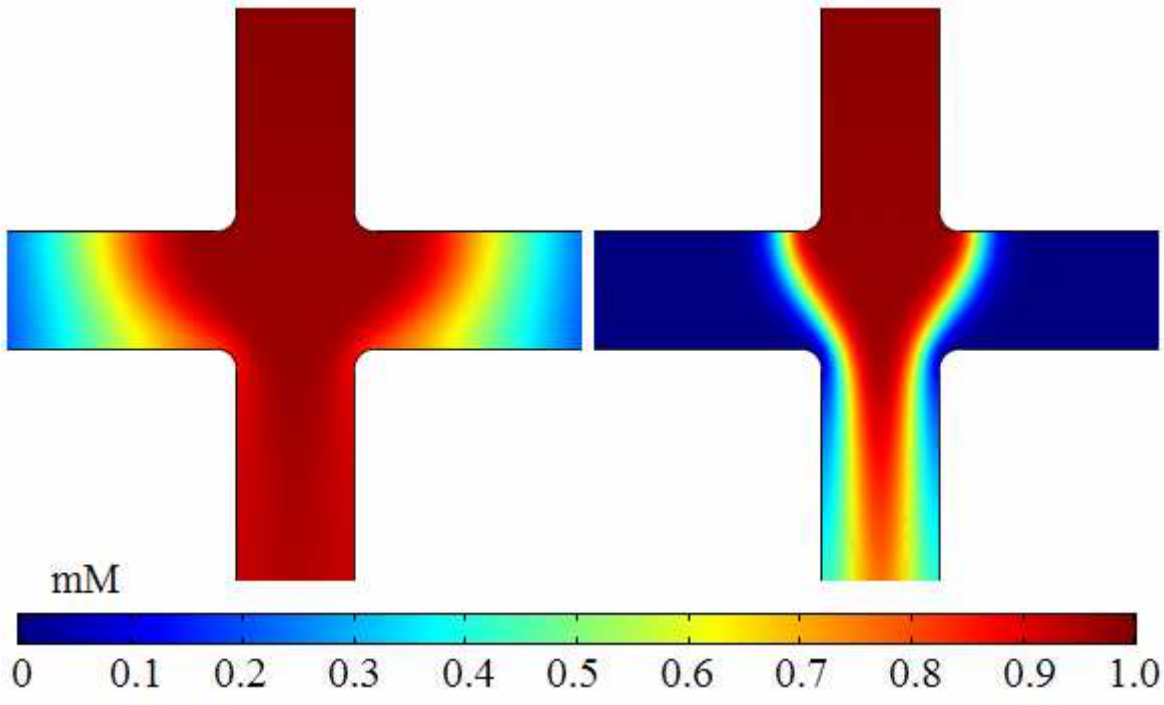

Fig. 26. Concentration profile of A_4 at t = 4 s. All analytes have the same concentration profiles in the injection step as they have equal mobilities as long they are in the vertical arm. The diffusion is of high significance (to be seen in left picture) when no constraint current is employed (0 → 0). Non-zero constraint current (right picture) confines the sample stream (0.333 → 0). The analytes are diluted in the sample waste arm.

The injection step is first five seconds. This time is found to be sufficiently long to reach the steady state for all constraint current density values employed (apart from the zero one). The electric field distribution is changed at 5 s (the change lasts 100 μs) and the separation step starts (lasts next 25 seconds). At the very first moment of the separation step, the sample stream is pulled from the channel intersection and forms the sample plug in the separation channel. The pull back current density is the quantity that is variable (Fig. 27) in the separation step. When no pull back current is applied, the diffusion causes the sample leakage from the vertical channel into the separation channel. The pull back current reduces the extent of this phenomenon as it diverts the sample into the sample reservoir and the sample waste (Fig. 28).

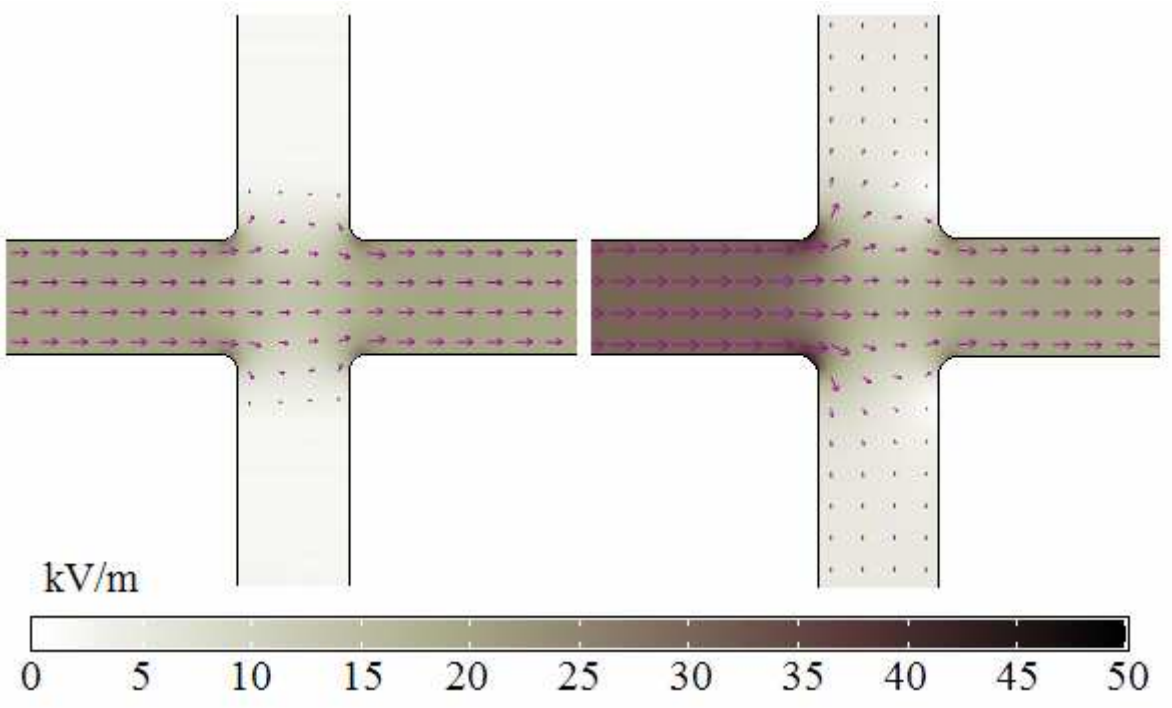

Fig. 27. Electric field distribution in the separation step (t = 6 s). No electric field is in the vertical arms (left picture) when no pull back current is employed (0 → 0). On the other hand, the electric field is in this region (right picture) when pull back current is applied (0 → 0.250).

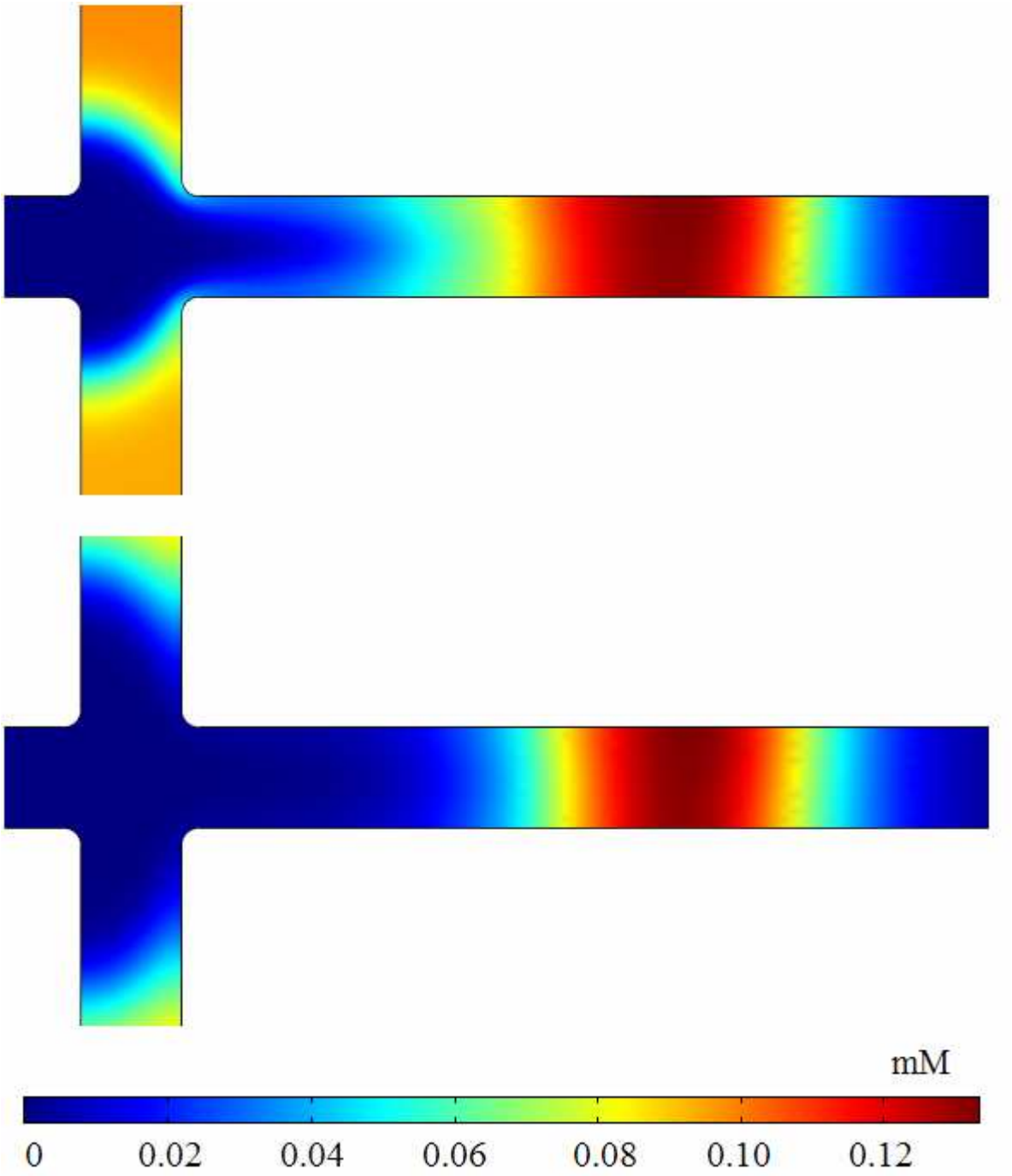

Fig. 28. Concentration profiles of A_4 at t = 5.7 s for 0 → 0 (the upper picture) and 0 → 0.250 (the lower picture). When no pull back current is applied the injected plug has a tailing shape as the analytes leak from the injection channel by the diffusion. The pull back current prevents the leakage from arising. In both cases, the analytes tend to concentrate at the start of the separation channel as there is a decrease in their mobility due to gel sieving environment.

The mobility of the analytes decrease when they enter the gel region due to sieving. Thus, they slow down at the gel edge and tend to enhance the concentration here (Fig. 29). This process is called the stacking. This may possibly increase the detection sensitivity as a zone of higher concentrations is supposed to reach the detector site. The analyte A_1 has the highest mobility change and its stacking is, thus, the most pronounced.

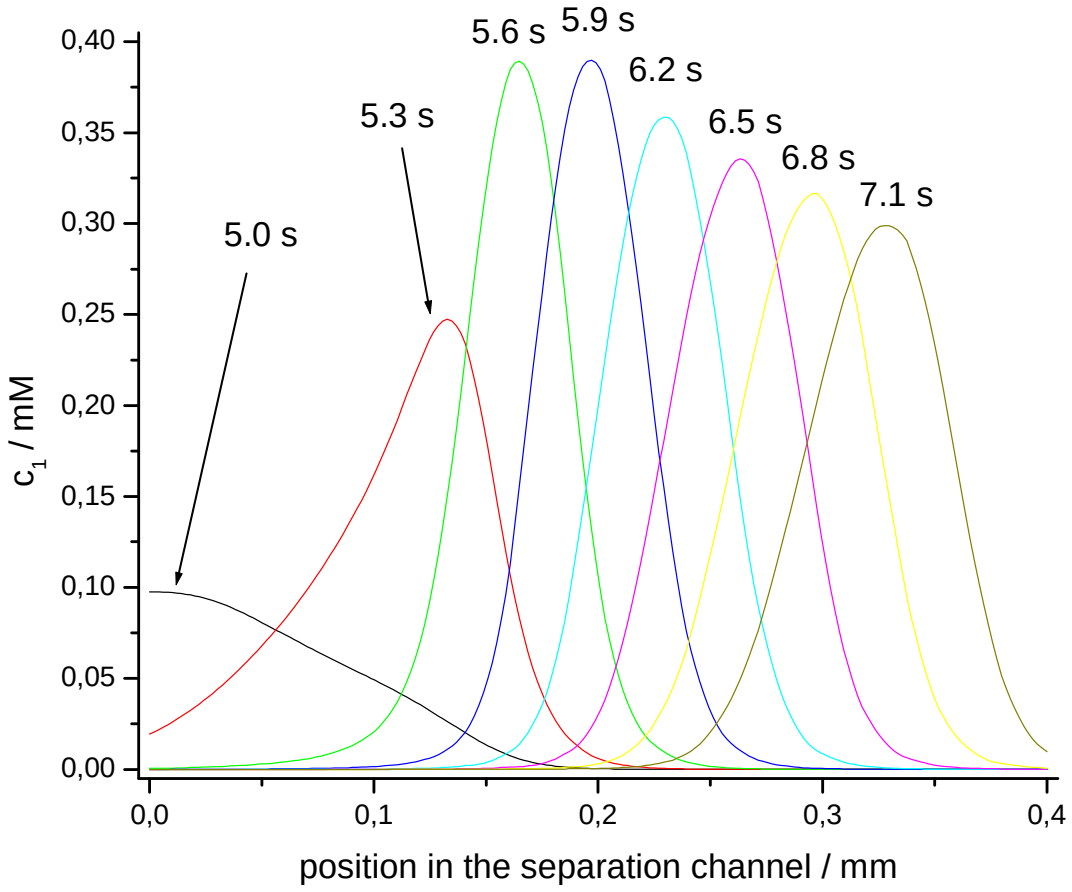

Fig. 29. Stacking of the analyte A_1 at the edge of the gel in the separation channel. The analyte concentration increases and its zone becomes more narrow. The concentration reaches its maximum at ~5.7 s and becomes four times higher than that in the sample reservoir. This effect may significantly enhance the detection sensitivity. Simulation conditions: 0 → 0.250. As a pull back current is employed, there is no sample leakage and the resulting peak is of nearly Gaussian shape.

It should be noticed that the sample injection is discriminative as the analytes have different mobility changes in the gel environment. The fastest analyte (A_4) has always of the lowest concentration. Conversely, the slowest has the highest concentration (Fig. 30).

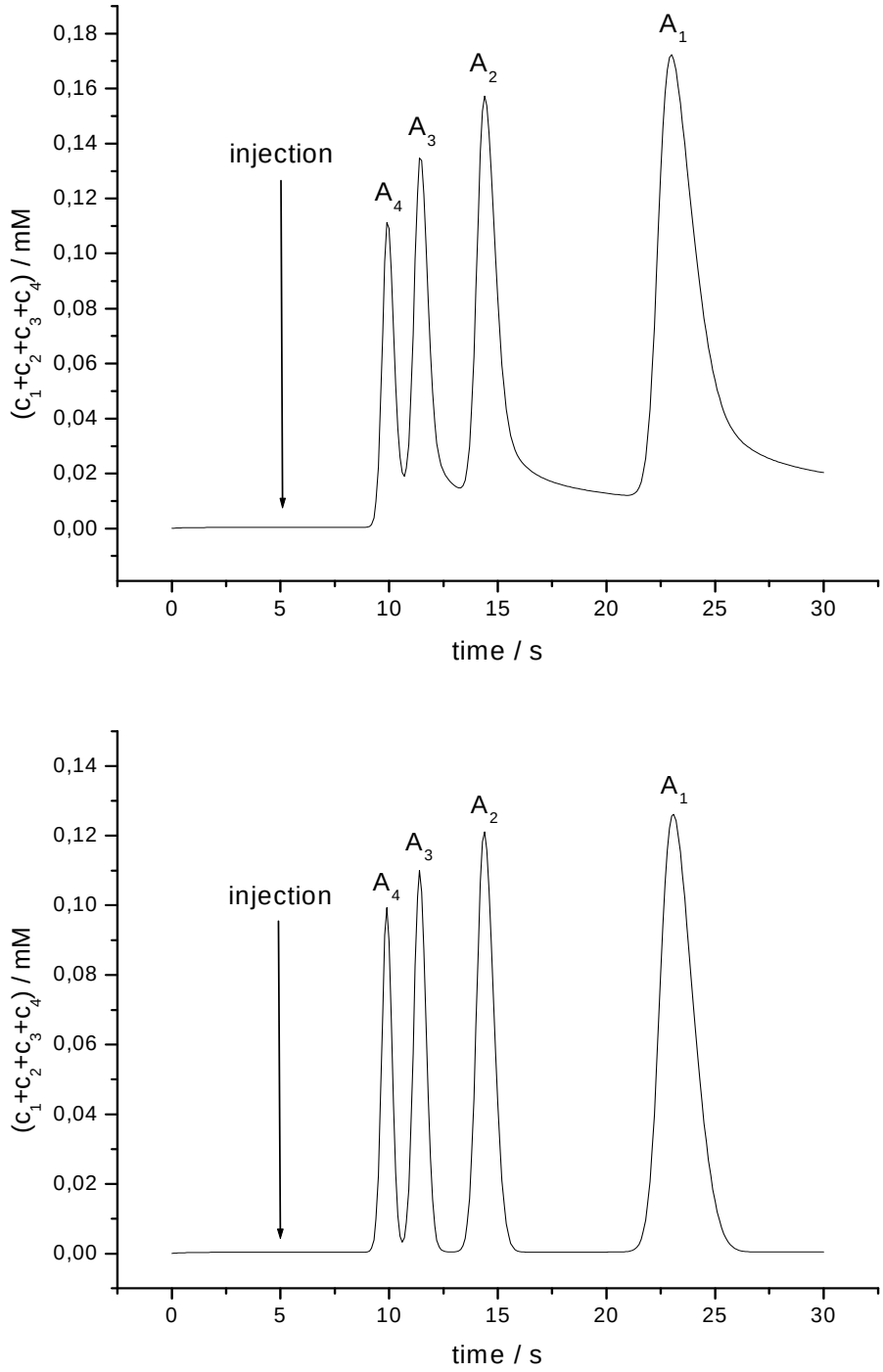

Fig. 30 Simulated electropherograms.
(A): Separation of analytes when no constraint and pull back currents (0 → 0) are employed. A strong leakage causes tailing peaks that deteriorate the analysis.
(B): The pull back current (0 → 0.250) strongly reduces the leakage and peaks are of Gaussian shape. The migration time of the analytes is the same as the electric field of constant strength is in the separation arm in all simulations. Notice that the peak heights are lowered when the pull back current is applied.

Migration times of the analytes have always the same values in all simulations (Fig. 30). This is in accordance with the constant field strength value that is in the separation arm in the separation step. The analytes A_3 and A_4 were selected to be investigated in terms of resolution. The resolution may be defined as

$$R_{3,4} = 1{,}18\frac{t_3 - t_4}{(w_3)_{1/2} + (w_4)_{1/2}} \tag{147}$$

Here t_3, t_4 and $(w_3)_{1/2}$, $(w_4)_{1/2}$ denote the migration times and full widths at half peak maxima, respectively, of the analytes A_3 and A_4.

One more quantity was defined *ad hoc* to describe the peak resolution. It resembles the above definition but employs the peak width at 5% of the its height

$$R^*_{3,4} = 2\frac{t_3 - t_4}{(w_3)_{1/20} + (w_4)_{1/20}} \tag{148}$$

This quantity is believed to describe the effect of the peak tailing. The peak shape can be evaluated by the asymmetry factor

$$(A_{F,i})_{1/20} = \frac{b_i}{a_i} \qquad a_i + b_i = (w_i)_{1/20} \qquad i = 3{,}4 \tag{149}$$

Here, a_i and b_i denote the horizontal distance from the peak maximum to the peak start and its end at 5% of its height, respectively.

Another quantity worth studying is the amount of the analyte that is injected into the separation channel. The concept of the peak areas is inapplicable here as there may happen the conditions where peaks never reach zero signal due to the constant diffusion leakage from the vertical channel. Rather, the concept of peak heights is utilized. In particular, we define the average concentration

$$\langle c \rangle_D = \frac{c_{3,D} + c_{4,D}}{2} \tag{150}$$

Here, $c_{3,D}$ and $c_{4,D}$ stand for the maximum concentrations of the analytes at the detector site.

Both $R_{3,4}$ and $R^*_{3,4}$ as well as $\langle c \rangle_D$ are wished to be as high as possible. Thus, we define the products $R_{3,4}\langle c \rangle_D$ and $R^*_{3,4}\langle c \rangle_D$ as criteria to find the optimal conditions for the analysis (Figs. 31, 32, 33,.34, 35 and 36).

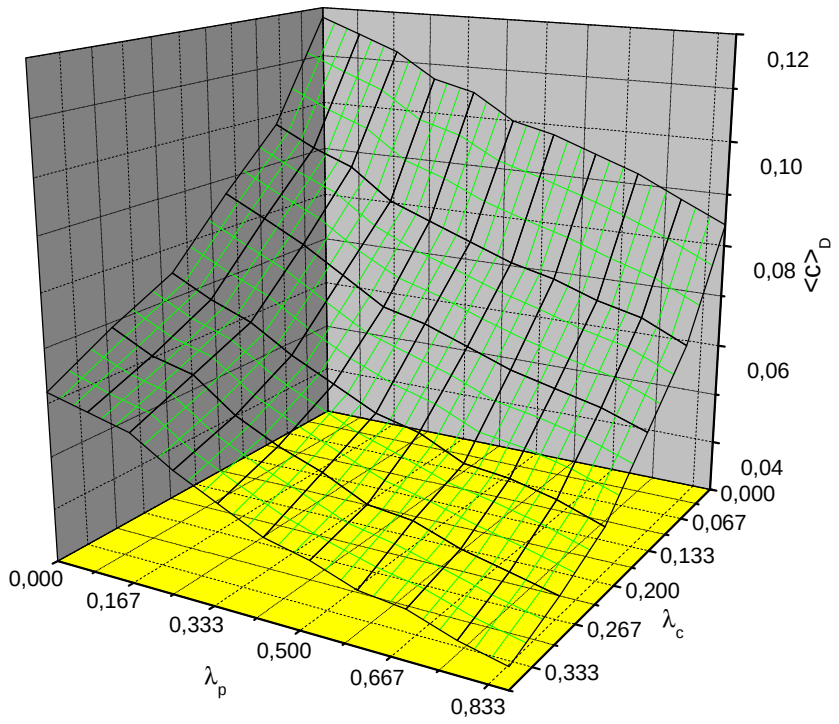

Fig. 31 Average concentration at the detector site $<c>_{D.}$ The arrangement $0 \rightarrow 0$ offers the highest possible concentration of the analytes to be injected into the separation channel. Both pull back and constraint currents tend to decrease the injected amount.

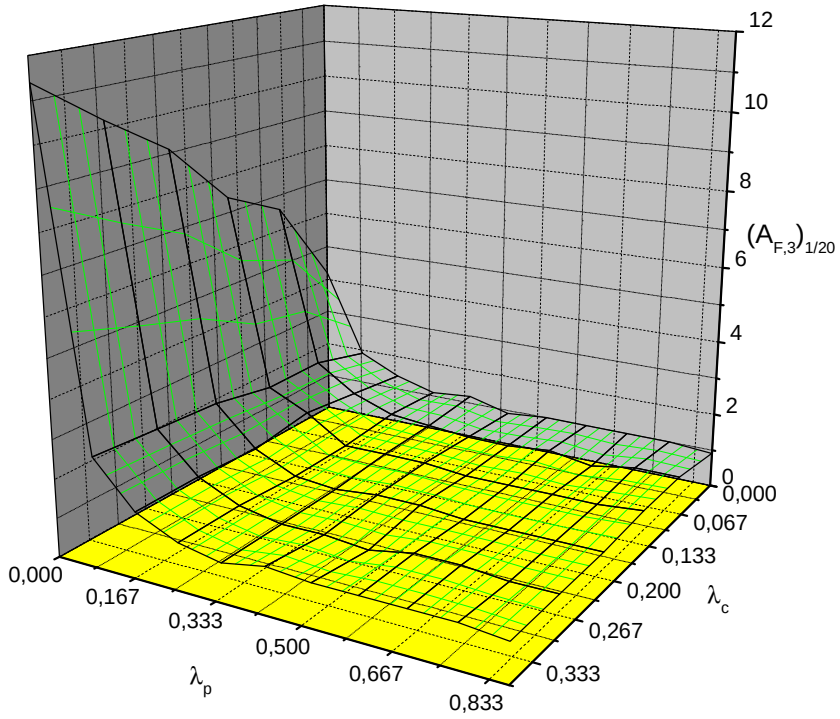

Fig . 32 Asymmetry factor $(A_{F,3})_{1/20}$ (determined at 5 % of the peak height). The peaks are symmetrical when pull back current density is high. (Evaluated for A_3.)

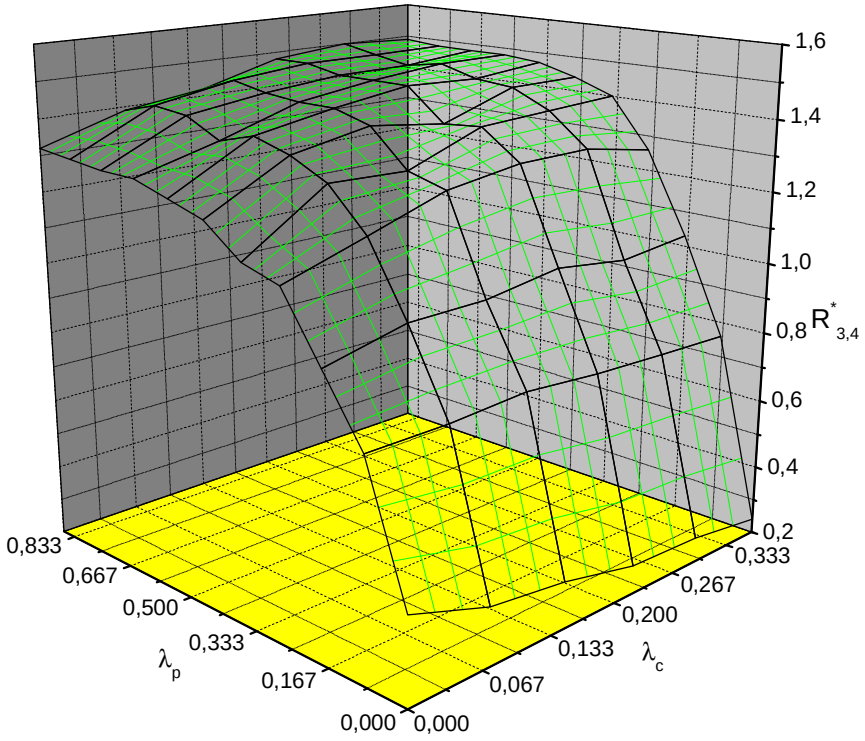

Fig. 33 The resolution $R^*_{3,4}$. Separation is enhanced when strong pull back current is applied. Dependence on the constraining current value is lesser.

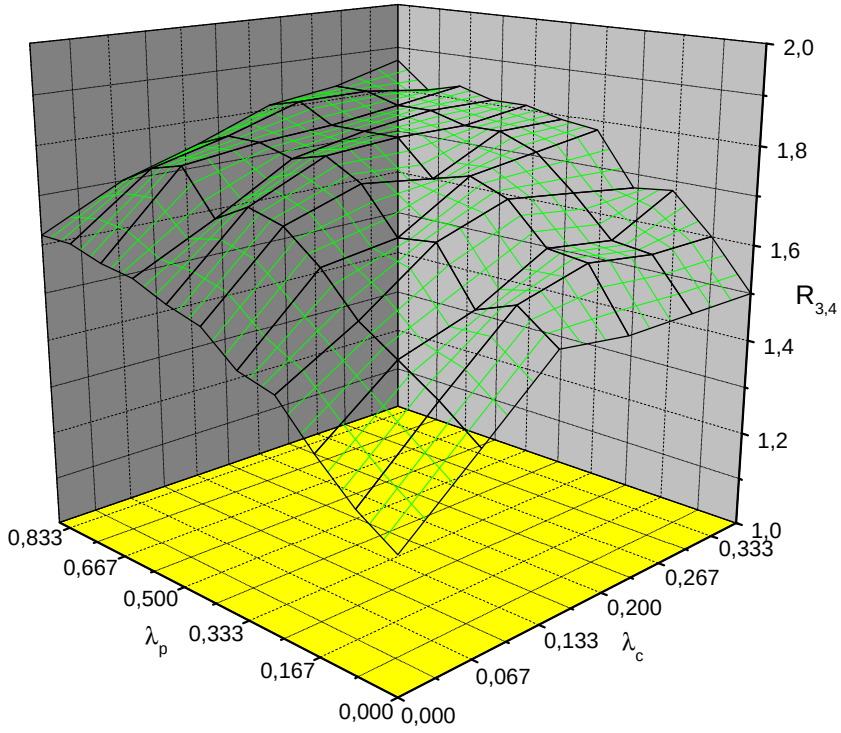

Fig. 34 The resolution $R_{3,4}$. Both constraint and pull back current tend to enhance the resolution.

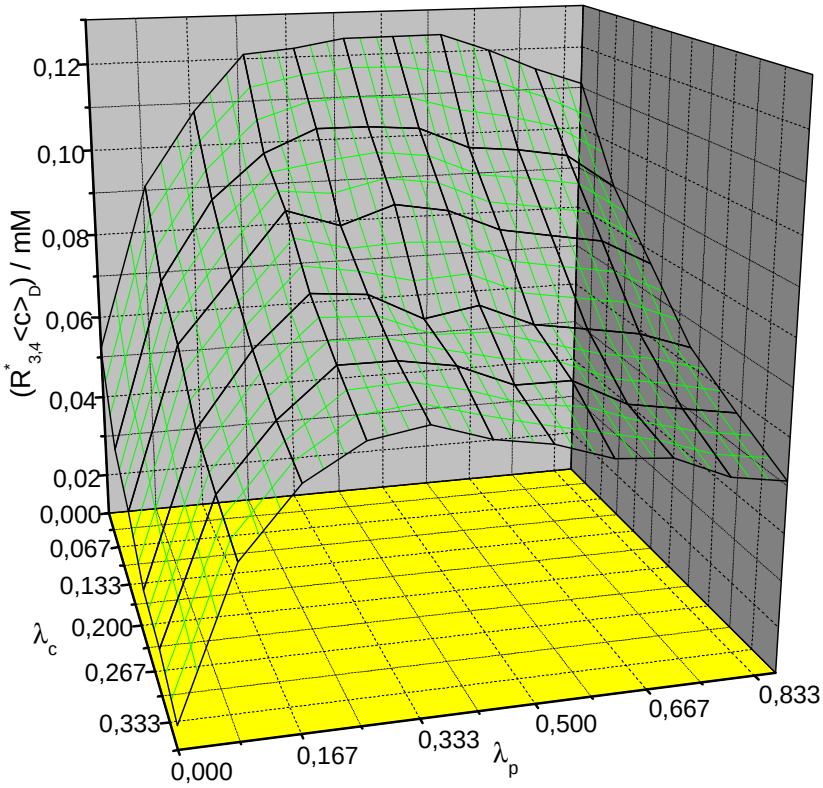

Fig. 35 The criterion $R^{*}_{3,4}\langle c\rangle_D$ *. Its value reaches the best value approximately at* $0 \to 0{,}417$ *.*

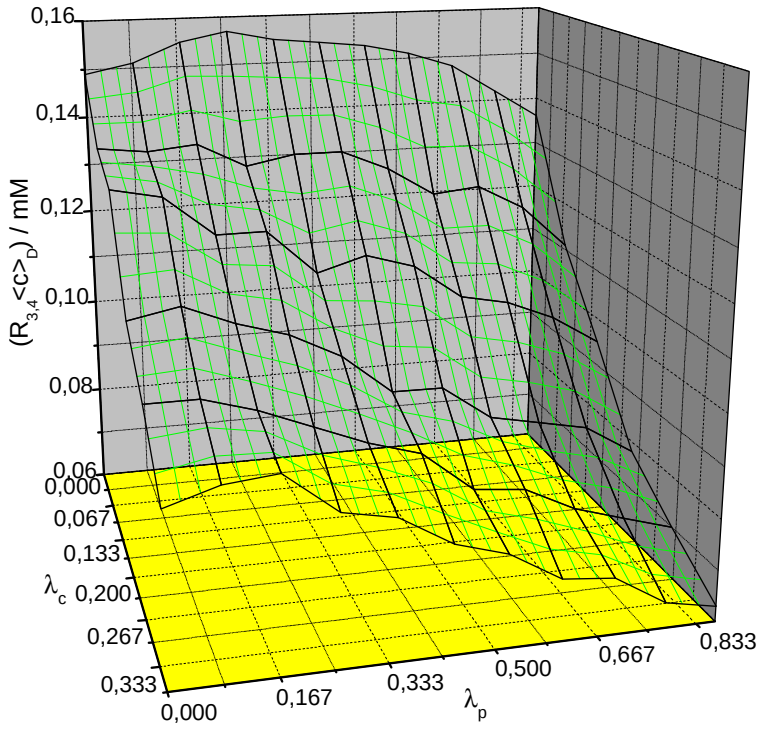

Fig . 36 The criterion $R_{3,4}\langle c\rangle_D$ *. The optimal value is at* $0 \to 0{,}167$ *.*

It has already been mentioned that the analytes are stacked when reaching the gel area in the separation channel. On the other hand, application of the constraining current or the pull back current decreases the injected amount (defined by Eq. (150) and to be seen in Fig. 31). Well resolved are to be found when a strong pull back current is applied.

Peak resolution $R_{3,4}$ (defined by Eq. (147)) shows only small absolute differences in the results (Fig. 34). This is what can be expected as the peak tailing tends to affect its lower part rather than its middle part (where the peak width is evaluated). On the contrary, higher differences are found in $R^{*}_{3,4}$ values (defined by Eq. (148)) as the peak width is assessed at 5 % of the peak height where the peak tailing is more pronounced (Fig. 33).

All this is related to the peak symmetry (Eq. (149). Symmetrical peaks are achieved when strong pull back currents are applied (Fig. 32).

Although there is a small discrepancy when using either $R_{3,4}\langle c\rangle_D$ or $R^{*}{}_{3,4}\langle c\rangle_D$, both approaches show the same qualitative results (Figs. 35, 36). Both criteria reach the maxima when no constraint current and moderate pull back current is applied.

This, strong constraint currents are meaningless to be imposed as they do not significantly enhance the resolution. Moreover, they make the detection limit worse as the smaller amount of the sample is injected. On the other hand, constraint current may be used when the detection limit is not the issue.

Pull back current is more appropriate to be used as it significantly enhances the resolution. However, its high values also decrease the injected sample amount.

This should be considered as the main result of this part of the thesis. The finite difference method enables one to find the best conditions for the analysis. The input data (analyte mobilities, their *pK* constants and the geometry arrangement) can be modified to investigate any particular lab-on-a-chip analysis.

4.4.3 Electromigration in Free-flow Electrophoresis

This method is employed when pure analytes are wished to result from the separation. Unlike the capillary methods, preparative amounts of analytes may be injected and separated. The method is based on the bulk-flow stream that delivers a mixture to the separation system. In it, perpendicularly imposed electric field diverts the charged species away from the course of the bulk flow. In principle, both cationic and anionic species can be treated at the same time. As the presented device is of small dimensions, it may be employed as a part of a separation chip.

4.4.3.1 Geometry

A separation chamber of rectangular shape is a main part of the device (Fig. 37). In its top part, fifteen channels feed it with the background electrolyte. Additionally, one channel contains a dissolved mixture to be separated (it is denoted by the red rectangle in Fig. 1). In the lower part of the chamber, fifteen channels divert the separated analytes to the collecting vessels (not considered in the model).
The chamber width is merely 590 μm. Its height is 300 μm. The width of the channels is 30 μm and their mutual distance is 10 μm. The chamber depth is supposed to be uniform and, thus, a 2-D model is employed.

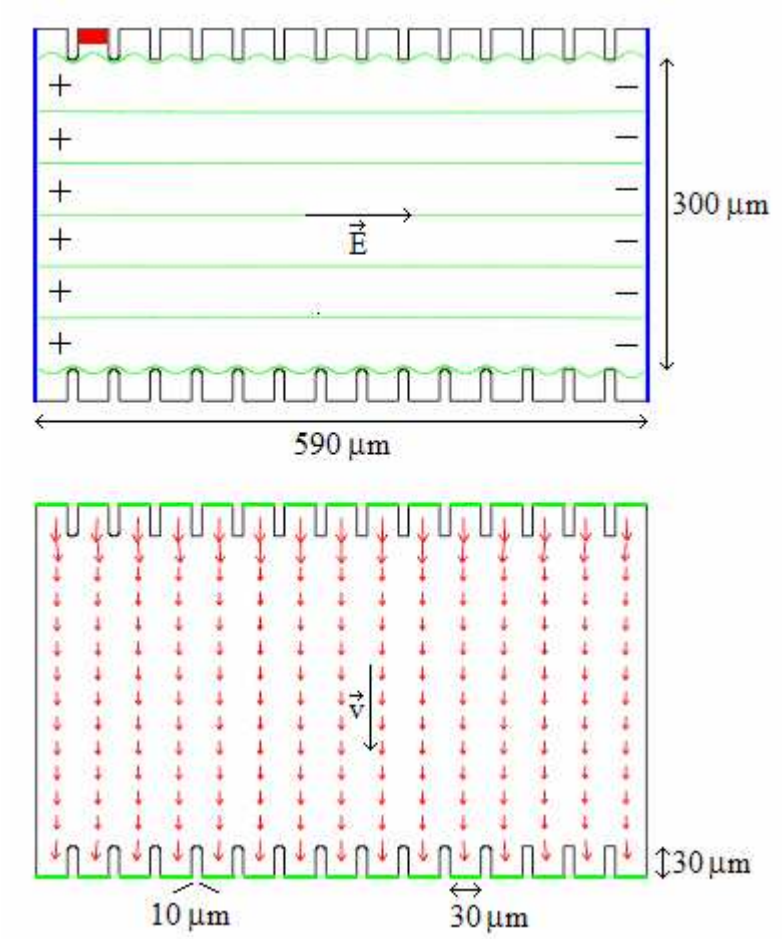

Fig. 37 Free-flow analyzer. The upper panel shows the electric field distribution. The green lines represent the electric field streamlines. The blue vertical walls denote the electrodes. Black-colored boundaries are non-conductive.
The lower panel shows the bulk flow velocity profile. Arrows indicate the velocity vector. Green (virtual) boundaries represent the inflow and the outflow channels. Here, the liquid is allowed to cross the boundary. The rest of system boundaries are impermeable (denoted by black colour).

4.4.3.2 BGE and Analytes

For the sake of simplicity, the buffer is of the same composition as it is in the simulations dealing with the separation in the injection cross (see Tab. 2 for a deeper

insight). The three weak cationic analytes (of mobilities 10, 20 and 30 e.u.) are considered. They match that ones in the injection cross section in their acid-base properties.

4.4.3.3 Electric field

The separation is carried out in the constant voltage mode. Two vertical chamber walls serve as the electrodes (denoted as blue lines in the upper panel in Fig. 37). Here, the constant Dirichlet boundary conditions are imposed. The rest of system boundaries are non-conductive (black walls). The zero Neumann boundary condition is imposed here.

4.4.3.4 Bulk Flow

As usual, the velocity profile is calculated by means of the Navier-Stokes equations. The inflow and the outflow channels are substituted by the virtual boundaries where the velocity vector is dictated by the constant Dirichlet boundary condition (denoted green). The upper channels serve as liquid reservoirs whereas the lower ones act as liquid sinks. The no slip boundary condition is imposed on all other walls (denoted black). No liquid may penetrate the boundary here.

4.4.3.5 Results

Besides the electrophoretic mobility, both the electric field strength value $\left|\vec{E}\right|$ and the bulk flow velocity value $\left|\vec{v}\right|$ affect the trajectory of the species in the chamber. In particular, the ratio of these two variables dictates the position analytes as they runs out of the chamber.
There is one more variable that is substantial for the resolution of the analytes – their residence time τ. It is given by

$$\tau = \frac{h}{\left|\vec{v}\right|} \tag{151}$$

Here h = 300 μm denotes the vertical distance traveled by the species and equals the chamber height. Short resident times prevent the diffusion from deteriorating the analysis (see Figs. 38 and 39).
As the chamber dimensions are very small, the steady state flow profile is achieved very quickly (after several hundreds of milliseconds). The total amount of the separated substances is dictated by the separation time that may be much greater than the residence time of analytes.

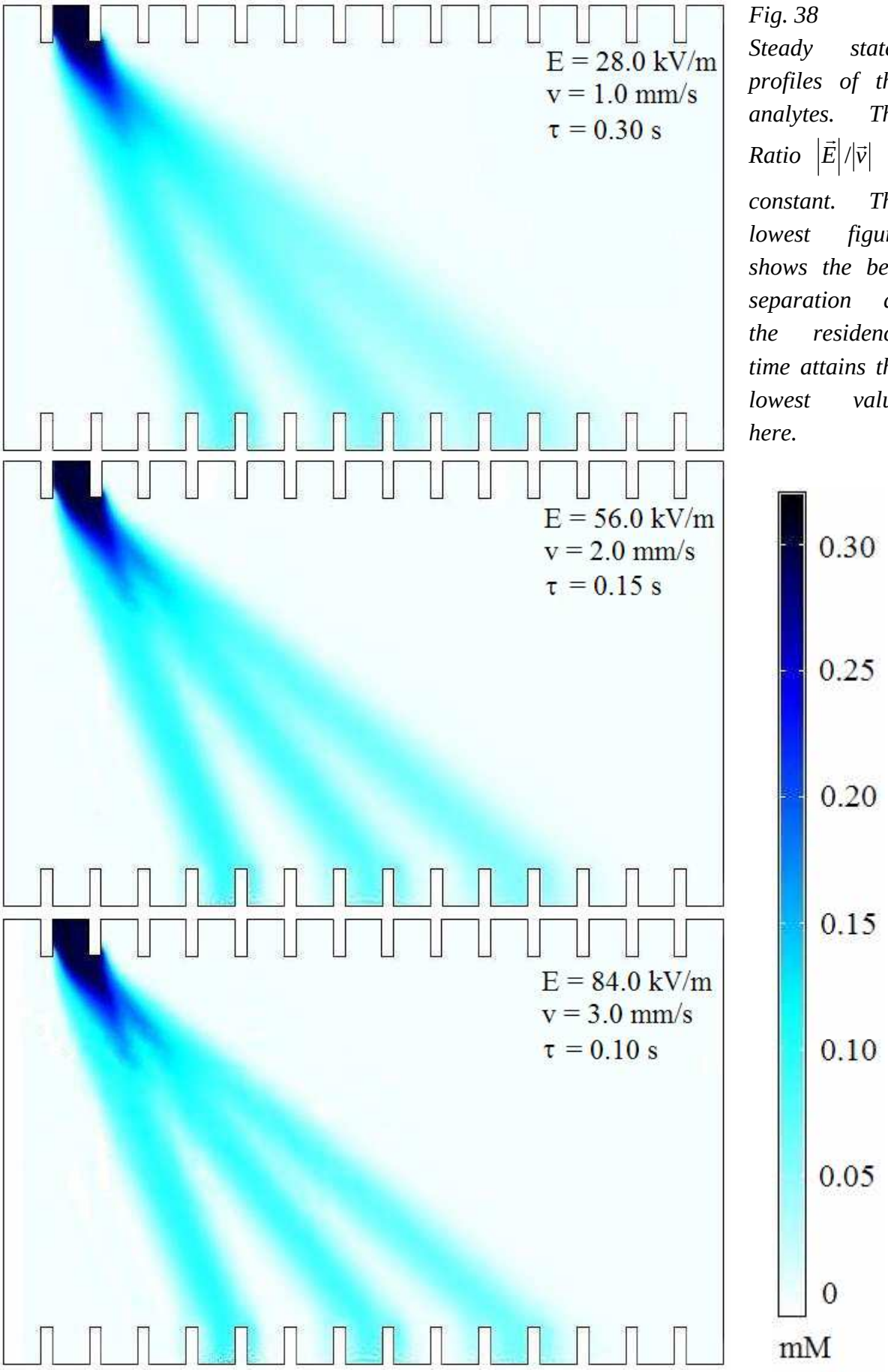

Fig. 38
Steady states profiles of the analytes. The Ratio $|\vec{E}|/|\vec{v}|$ *is constant. The lowest figure shows the best separation as the residence time attains the lowest value here.*

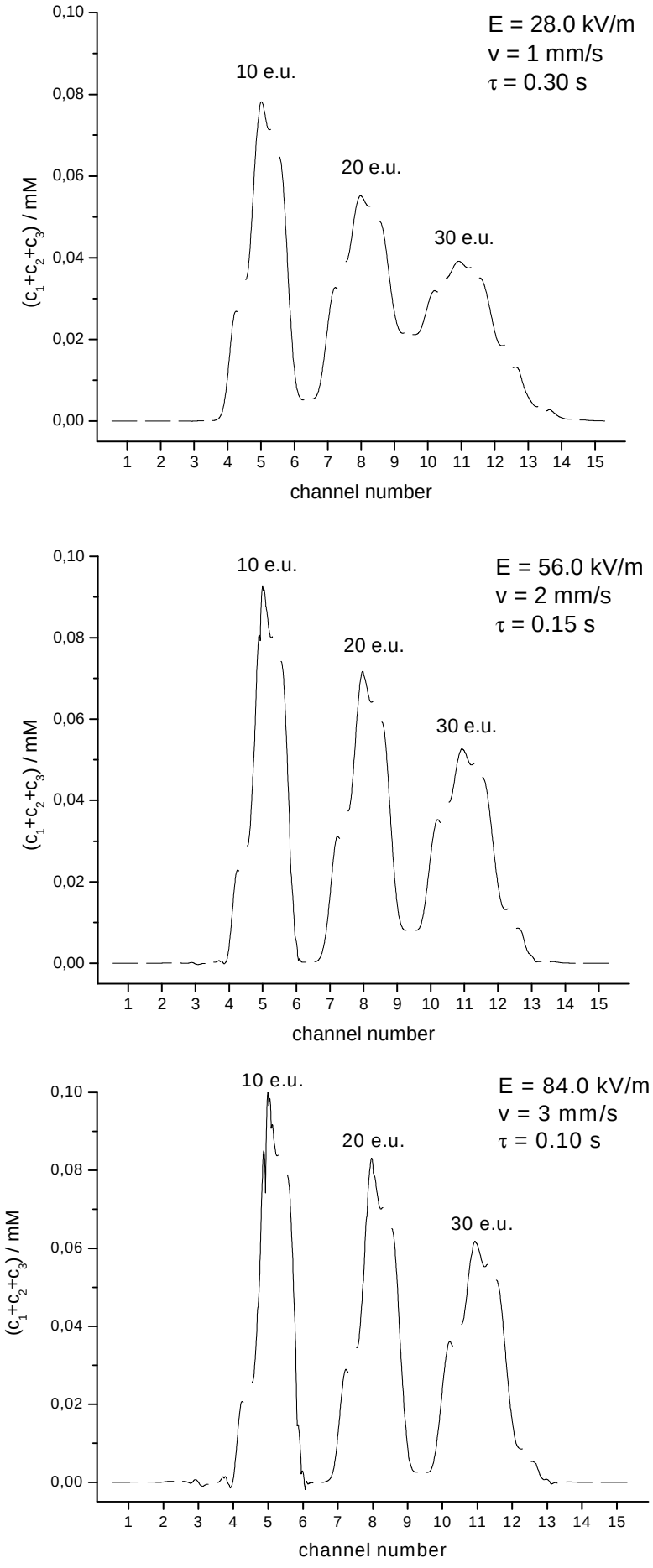

Fig 39. Pictures show the steady-state separation of the analytes. The numbers denote the position of outflow channels. The best resolution is achieved in the lowest picture where the highest field strength and bulk flow velocity values are applied.

4.4.4 Joule Heating in Electrophoresis

The temperature rises as the electric current passes through an electrolyte. This is known as Joule heating. This part of the thesis shows the possibility of simulating this phenomenon. In particular, capillary cooling by the aid of air and water (coolants) is investigated here.

4.4.4.1 Geometry

The capillary is of the main interest as Joule heating originates here (see Fig. 40).

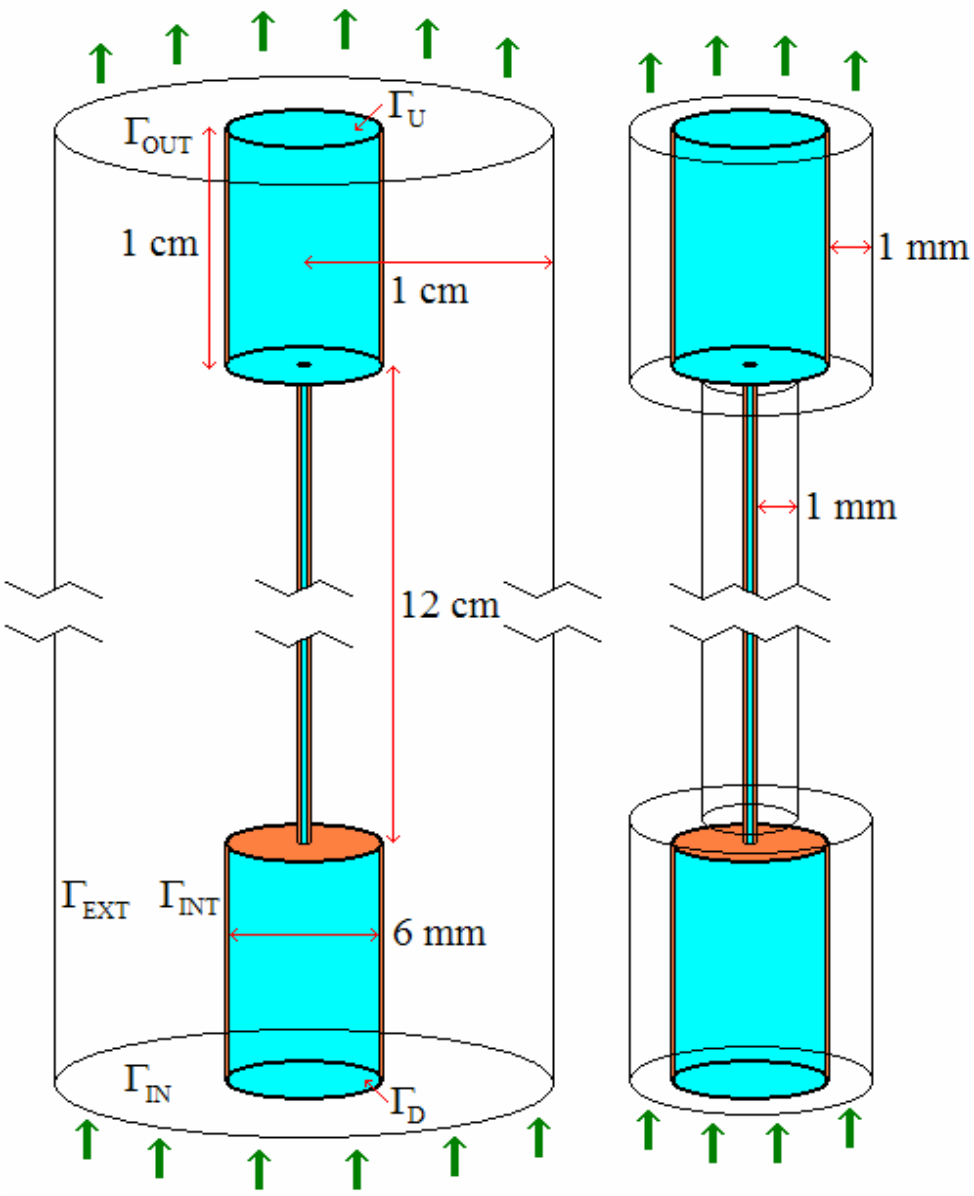

Fig. 40 Two geometry arrangements: I (left picture) and II (right picture). The blue colour is used to denote the region filled with the background electrolyte. Orange colour depicts the silica glass region. Colourless regions denote the coolant (either water or air). Green arrows indicate the entry and the exit of the coolant.

Its inner and outer diameter is 75 μm and 365 μm, respectively. Thus, the capillary wall thickness is 145 μm. The capillary length is 12 mm and both its ends are connected to vessels. The vessel diameter is 6 mm and its height is 1 cm. For the sake of simplicity, the vessel wall is of the same thickness as the capillary wall.
The two particular geometries are considered. The first arrangement (denoted *I* in Fig. 40) deals with the capillary and the vessels immersed in the figure of cylindrical shape of uniform radius (1 cm). In the second arrangement (*II*), the capillary and the vessels are immersed in the figure that leaves a gap (of size 1 cm) around them. In both cases, the figure is filled either by air or by water.

4.4.4.2 Symmetry

The geometry is of cylindrical shape and, thus, the cylindrical symmetry is employed.

4.4.4.3 Background Electrolyte

The capillary and the vessels are filled with the BGE. It is composed of phosphoric acid and potassium. Both BGE constituents are regarded as weak electrolytes (Tab. 3). No analyte is considered.

Tab. 3

	c/mM	u(+1)/e.u	u(-1)/e.u	u(-2)/e.u	u(-3)/e.u	pK(+1)	pK(-1)	pK(-2)	pK(-3)
K^+	7.5	76.2	-	-	-	13.0	-	-	-
Ph.	5.0	-	34.6	61.4	71.5	-	2.16	7.21	12.67

Ph. – Phosphate
e.u. – electrophoretical unit

4.4.4.4 Assumptions

The BGE composition is supposed to be maintained in time. This can be achieved by employing virtual buffer reservoirs connected to both upper and the lower vessel through the outer horizontal vessel boundary parts Γ_U and Γ_D (circle surfaces, see Fig. 40).
The continuity equations for potassium and phosphate as well as the electric field distribution are not solved in the walls and in the coolant region. They are only solved in the capillary and in the vessel region. Moreover, as the buffer composition is supposed to be constant, these equations need not be solved in time. Their stationary state solution is calculated at $t = 0$ and is employed in the time propagation.
The heat transfer equation and the Navier-Stokes equations are solved in entire computational domain. The Navier-Stokes equations are not solved in time as the profile of applied coolant flow is supposed to be constant in time. It means that the heat transfer equation is the only equation solved in time. It accounts for both thermal diffusion and thermal convection. The

Joule heating is the only heat source considered in the model. No thermal sinks are taken into account. No ionic strength correction and EOF is considered.

4.4.4.5 Electric Field

The analysis is carried out in the constant voltage mode. The field strength attains the value 40.0 kV/m in the capillary region. It is not supposed to change in time as no changes in the BGE composition are assumed.

4.4.4.6 Boundary Conditions

The mixed boundary condition is stated to the mass conservation laws for both BGE constituents. In particular, the constant Dirichlet BC is imposed on the outer horizontal vessel boundary parts (Γ_U and Γ_D). The zero Neumann condition is imposed on the capillary and rest vessel boundary parts (internal boundary parts collectively denoted Γ_{INT}) and, thus, no matter may penetrate through these boundary parts.
The boundaries Γ_U and Γ_D serve as the upper and the lower electrode, respectively. Thus, the constant Dirichlet BC is imposed here when dealing with the electric field distribution. The zero Neumann BC is imposed on Γ_{INT} as these walls are supposed to be non-conductive.
As no bulk flow is considered in the capillary, no external force is imposed in the capillary and vessels when solving the Navier-Stokes equations. The neutral BC is imposed on Γ_U and Γ_D. The no slip BC is imposed on Γ_{INT} and Γ_{EXT}. The inflow velocity BC determines the velocity profile on the inflow boundary part Γ_{IN} (the coolant enters the computational domain through its lower part). The normal flow BC is imposed on Γ_{OUT}.
No thermal insulation or heat discontinuity effects are considered. The constant temperature BC is imposed on Γ_{IN}, Γ_{OUT}, Γ_D and Γ_U as the system is supposed to be placed in the infinitely large surrounding of constant temperature (T_0 = 298.15 *K*). The heat continuity BC is imposed on the internal boundaries Γ_{INT}.
As usual, the zero Dirichlet BC stated to the electroneutrality condition is imposed on all boundary parts.

4.4.4.7 Physical Properties of Materials

For the sake of simplicity, all physical properties of the materials are taken as temperature-independent. The property values hold for 298.15 *K*. However, the model can also, in principle, handle the physical properties that depend on temperature.

Density of water (applied also to the phosphate buffer) is $\rho(H_2O)$ = 996.8 $kg.m^{-3}$.
Density of silica glass is $\rho(glass)$ = 2203 $kg.m^{-3}$.
Air is supposed to obey the ideal gas law and, thus, its density is given by

$$\rho(air) = p_0 M / RT_0 = 1.19\ kg.m^{-3} \qquad (152)$$

The air is assumed to be pumped under constant (atmospheric) pressure p_0 = 101325 *Pa*. Average molar mass of the air is M = 29,0.10^{-3} *kg.mol*$^{-1}$.

Dynamic viscosity of water (or of phosphate buffer) is $\eta(H_2O)$ =9,13.10^{-4} *Pa.s*.
Dynamic viscosity of glass is a quantity that is very difficult to be determined. The value $\eta(glass)$ = 1 *Pa.s* is employed here. This value is supposed to be sufficiently high to prevent any flow from arising in the glass region.
Dynamic viscosity of air is $\eta(air)$ = 1,77.10^{-5} *Pa.s* (this value holds for 101325 *Pa*).

Thermal conductivity of water (or phosphate buffer) is $\lambda(H_2O)$ =0,616 *W.m*$^{-1}$*.K*$^{-1}$.
Thermal conductivity of glass is $\lambda(glass)$ = 1.38 *W.m*$^{-1}$*K*$^{-1}$.
Thermal conductivity of air is $\lambda(air)$ = 0.0262 *W.m*$^{-1}$*K*$^{-1}$ (holds for 101325 *Pa*)

Specific heat capacity (at constant volume) of water (also applied to phosphate buffer) is $c_v(H_2O)$ = 4200 *J.kg*$^{-1}$*K*$^{-1}$.
Specific heat capacity of glass is $c_v(glass)$ = 703 *J.kg*$^{-1}$*K*$^{-1}$.
Specific heat capacity of air is $c_v(air)$ = 1100 *J.kg*$^{-1}$*K*$^{-1}$.

It should be mentioned that the values of density, dynamic viscosity, thermal conductivity and specific heat capacity are taken from the database of Comsol Multiphysics 3.3 Program. The values were also discussed with Ref. [13].

4.4.4.8 Results

Geometry arrangement I
In this geometry, the velocity field tends to create the vortex above the lower vessel (Fig. 41). The coolant velocity attains low values in the upper part of the capillary and, thus, convective heat flow is ineffective here. The heat cumulates here and the temperature change is pronounced mainly in this region.

Geometry arrangement II
This geometry arrangement was selected to be analyzed in detail. Fig. 42 shows the velocity and temperature profile when the air is used as a coolant. The air cooling works more effectively in this geometry arrangement as the air flows directly around the capillary where the heat is produced. As seen from Fig. 43, the water cooling works even more effectively. In both types of cooling, the temperature tends to decrease as the coolant flows faster. Fig. 44 shows the temperature profile across the BGE, the capillary wall and the coolant (air is employed). A parabolic profile is found in the BGE region whereas it is of logarithmic shape in the glass and in the coolant region.

It should be mentioned that higher coolant velocities were not able to be investigated because of computational problems that arose when solving the stationary Navier-Stokes equations.

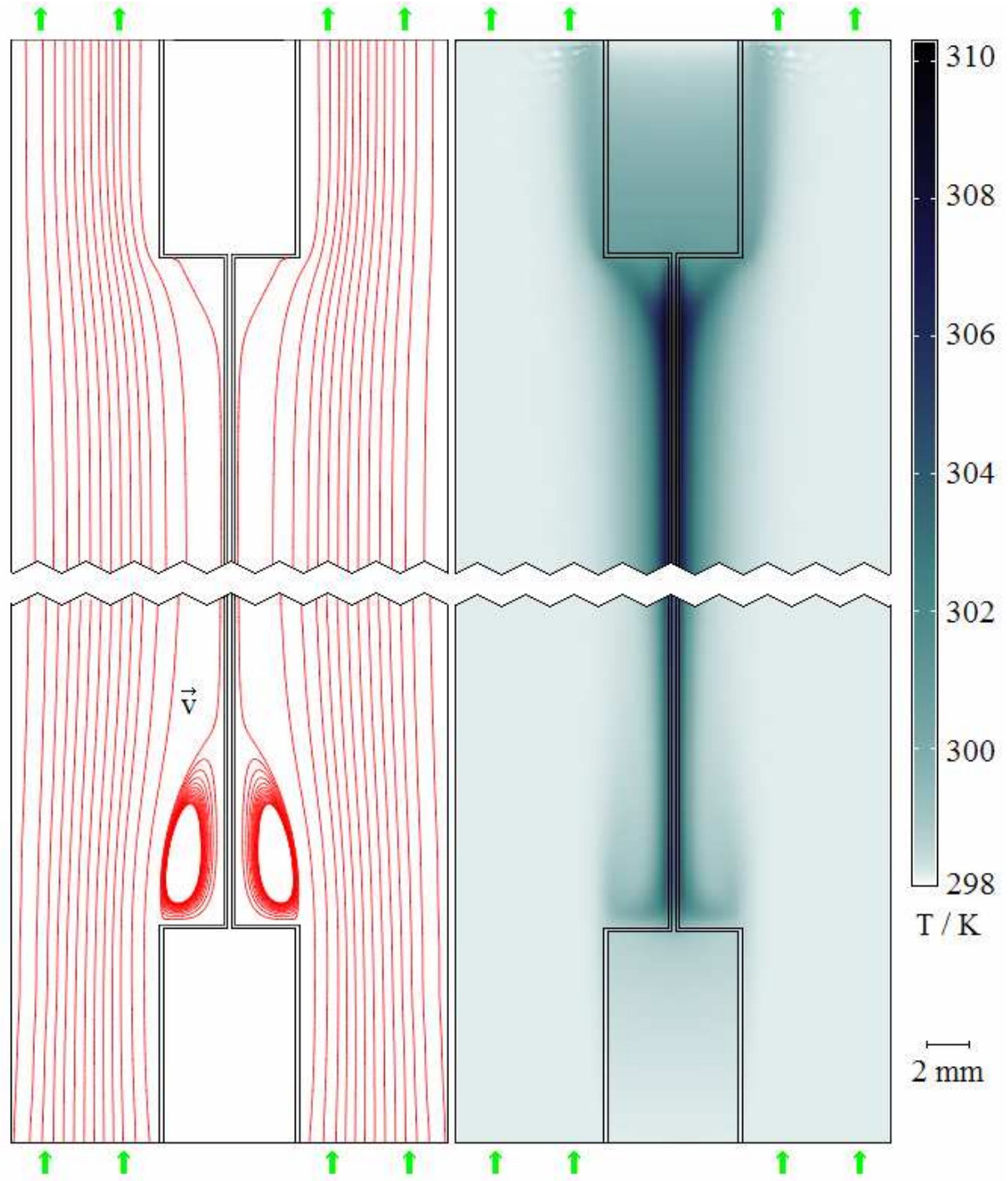

Fig. 41. Geometry arrangement I with air cooling. Velocity field streamlines (left picture) and temperature map (right picture) are pictured. The velocity field tends to create vortex above the lower vessel. Temperature attains its maximum value in the upper part of the capillary as the air cooling is not effective here. Green arrows indicate the entry and the exit of the coolant. Air inflow velocity: 0.5 m/s

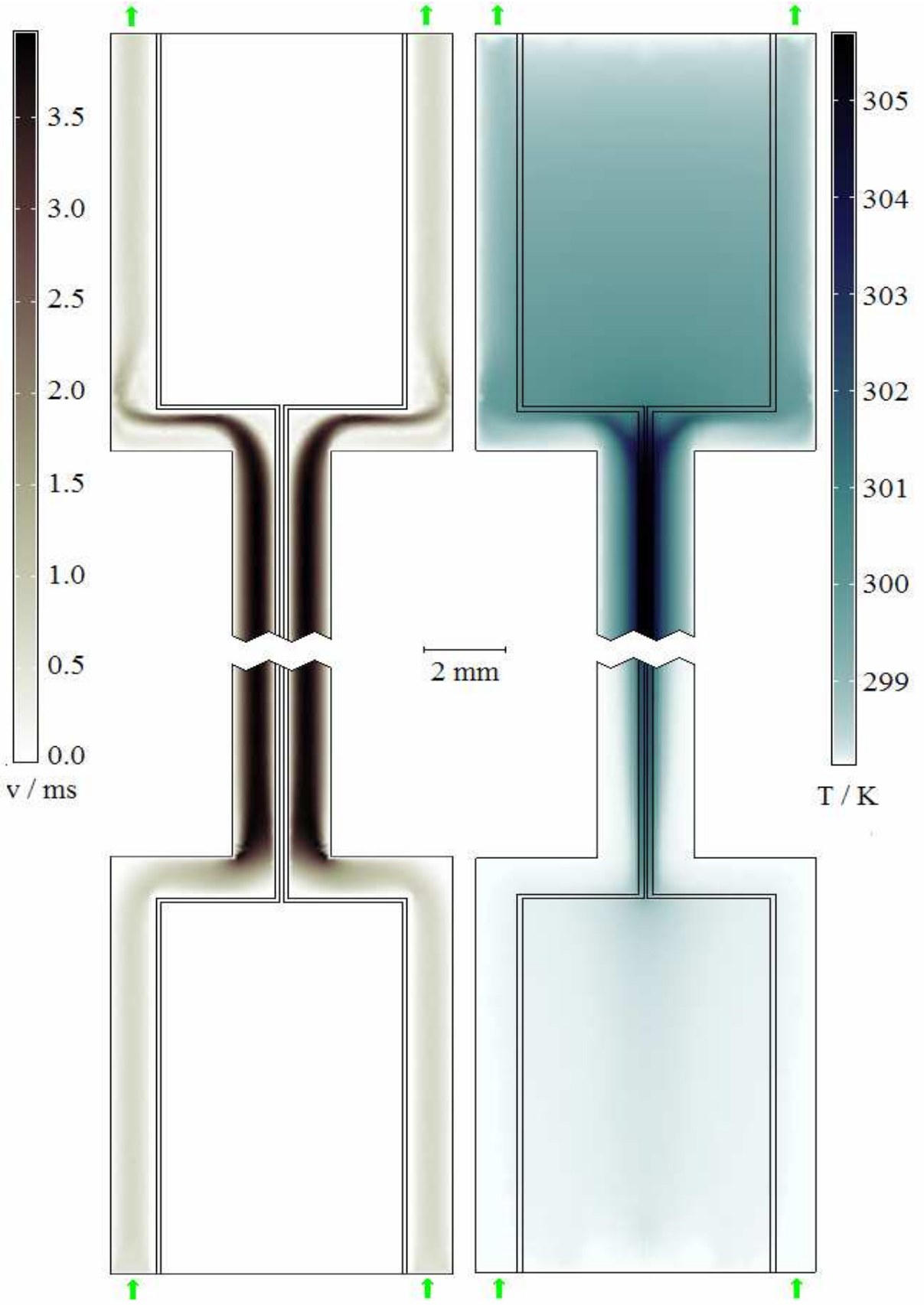

Fig. 42. Geometry arrangement II with air cooling. Velocity value (left picture) and temperature map (right picture) are pictured. Green arrows indicate the entry and the exit of the coolant. No vortices originate in the airflow in this geometry. Air inflow velocity: 0.5 m/s

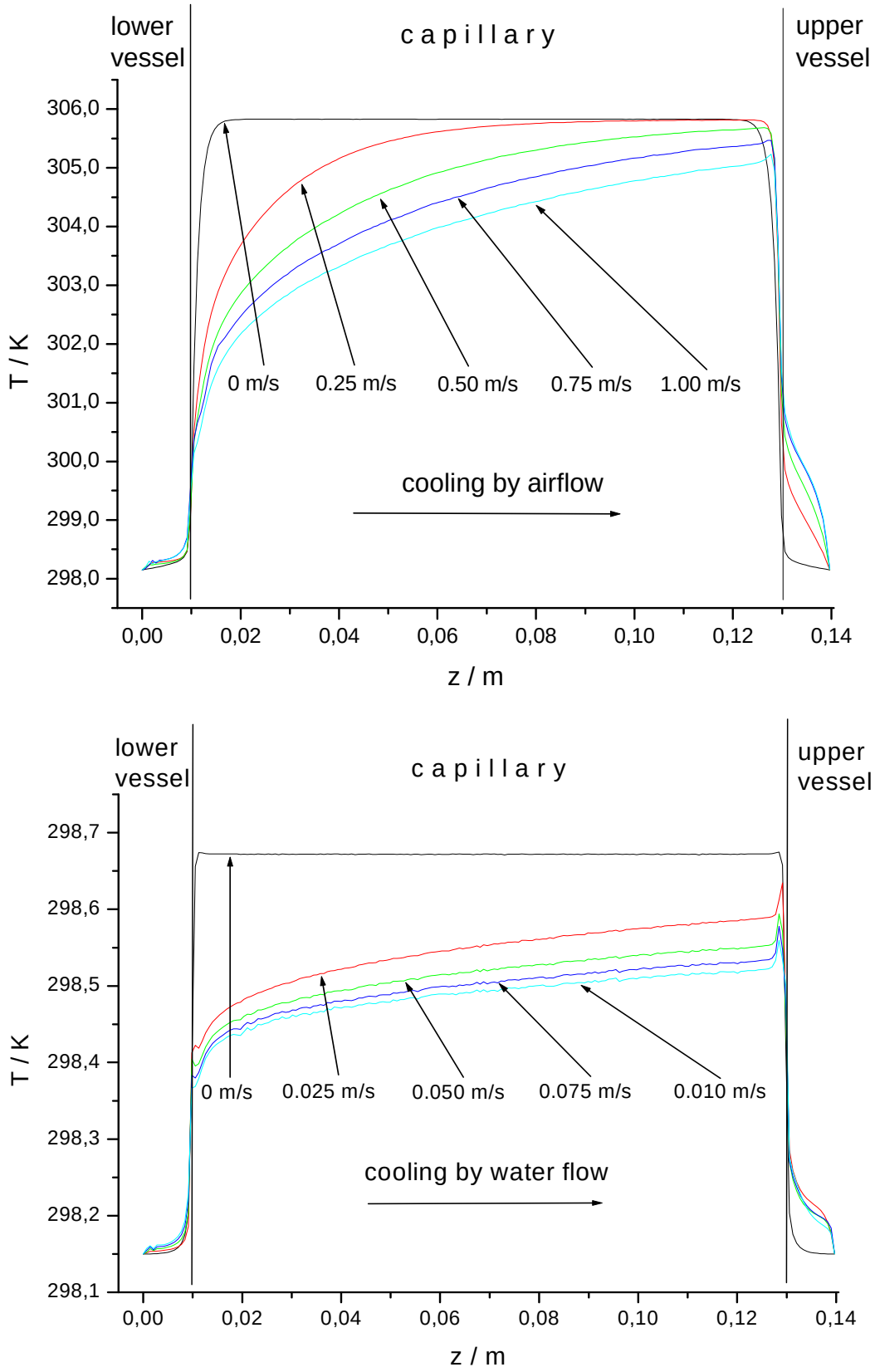

Fig. 43 Axial temperature profiles (at the centre of the capillary and the vessels) for air (upper picture) and water (lower picture) cooling at various velocities. The water cooling works very effectively. In both types of cooling, the temperature decreases as the coolant flows faster. Notice the difference in temperature scales in the pictures.

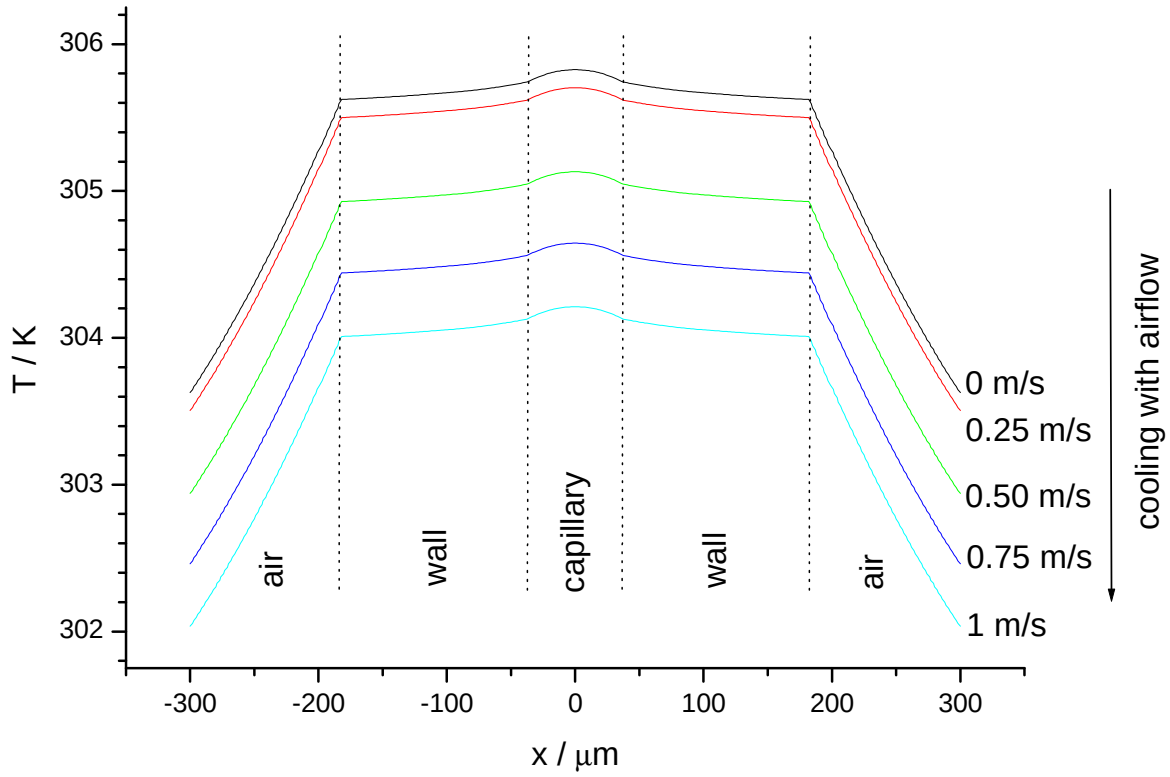

Fig. 44 Temperature profiles across the BGE, capillary wall and coolant (at the centre of the capillary) at various velocities. Temperature decreases as the coolant flows faster. A parabolic temperature profile is found in the BGE region whereas the capillary wall and the coolant region are of logarithmic temperature profiles. The air was used as a coolant.

5 Concluding Remarks

The presented thesis shows the ability of simulating 2-D and 3-D electrophoretic tasks by means of the finite element method. The introduced computational model handles many kinds of phenomena encountered in real experiments in electrophoresis. Four particular tasks are chosen to be solved.

The first task focuses on the electrophoresis in the 3DCE equipment. Changes in the electrolyte composition due to electrolysis are investigated. The sodium/acetic buffer is selected as a representative buffer example. The acetate ion tends to cumulate in the vicinity of the positively charged electrode. On the other hand, sodium ion moves away. The pH value decreases in the vessel and, subsequently, also in the capillary. The extent of this change is inspected. The arrangement with the capillary hidden in the electrode shows fast pH changes as no hindrance is placed between the electrode and the capillary inner region. The arrangements with long capillary tips require much longer times to alter the buffer pH in the capillary region. The bulk flow driven by electroosmosis is also investigated. Electroosmotic flow of upward direction (assessed in the capillary) speeds up the pH change as an altered buffer is pumped into the capillary by convection. On the contrary, reversed EOF slows down the pH change. This kind of simulation may be useful when planning a new geometry arrangement for the electrophoresis.

The second task deals with the injection cross that is a common part of separation microdevices. The task shows that the simulation can also be carried out in the constant current mode. The resolution of analytes is inspected under various conditions. Optimal conditions for the analysis are found. The task demonstrates the importance of constraint current and pullback current in the lab-on-a-chip analysis. They control the analyte concentration in the separation and they can also avoid the peak tailing that originates due to the diffusion. The presented computational model is also able to handle more complicated chip structures (results not shown).

The third task concerns the free-flow electrophoresis equipment. It can possibly be used also as a chip structure. The simulations reveal spatial profiles of the analytes under various conditions. This kind of simulation may be useful when searching for a free-flow device of appropriate dimensions as well as when optimizing the free-flow separation.

The fourth task focuses on the temperature effects in the capillary. The simulations reveal stationary temperature profiles in two particular geometry arrangements. The temperature rises as the electric current passes through the electrolyte. Furthermore, the air and the water cooling are inspected. The temperature decreases as a coolant flows faster around the capillary. The water cooling is more effective than that employing the air. This kind of simulation may be of great interest when heat-sensitive analytes are to be separated.

The finite element method is a powerful tool when solving the tasks in the natural sciences, especially in the physics. The presented thesis would like to show that it can also lend a helping hand when solving the tasks in electrophoresis. I believe that the introduced mathematical model will be further improved and applied also to other tasks that deal with the computer simulations of experiments in electrophoresis.
Last of all, I suppose that I have fulfilled all the aims of the presented thesis.

6 References

[1] W. Thormann, R. A. Mosher, Electrophoresis 6 (19-85) 413-418

[2] R. A. Mosher, D. Dewey, W. Thormann, W. Saville, M. Bier, Anal.Chem 61 (1989) 362

[3] R. A. Mosher, D. A. Saville W. Thormann, The Dynamics of Electrophoresis, VCH, Weinheim, New York, Basel, Cambridge, 1992

[4] B. Gaš, J. Vacík, I. Zelenský, J. Chromatogr. 545 (1991) 225-237

[5] C. Schwer, B. Gaš, F. Lottspeich, E. Kenndler, Anal.Chem. 65 (1993) 2108-2115

[6] E. V. Dose, G. A. Guiochon, Anal.Chem. 63 (1991) 1063-1072

[7] S. V. Ermakov, O. S. Mazhorova, M. Y. Zhukov, Electrophoresis 13 (1992) 838-848

[8] S. V. Ermakov, M. S. Bello, P. G. Righetti, J. Chromatogr. A 661 (1994) 265-278

[9] J. H. P. A. Martens, J. C. Reijenga, J. H. M. T. Boonkkamp, R. M. M. Mattheij, F. M. Everaerts, J.Chromatogr. A 772 (1997) 49-62

[10] N. Ikuta, T. Hirokawa, J. Chromatogr. A 802 (1998) 49-57

[11] J. C. Reijenga, E. Kenndler, J. Chromatogr. A 659 (1994) 403-415

[12] J. C. Reijenga, E. Kenndler, J. Chromatogr. A 659 (1994) 417-426

[13] P. W. Atkins et al., Physical Chemistry

[14] B. Gaš, P. Coufal, M. Jaroš, J. Muzikář, I. Jelínek, J. Chromatogr. A 905 (2001) 269-279

[15] F. Kohlrausch, Ann. Phys. 62 (1897) 209-239

[16] P. Gebauer, P. Borecká, P. Boček, Anal.Chem. 70 (1998) 3397

[17] P. Gebauer, P. Boček, Anal. Chem. 69 (1997) 1557-1563

[18] P. Gebauer, P. Pantůčková, P. Boček, Anal.Chem. 71 (1999) 3374-3381

[19] M. Jaroš, K. Včeláková, I. Zusková, B. Gaš, Electrophoresis 23 (2003) 2667-2677

[20] L. Onsager, Physik. Z. 27 (1926) 388-392

[21] L. Onsager, Physik. Z. 28 (1927) 277-298

[22] L. Onsager, R. M. Fuoss, J. Phys. Chem. 36 (1932) 2689-2778

[23] H. Poppe, J.Chromatogr. 506 (1990) 45-60

[24] H. Poppe, Anal.Chem. 64 (1992) 1908-1919

[25] G. J. M.Bruin, A. C. van Asten, X. Xu, H. Poppe, J.Chromatogr. 608 (1992) 97-107

[26] X. Xu, W. Th. Kok, H. Poppe, J.Chromatogr. A 742 (1996) 211-227

[27] H. Poppe, J. Chromatogr. A 831 (1999) 105-121

[28] J. Crommen, G. Schill, D. Westerlund, L. Hackzell, Chromatografia 24 (1987) 252

[29] P. Gebauer, C. Desiderio, S. Fanali, P. Boček, Electrophoresis 19 (1998) 701

[30] M. Horká, K. Šlais, Electrophoresis 21 (2000) 2814-2827

[31] M. Štědrý, M. Jaroš, B. Gaš, J.Chromatogr. A 960 (2002), 187-198

[32] M. Štědrý, M. Jaroš, K. Včeláková, B. Gaš, Electrophoresis 24 (2003) 536-547

[33] F. E. P. Mikkers, F. M. Everaerts, T. P. E. M. Verheggen, J. Chromatogr. 169 (1979) 1-10

[34] E. S. Yeung, W. G. Kuhr, Anal.Chem. 63 (1991) 275A-282A

[35] J. L. Beckers, Chromatogr. A 679 (1994) 153-165

[36] P. Gebauer, P. Boček, J. Chromatogr. A, 772 (1997) 73-79

[37] C. Desiderio, S. Fanali, P. Gebauer, P. Boček, J. Chromatogr. A 772 (1997) 81-89

[38] M. Macka, P.R. Haddad, P. Gebauer, P. Boček, Electrophoresis, 18 (1997) 1998-2007

[39] J. L. Beckers, J. Chromatogr. A 844 (1999) 321-331

[40] P. Gebauer, P. Boček, Electrophoresis 21 (2000) 2809-2813

[41] P. Gebauer, P. Pantůčková, P. Boček, J.Chromatogr. A 894 (2000) 89-93

[42] P. Boček, P. Gebauer, J. L. Beckers, Electrophoresis 22 (2001) 1106-1111

[43] J. L. Beckers, P. Gebauer, P. Boček, J. Chromatogr. A 916 (2001) 41-49

[44] J. L. Beckers, P. Boček, Electrophoresis 23 (2002) 1942-1946

[45] J. L. Beckers, Electrophoresis 22 (2001) 2684-2690

[46] M. Štědrý, M. Jaroš, V. Hruška, B. Gaš, Electrophoresis 25 (2004) 3071-3079

[47] M. Jaroš, V. Hruška, M. Štědrý, I. Zusková, B. Gaš, Electrophoresis 25 (2004) 3080-3085

[48] T. Hirokawa, Y. Kiso, J. Chromatogr. 248 (1982) 341-362

[49] T. Hirokawa, M. Nishimo, N. Aoki, Y. Kiso, Y. Sawamoto, T. Yagi, J. Akiyama, J. Chromatogr. 271 (1983) D1-D106

[50] T. Hirokawa, T. Gojo, Y. Kiso, J. Chromatogr. 369 (1986) 59-81

[51] T. Hirokawa, T. Gojo, Y. Kiso, J. Chromatogr. 390 (1987) 201-223

[52] T. Hirokawa, Y. Kiso, B. Gaš, I. Zusková, J. Vacík, J. Chromatogr. 628 (1993) 283-308

[53] K. Včeláková, I. Zusková, E. Kenndler, B. Gaš, Electrophoresis 25 (2004) 309-317

[54] P. C. Haarhoff, H. J. van der Linde, Anal. Chem. 38 (1966) 573-582

[55] V. Hruška, M. Jaroš, B. Gaš, Electrophoresis 27 (2006) 984-991

[56] http://www.natur.cuni.cz/~gas

[57] K. Rektorys, Survey of Applicable Mathematics, Iliffe Books, London 1969

[58] A. Ralston, A First Course in Numerical Analysis. McGrawHill, New York 1985

[59] S. V. Ermakov, M. Y. Zhukov, L. Capelli, P. G. Righetti, Electrophoresis 19 (1998) 192

[60] S. V. Ermakov, M. Y. Zhukov, L. Capelli, P. G. Righetti, Anal.Chem. 66 (1994) 4034-4042

[61] B. Gaš, E. Kenndler, A. Rizzi, M. Štědrý, Electrophoresis 16 (1995) 958-967

[62] S. V. Ermakov, M. Y. Zhukov, L. Capelli, P. G. Righetti, J.Chromatogr. A 699 (1995) 297-313

[63] B. Gaš, J. Chromatogr. 644 (1993) 161-174

[64] R. L. Williams, B. Childs, E.V. Dose, G. Guiochon, G. Vigh, Anal.Chem 69 (1997) 1347-1354

[65] V. Hruška, M. Jaroš, B. Gaš, Electrophoresis 27 (2006) 513-518

[66] D. J. Harrison, A. Manz, Z. Fan, H. Lüdi, H. M. Widmer, Anal.Chem. 64 (1992) 1926

[67] A. Manz, D. J. Harisson, E. M. J. Verpoorte, J. C. Fettinger, A. Paulus, H. Lüdi, H. M. Widmer, J. Chromatogr. 593 (1992) 253

[68] C. S. Effenhauser, A. Manz, H. M. Widmer, Anal.Chem. 65 (1993) 2637

[69] K. Seiler, D. J. Harisson, A. Manz, Anal.Chem 65 (1993) 1481

[70] D. J. Harisson, K. Fluri, K. Seiler, Z. Fan, C. S. Effenhauser, A. Manz, Science 261 (1993) 895

[71] S. C. Jacobson, R. Hergenröder, L. B. Koutny, R. J. Warmack, J. M. Ramsey, Anal.Chem. 66 (1994) 1107

[72] S. C. Jacobson, R. Hergenröder, L. B. Koutny, J. M. Ramsey, Anal.Chem. 66 (1994) 1114

[73] L. B. Koutny, D. Schmalzing, T. M. Taylor, M. Fuchs, Anal.Chem. 68 (1996) 18

[74] B. Ekstrom, G. Jacobson, O. Ohman, H. Sjodin, International Patent WO 91/16966, 1990, Adv. Chromatogr. 33 (1993) 1

[75] C. S. Effenhauser, A. Paulus, A. Malz, H. M. Widmer, Anal. Chem. 66, (1994) 2949

[76] A. T. Woolley, R. A. Mathies, Proc. Natl. Acad. Sci. U.S.A. 91 (1994) 11384

[77] A. T. Woolley, R. A. Mathies, Anal. Chem. 67 (1995) 3676

[78] S. V. Ermakov, S. C. Jacobson, J. M. Ramsey, Anal.Chem. 70 (1998) 4494-4504

[79] M. Jansson, A. Emmer, J. Roeraade, J. High Resolut. Chromatogr. 12 (1989) 797

[80] S. C. Jacobson, J. M. Ramsey, Anal. Chem. 69 (1997) 3212

[81] S. V. Ermakov, S. C. Jacobson, J. M. Ramsey, Anal.Chem. 72 (2000) 3512-3517

[82] S. C. Jacobson, S. V. Ermakov, J. M. Ramsey, Anal. Chem. 71 (1999) 3273-3279

[83] A. Chatterjee, J. Micromech. Microeng. 13 (2003) 758-767